University of Alberta

The Development and Application of a Time-Lag Focusing Matrix-Assisted Laser Desorption/Ionisation Time-of-Flight Mass Spectrometer

by

Randy Murray Whittal

A thesis submitted to the Faculty of Graduate Studies and Research in partial fulfilment of the requirements for the degree of Doctor of Philosophy

Department of Chemistry

Edmonton, Alberta

Fall 1996

National Library of Canada

Acquisitions and Bibliographic Services Branch

395 Wellington Street
Ottawa, Ontario
K1A 0N4

Bibliothèque nationale du Canada

Direction des acquisitions et des services bibliographiques

395, rue Wellington
Ottawa (Ontario)
K1A 0N4

Your file *Votre référence*

Our file *Notre référence*

The author has granted an irrevocable non-exclusive licence allowing the National Library of Canada to reproduce, loan, distribute or sell copies of his/her thesis by any means and in any form or format, making this thesis available to interested persons.

L'auteur a accordé une licence irrévocable et non exclusive permettant à la Bibliothèque nationale du Canada de reproduire, prêter, distribuer ou vendre des copies de sa thèse de quelque manière et sous quelque forme que ce soit pour mettre des exemplaires de cette thèse à la disposition des personnes intéressées.

The author retains ownership of the copyright in his/her thesis. Neither the thesis nor substantial extracts from it may be printed or otherwise reproduced without his/her permission.

L'auteur conserve la propriété du droit d'auteur qui protège sa thèse. Ni la thèse ni des extraits substantiels de celle-ci ne doivent être imprimés ou autrement reproduits sans son autorisation.

ISBN 0-612-18131-6

Canada

University of Alberta

Library Release Form

Name of Author: Randy Murray Whittal

Title of Thesis: The Development and Application of a Time-Lag Focusing Matrix-Assisted Laser Desorption/Ionisation Time-of-Flight Mass Spectrometer

Degree: Doctor of Philosophy

Year This Degree Granted: 1996

Permission is hereby granted to the University of Alberta Library to reproduce single copies of this thesis and to lend or sell such copies for private, scholarly, or scientific research purposes only.

The author reserves all other publication and other rights in association with the copyright in the thesis, and except as hereinbefore provided, neither the thesis nor any substantial portion thereof may be printed or otherwise reproduced in any material form whatever without the author's prior written permission.

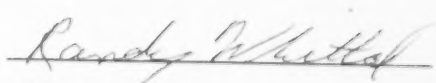

15 James Street
Bright, Ontario
Canada
N0J 1B0

September 30, 1996

University of Alberta

Faculty of Graduate Studies and Research

The undersigned certify that they have read, and recommend to the Faculty of Graduate Studies and Research for acceptance, a thesis entitled The Development and Application of a Time-Lag Focusing Matrix-Assisted Laser Desorption/Ionisation Time-of-Flight Mass Spectrometer submitted by Randy Murray Whittal in partial fulfillment of the requirements for the degree of Doctor of Philosophy.

Dr. L. Li, Associate Professor of Chemistry

Dr. N. J. Dovichi, Professor of Chemistry

Dr. O. Hindsgaul, Professor of Chemistry

Dr. G. Horlick, Professor of Chemistry

Dr. M. C. Williams, Professor of Chemical Engineering

Dr. T. B. McMahon, Professor of Chemistry

Sept. 27, 1996

to my parents

William and Jacqueline

Abstract

Decoupling ion desorption from ion extraction in matrix-assisted laser desorption/ionisation (MALDI) on a time-of-flight mass spectrometer provides substantial benefits. Inserting the sample probe through the repeller ensures that the resultant ions are directed forward in a direction parallel to the flight axis. Spatial aberrations are minimized in this geometry. Thus, a relationship between an ion's velocity (energy) and its initial position exists before the extraction pulse is applied. Time-lag focusing can be used to compensate for the initial energy distribution of MALDI formed ions providing a significant increase in resolution. The energy deficit observed in continuous extraction MALDI was not observed with time-lag focusing. The opposite effect was seen, an energy excess that increased with mass. A method was developed to overcome the effect of the energy excess on the time-of-flight calibration curve. The dependence of ion flight time on laser power is significantly reduced in time-lag focusing. The small laser power dependent energy deficit that remains decreases slightly with increasing mass, consistent with source discharge.

A good sample preparation method is necessary to obtain consistent external mass accuracy and mass resolution. Preferably, samples should be prepared in thin layers of matrix microcrystals. The instrument is applied to the analysis of peptides, proteins, oligonucleotides, modified oligosaccharides from crude samples, and end-labelled polyethylene glycol polymers.

A technique called microspot MALDI was developed to improve the sensitivity of the MALDI method. Microcapilleries were used to deposit analyte onto a specific location on the sample probe to use the sample more efficiently. The sample preparation method is described.

Acknowledgment

I would like to thank my supervisor Dr. Liang Li for his encouragement, advice, inspiration and enthusiasm over the past four years. Dr. Li has always been available for discussion and help. Dr. Li was also the recruitment officer when I applied to this department. I thank him for his hard work, personal contact and the arrangements he made for prospective students, such as me, to visit this department.

I also thank the other members of my supervisory committee Professor N. J. Dovichi and Professor O. Hindsgaul and the rest of my examining committee Professor G. Horlick, Professor M. C. Williams and Professor T. B. McMahon for their review and comments regarding this thesis.

I gratefully acknowledge the participation of the persons with whom I collaborated. I thank Professor M. M. Palcic for providing the facilities of her laboratory and for doing the enzyme incubations. I also thank Ms. C. Compston for doing the sulphatase enzyme incubations. I thank Professor O. Hindsgaul and members of his research group (Mr. R. Beever and Mr. P. Diedrich) for providing the tetramethylrhodamine-labelled and unlabelled oligosaccharides. I also thank Professor's Palcic and Hindsgaul for the many helpful discussions we had about the oligosaccharide work. I thank Dr. S. Lee and Professor M. A. Winnik from the University of Toronto who synthesized the pyrene end-labelled poly(ethylene glycol) polymers and did the ^{1}H NMR and gel permeation chromatography analysis. I thank Dr. S. R. Weinberger from the Hewlett-Packard Company in Palo Alto, CA for his many valuable discussions and ideas on the final design of the time-lag focusing instrument. From Dr. L. Li's research group, I thank Dr. L. M. Russon for his valued ideas on the final design of the instrument, his helpful discussions, and his many hours simulating ion trajectories with SIMION. I also thank Ms. Y. Dai who collected the confocal images (Chapter's 4 and 7) and the oligonucleotide spectra (Chapter 2). I thank Mr. R. E. Golding for constructing the microspot sample loading apparatus and his assistance in developing the sample preparation protocol (Chapter 7). His vast knowledge and experience were valued assets in many areas. I also thank other members of the group with whom I have worked, especially Mr. R. W. Purves for his assistance in the initial pulsed extraction experiments and

Mr. D. C. Schriemer and Mr. C. Bridges for their assistance in developing the polymer analysis protocol. I thank all of the members of Dr. Li's research group for their ideas and discussions throughout the four years of my stay. I thank Ms. N. Chan (Professor Palcic's group) for answering the many questions I posed to her over the last few years.

I thank Professor G. Horlick for the loan of the Photochemical Research Associates LN1000 nitrogen laser (Chapter's 2 and 5). I thank Dr. X. Le and Dr. I. H. Lee of Professor N. J. Dovichi's group for checking the purity of the samples used for the confocal imaging work. I thank Mr. P. Semchuk at the Centre of Excellence in Protein Engineering for the generous gift of the synthetically generated peptides. I thank Allan Crawford Associates of Mississauga, ON for the loan of the LeCroy 9354M oscilloscope. I thank the Hewlett-Packard Company of Palo Alto, CA for the loan of the Molectron laser energy meter and the HP Vectra 486/66XM computer.

I thank the personnel in the machine shop and electronics shop of the chemistry department, without whom this work would not be possible. I especially thank Mr. Eric Schartner of the machine shop for all of the help he gave me regarding a practical design on the many projects that he worked. Many examples of his fine work can be seen throughout the laboratory.

I thank the Department of Chemistry and the University of Alberta for providing the facilities. I was impressed with the excellent facilities of this department and this strongly influenced my decision to pursue graduate studies here. I thank the University of Alberta for the Entrance Scholarship and the Walter H. Johns Scholarship for four years, 1992-1996. I thank the Faculty of Graduate Studies and Research, the University of Alberta, and the Vice-President (Research) for the Mary Louise Imrie Graduate Student Award. I thank the Natural Sciences and Engineering Research Council of Canada (NSERC) for the Post-Graduate Scholarships, PGS A and PGS B for four years, 1992-1996. I thank NSERC for providing funding through both operating grants and its Industrially Oriented Research Grants. I thank the Polymer Structure Research Program of the Environmental Science and Technology Alliance Canada and the Hewlett-Packard Company of Palo Alto, CA for further funding of this work.

Table of Contents

Chapter 1 1

Introduction: Time-Lag Focusing in Linear Time-of-Flight Mass Spectrometers 1

1.1 Introduction to MALDI. 1

1.2 Why Use the Time-of-Flight Analyser? 3

1.3 The Resolution Problem. 4

1.4 Solutions to the Resolution Problem 5

1.4.1 The Ion Mirror (Reflectron) 7

1.4.2 Impulse-Field Focusing 8

1.4.3 Velocity Compaction 8

1.4.4 Dynamic-Field Focusing 9

1.4.5 Post-Source Pulse Focusing 9

1.4.6 Time-Lag Focusing 10

1.5 Time-Lag Focusing and MALDI 14

1.6 Literature Cited 18

Chapter 2 22

High Resolution Matrix-Assisted Laser Desorption/Ionisation in a Linear Time-of-Flight Mass Spectrometer 22

2.1 Introduction 22

2.2 Experimental 24

2.2.1 Peptides and Proteins 25

2.2.2 Oligonucleotides 26

2.3 Results and Discussion 27

2.4 Literature Cited 37

Chapter 3 40

Functional Wave Time-Lag Focusing Matrix-assisted Laser Desorption/Ionisation in a Linear Time-of-Flight Mass Spectrometer; Improved Mass Accuracy 40
3.1 Introduction 40
3.1.1 Model 43
3.2 Experimental 45
3.2.1 Instrument 45
3.2.2 Sample Preparation 47
3.3 Results and Discussion 48
3.4 Literature Cited 57

Chapter 4 60

Confocal Fluorescence Microscopic Imaging for Investigating the Analyte Distribution in MALDI Matrices 60
4.1 Introduction 60
4.2 Experimental 62
4.2.1 MALDI and Sample Preparation 62
4.2.2 Confocal Microscopy 63
4.2.3 Application Notes 64
4.3 Results and Discussion 65
4.4 Literature Cited 76

Chapter 5 79

Direct Analysis of Enzymatic Reactions of Oligosaccharides in Human Serum Using Matrix-Assisted Laser Desorption/Ionisation Mass Spectrometry 79
5.1 Introduction 79
5.2 Experimental 80
5.2.1 Preparation of labelled oligosaccharides 80

5.2.2 Enzyme reactions 81
5.2.3 MALDI sample preparation 82
5.2.4 Time-of-flight mass spectrometry 82
5.3 Results and Discussion 83
5.4 Literature Cited 97

Chapter 6 99

Characterization of End-Labelled Polyethylene Glycol by High Resolution Matrix-Assisted Laser Desorption/Ionisation Time-of-Flight Mass Spectrometry 99
6.1 Introduction 99
6.2 Experimental 102
6.2.1 Synthesis of α,ω-poly(ethylene glycol)-di-4-(1-pyrenyl)butyrate 102
6.2.2 Synthesis of α,ω-poly(ethylene glycol 4100) bis[methoxy poly(ethylene glycol X) 4-(1-pyrenyl)butyl phosphate] 102
6.2.3 Materials 102
6.2.4 MALDI Mass Spectrometry 102
6.2.5 Gel Permeation Chromatography and ^{1}H NMR 103
6.3.1 Time-Lag Focusing MALDI and Polymer Analysis 103
6.3.2 Applications of Time-Lag Focusing MALDI to Polymer Analysis: 105

Chapter 7 125

Microspot Matrix-Assisted Laser Desorption/Ionisation and Its Application to Single Cell Analysis 125
7.1 Introduction 125
7.2 Experimental 126
7.2.1 Sample Preparation 126

7.2.1.1 Preparing the Capillaries 127
7.2.1.2 Peptide Analysis 127
7.2.1.3 Protein Analysis 127
7.2.1.4 Loading the Analyte 127
7.2.1.5 Analysis of Cells 128
7.2.2 MALDI Analysis 130
7.2.3 Sample Imaging 130
7.3 Results and Discussion 132
7.4 Literature Cited 140

Chapter 8 143

Conclusions and Future work 143

List of Tables

Table 2.1 Mass Accuracy and Reproducibility of a DNA 35-mer $(M+H)^+$ with a mass of 10637.02 Da 37

Table 3.1 Internal Mass Accuracy for Time-Lag Focusing (TLF) MALDI Using a Square Wave and a Modified Wave Shape 49

Table 3.2 Resolution of Proteins in Continuous Extraction and Time-Lag Focusing Extraction MALDI 54

Table 3.3 External Mass Accuracy and Reproducibility of Modified Pulse Time-Lag Focusing MALDI 56

Table 6.1 Molecular Weight Data for the Poly(ethylene glycol) Used as the Starting Material for **1**, **2**, **3**, **4**, and **5** 109

Table 6.2 Summary of the Molecular Weight Data for the Bis(phosphates), Obtained by MALDI, Gel Permeation Chromatography (GPC), and ^1H NMR Spectroscopy, and Their Comparison with the Calculated M_n Values . 119

List of Figures

Figure 1.1 Schematic of a time-of-flight instrument with (A) a single-stage extraction source and (B) a dual-stage extraction source. Ions are accelerated in the source; all ions starting at a position *s* receive the same kinetic energy from the power supply. The ions enter a field-free region where the separate according to their velocity or mass-to-charge ratio; lighter ions (higher velocity) reach the detector first. 2

Figure 1.2 In MALDI, the sample probe is inserted through the repeller. The sample of interest is mixed with a matrix, whose electronic transition matches the wavelength of the laser. The laser desorbs/ionises the matrix along with the sample. 6

Figure 1.3 Time-Lag focusing in a time-of-flight mass spectrometer. (A) Ions are desorbed into a field-free region where they separate according to their initial velocity. Ions of the same mass with higher initial velocity (energy) move further from the repeller. (B) As the extraction pulse is applied, the initially more energetic ions receive less energy from the extraction pulse than the initially less energetic ions. (C) The initially less energetic ions catchup to the initially more energetic ions at the detector plane, greatly improving resolution. 11

Figure 1.4 A simulated demonstration of time-lag focusing. Using equation (14), the difference in flight time of insulin ions desorbed from a surface was calculated assuming initial velocities ranging from 300 to 900 m s^{-1}. The smallest time difference (predicted < 1ns) represents the highest resolution. The effect of time lag and extraction voltage is shown. See text for details. 16

Figure 2.1 MALDI mass spectra for a total loading of 1 pmol of a synthetic peptide, Ac-ELEKLLKELEKLLKEAEK-Am (monoisotopic, $(M + H)^+$ = 2224.317 Da), obtained by using (A) DC ion extraction and (B) time-lag focusing ion extraction with a 2.00 kV pulse. Each spectrum is the result of signal

averaging of 100 shots on the oscilloscope. 28

Figure 2.2 Time-lag focusing MALDI mass spectra for a total loading of 1 pmol of peptide for several peptides using α-cyano-4-hydroxycinnamic acid as matrix, the pulse potential used is given in brackets. (A) Bradykinin, $(M+H)^+$ = 1060.569 Da, (0.90 kV), (B) LYPVKLYPVK, $(M+H)^+$ = 1219.746 Da, (1.00 kV), (C) Ac- KLEALEAKLEALEA-Am, $(M+H)^+$ = 1568.290 Da, (1.30 kV), (D) Ac-EAEKAAKEAEKGAKEAEK-Am, $(M+H)^+$ = 1958.020 Da, (1.75 kV), (E) Ac-ELEKLLKECEKLLKELEK-Am, $(M+H)^+$ = 2256.289 Da, (2.05 kV), (F) Ac- KLEALEAKLEALEAKLEALEAKLEALEA-Am, $(M+H)^+$ = 3077.735 Da, (2.50 kV) 29

Figure 2.3 Single shot mass spectrum for a total loading of 1 pmol of synthetic peptide Ac-EAEKAAKEAEKGAKEAK-Am using α-cyano-4-hydroxycinnamic acid as matrix. The pulse potential used is 1.75 kV. 31

Figure 2.4 Time-lag focusing MALDI mass spectrum of a mixture of peptides (1 pmol of each peptide is loaded to the sample probe) using α-cyano-4-hydroxycinnamic acid as matrix. The pulse potential used is 1.20 kV. The peptide sequence of the two synthetic peptides is given in Figure 2.2. . . 33

Figure 2.5 Time-lag focusing MALDI mass spectra for a total loading of 1 pmol of (A) bovine insulin $(M + H)^+$ = 5734.37 Da using α-cyano-4-hydroxycinnamic acid as matrix, pulse potential 2.75 kV (B) equine cytochrome *c* using sinapinic acid as matrix, pulse potential 3.50 kV (C) equine apomyoglobin using α-cyano-4-hydroxycinnamic acid as matrix, pulse potential 4.50 kV. 34

Figure 2.6 MALDI mass spectra of 7 pmol of a DNA 35-mer analysed in (A) positive-ion and (B) negative-ion modes using a 1-μs time-lag and (A) 2.95 kV, (B) −3.15 kV pulsed-extraction potential 36

Figure 3.1 In time-of-flight instruments calibrations are done assuming there is a linear relationship between (flight time)^2 and m/z. This does not account for the initial energy of an ion. If an initial ion velocity of 500 m/s is assumed for all MALDI ions, then a linear relationship no longer holds. The effect upon the

calibration is shown. 42

Figure 3.2 The predicted pulse shape that is required to maintain constant total kinetic energy for all ions by delivering less imparted kinetic energy to ions of higher mass. The times at which a 5 kDa and a 30 kDa ion exit the region between the repeller and the first extraction plate are labelled on the graph. The effect of a change in the time lag is shown. The inset figure shows the overall pulse shape between 0 and 3.9 kV. See the text for details. 46

Figure 3.3 Changes in ion flight time with laser power for (A) bovine insulin and (B) bovine carbonic anhydrase II. Four spectra were averaged for each point. The error bars represent one SD in the observed flight time. Charge depletion on the repeller is proposed for the time shift with increasing laser power. See text for details. 51

Figure 3.4 The dependence of the flight time of human insulin ions on the laser energy used for desorption in continuous extraction MALDI. Increasing the source capacitance decreases the effect of laser energy. See the text for details. 53

Figure 3.5 MALDI spectra of a mixture of insulin, cytochrome *c*, myoglobin, trypsinogen and carbonic anhydrase II in (A) continuous extraction and (B) time-lag focusing extraction with focusing centred at carbonic anhydrase using a 1-μs time lag. 55

Figure 4.1 MALDI mass spectrum of 1 pmol bovine insulin-FITC using sinapinic acid as the matrix. 66

Figure 4.2 Confocal microscopic images (scale bars in μm) of bovine insulin-FITC in: (A) 2,5-dihydroxybenzoic acid matrix crystals and (B) sinapinic acid matrix crystals, obtained by superimposing the transmission phase-contrast images of crystals (in red background) and the analyte fluorescence images (in green),prepared on a glass slide using the dried-droplet method. (C) 2,5-Dihydroxybenzoic acid matrix crystals and (D) sinapinic acid matrix crystals, obtained by superimposing the phase-contrast reflectance images of crystals (in red background) and the analyte fluorescence images (in green), prepared

on a MALDI probe using the dried-droplet method. (E) A sinapinic acid matrix crystal prepared by a controlled slow-growth process. Sinapinic acid matrix crystals prepared by (F) the fast solvent evaporation method, (G) the crushed-crystal method, and (H) the uniform submicron-crystal formation method described in this work. Colour-coded confocal fluorescence images of bovine insulin-FITC (in green) and αGal(1→3)[αFuc(1→2)]βGal-TMR (in blue), see text for details. The sample is prepared by (I) the dried-droplet method with 2,5-dihydroxybenzoic acid as the matrix and (J) the fast evaporation method with sinapinic acid as the matrix. Note that the MALDI desorption laser is typically 50–100 μm. 67

Figure 4.3 MALDI mass spectrum of trypsinogen. The sample was prepared by dissolving sinapinic acid in a solvent mixture of 39% acetone, 60% methanol, 1% of 0.1% trifluoroacetic acid (aq.) (v/v) and depositing 1 μL to the sample probe to form a thin layer of matrix crystals, followed by adding a 0.5 μL of a 1:1 mixture of 1.2 pmol/μL trypsinogen (aq.) and sinapinic acid dissolved in 30% acetonitrile, 20% methanol, 50% water (v/v) to the top of the first matrix layer. 74

Figure 5.1 MALDI mass spectrum of a mixture of three derivatives of an oligosaccharide using 2,5-dihydroxybenzoic acid as the matrix: 10 pmol Le^b-OCH_3, 1 pmol Le^b-MCO and 0.2 pmol Le^b-TMR. 84

Figure 5.2 MALDI mass spectrum of 0.2 pmol Le^b-TMR obtained using α-cyano-4-hydroxycinnamic acid as the matrix. 86

Figure 5.3 MALDI mass spectrum of a mixture of 30 pmol Le^b-OCH_3, 10 pmol Le^b-MCO, and 0.5 pmol Le^b-TMR spiked into human serum with buffers and other reagents added. α-Cyano-4-hydroxycinnamic acid is used as the matrix with the new sample/matrix preparation method. Le^b-TMR is the only oligosaccharide derivative observed. The inset graph is an expansion of the peak at m/z 1287.4. 88

Figure 5.4 MALDI mass spectra of B-TMR obtained with A) a pure sample and B) from buffered serum spiked with B-TMR. α-Cyano-4-hydroxycinnamic acid is

used as the matrix with the new sample/matrix preparation method. Spectra collected with a 1ns/point digitizer. The theoretical exact mass of B-TMR is 1099.497 Da. 90

Figure 5.5 MALDI for monitoring the αGal(1→3) transferase enzyme reaction in vitro. MALDI mass spectra of the serum samples after a 90-min incubation with no UDP-Gal donor added (A) and with UDP-Gal donor added (B) α-cyano-4-hydroxycinnamic acid is used as the matrix with the new sample/matrix preparation method. 92

Figure 5.6 MALDI spectra of the acceptor disac-TMR after a 90-min incubation in human serum. (A) An unexplained peak appears at 102.0 mass units above the disac-TMR$^+$ peak. (B) After a 120 min incubation of the sample in (A) with Limpet sulphatase, the unexplained peak disappears. 94

Figure 5.7 Calibration curve for quantitation of B-TMR product. The peak intensity of B-TMR is measured relative to Le^b-TMR. The error bars represent ±2 SD for five samples at each concentration. 95

Figure 6.1 MALDI spectra of a mixture of poly(ethylene glycol) 2000 and 4100 in (A) continuous extraction and time-lag focusing with (B) a 1.40 kV pulse and (C) a 2.00 kV pulse. 104

Figure 6.2 MALDI spectra of poly(ethylene glycol) 10000 in (A) continuous extraction and (B) time-lag focusing extraction. The resolution in (B) is ~1100 fwhm at 13 kDa. 106

Figure 6.3 Spectra of poly(ethylene glycol) 3350 collected at two different pulse potentials. (A) the pulse potential is optimized for ~3 kDa and (B) the pulse potential is optimized for ~5 kDa. 107

Figure 6.4 MALDI mass spectrum of the poly(ethylene glycol) 4100 molecular weight standard used as the starting material in the esterification reaction with pyrenebutyric acid, i.e., to make **1**. 108

Figure 6.5 Gel permeation chromatography trace of **1**. Solid line: refractive index detector. Dashed line: fluorescence detector measuring the excitation signal at 345 nm. The minor, nonabsorbing impurity at low molecular weight is

unidentified. 111

Figure 6.6 MALDI mass spectrum of **1**. D represents the doubly-labelled **1**. S2 is singly-labelled **1**. S1 is most likely the sodium salt of S2. All peaks are sodium cationised. See text for details. 112

Figure 6.7 MALDI spectrum of **2**. M_n = 4692, M_w = 4714. See text for details. . . 114

Figure 6.8 MALDI spectrum of **3**. M_n = 5607, M_w = 5628. See text for details. . . 115

Figure 6.9 MALDI spectrum of **4**. M_n = 5897, M_w = 5920. See text for details. . . 116

Figure 6.10 MALDI spectrum of **5**. M_n = 8409, M_w = 8427. See text for details. . . 117

Figure 6.11 MALDI spectrum of **6**. The mass accuracy is 56 ± 38 ppm external for poly(ethylene glycol) bis(acetaminophen). See text for details. 121

Figure 6.12 MALDI spectrum of **7**. The mass accuracy is 40 ± 35 ppm external for poly(ethylene glycol) bis(ephedrine). See text for details. 122

Figure 7.1 Microspot MALDI delivery system. It consists of a sample and probe tip holder and a movable x-y stage. Two fused silica capillaries are attached to the x-y stage and connected to disposable syringes. During sample loading, the sample vial is placed on the sample holder and the x-y stage is moved to allow the capillary to contact the sample solution. A measured volume of a sample is then withdrawn using the syringe under microscopic observation. Some air is then drawn into the capillary. The sample vial is replaced with the MALDI probe that is precoated with a thin layer of a matrix. The capillary loaded with the sample is then moved to the probe surface and the sample is deposited onto the matrix layer. For protein analysis, a second layer of matrix is loaded on top of the sample. 129

Figure 7.2 Schematic of the cell loading process for human erythrocytes. (A) Before loading the cell suspension the capillary was filled with ~0.5-1 nL of water. The cell suspension was first loaded to a deactivated-glass tube with a diameter of 1.3 mm. The 20-μm-ID sample capillary, whose external diameter was reduced to 48 μm, was inserted in the tube containing the cell suspension. For single cell loading, the volume withdrawn from the cell suspension was ~100 pL. (B) The exact number of cells was verified using

a larger microscope magnification. (C) The cell suspension was then delivered to the probe tip that was previously covered with a thin layer of matrix. A second layer of matrix (20 nL) was added on top of the sample using the auxiliary capillary. 131

Figure 7.3 (A) Confocal fluorescence microscopic image of a conventional sample preparation and (B) a microspot MALDI sample preparation of a tetramethylrhodamine labelled trisaccharide loaded on the second layer of α-cyano-4-hydroxycinnamic acid. 133

Figure 7.4 The sample spot area and diameter which is observed by fluorescence microscopy for a tetramethylrhodamine-labelled trisaccharide on α-cyano-4-hydroxycinnamic acid for a 10-μm-ID and 144-μm-OD capillary. . . . 134

Figure 7.5 Microspot MALDI spectra of (A) 195 pL of a 5.0 nM solution or 0.97 amol of substance P (oxidized form) and (B) 230 pL of a 20 nM solution or 4.6 amol bradykinin. The samples were loaded on top of the second layer of matrix. See the text for details. 137

Figure 7.6 Microspot MALDI spectra of (A) 13 amol of human insulin and (B) 54 amol of equine myoglobin using sinapinic acid as the matrix. See the text for details. 138

Figure 7.7 Application of microspot MALDI to the analysis of human erythrocytes. (A) three cells loaded and (B) one cell loaded. See text for details. 139

List of Abbreviations

CCD	charge-coupled device
Da	daltons, 1 Da ≡ 1 u (atomic mass standard)
DC	direct current
DNA	deoxyribonucleic acid
eV	electron Volt, 1 eV = 1.60218×10^{-19} J
fwhm	full width at half maximum
FITC	fluorescein isothiocyanate
^{1}H NMR	proton nuclear magnetic resonance spectroscopy
ID	internal diameter
MALDI	matrix-assisted laser desorption/ionisation
M_n	number average molecular weight
M_w	weight average molecular weight
m/z	mass-to-charge ratio
Nd:YAG	neodymium: yttrium aluminium garnet
ppm	parts per million
SD	standard deviation
TMR	tetramethylrhodamine
UV-VIS	ultraviolet-visible
v/v	volume-to-volume ratio
w/w	weight-to-weight ratio

Chapter 1

Introduction: Time-Lag Focusing in Linear Time-of-Flight Mass Spectrometers

Decoupling ion formation from ion extraction in a two-stage ion source provides substantial benefits to the analysis of ions formed by matrix-assisted laser desorption/ ionisation (MALDI). The time lag or delay inserted between ion formation and extraction allows ions of the same mass but different initial energy to be focused at the detector of a time-of-flight mass spectrometer simultaneously. This technique is called time-lag focusing.

1.1 Introduction to MALDI.

The current interest in time-of-flight mass spectrometers is due largely to the development of MALDI, independently in two laboratories in 1987 with the first high mass results published in 1988. Tanaka and coworkers at Shimadzu in Japan used a nitrogen laser (337 nm) to desorb intact carboxypeptidase-A ions (34.5 kDa) from a slurry of glycerol and ultra-fine metal powder for analysis by a time-of-flight instrument.[1,2] Hillenkamp and Karas at the University of Münster in Germany used a frequency-quadrupled Nd:YAG laser (266 nm) to desorb peptides from 3-nitrobenzyl alcohol, 2-nitrophenyl octyl ether, and nicotinic acid for analysis by an LAMMA-1000 (LAser Microprobe Mass Analyser) time-of-flight mass spectrometer.[3] Using nicotinic acid, the same instrument was applied to the analysis of several proteins up to bovine albumin (66.4 kDa).[4] The method of Hillenkamp and Karas has been more readily adapted, mainly due to its higher sensitivity.

In MALDI, desorption of the compound of interest takes place under a vacuum (<600 μPa) inside the ion source of the instrument using a pulsed laser (~1 - 10 ns duration). A high continuous voltage is applied to the ion source to accelerate the ions out (see Figure 1.1A). MALDI is generally considered a soft-ionisation method, i.e., generally only pseudomolecular (usually protonated molecular or $(M + H)^+$) ions are observed. However, MALDI ions do receive enough internal energy to undergo unimolecular decay or to

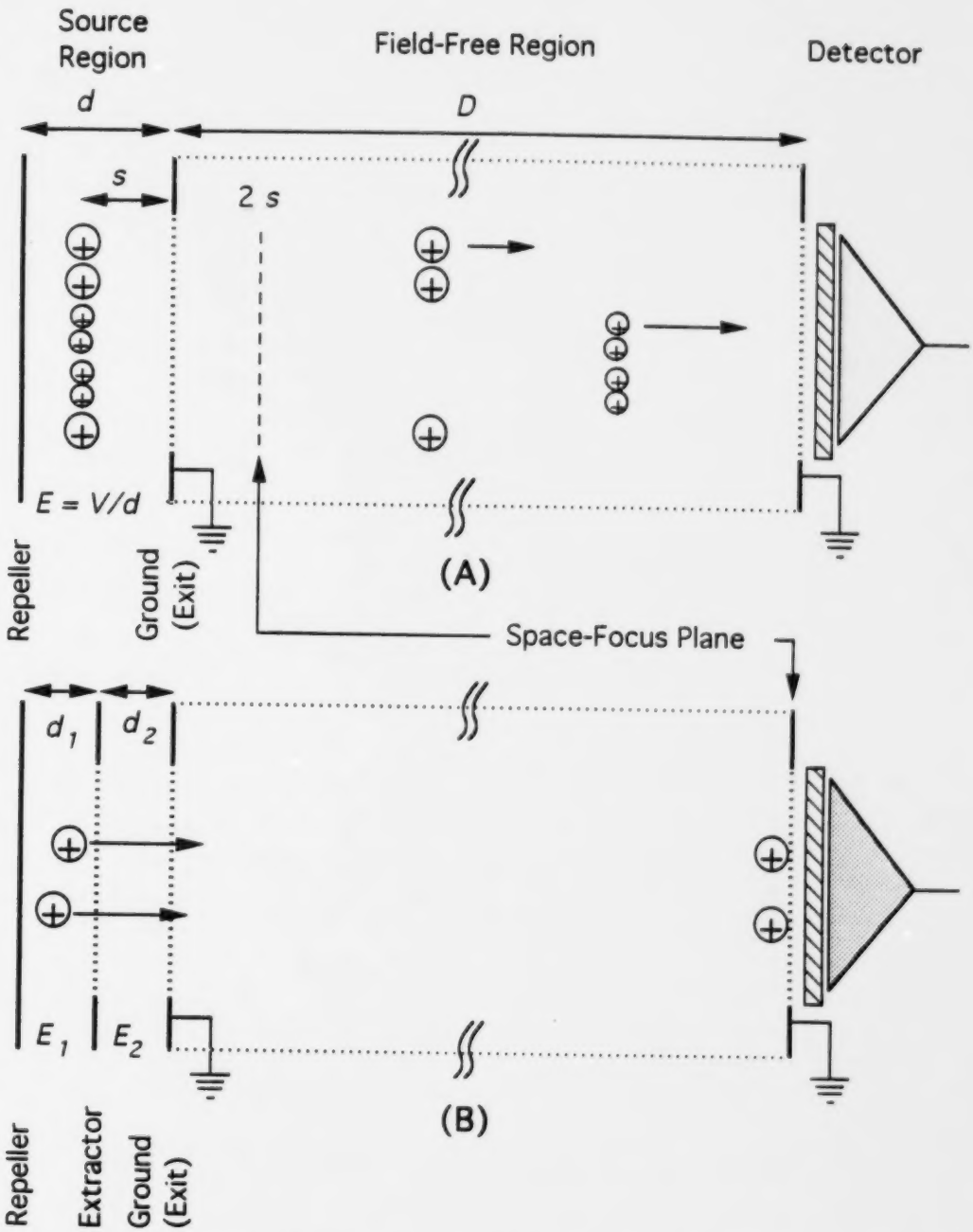

Figure 1.1 Schematic of a time-of-flight instrument with (A) a single-stage extraction source and (B) a dual-stage extraction source. Ions are accelerated in the source; all ions starting at a position *s* receive the same kinetic energy from the power supply. The ions enter a field-free region where the separate according to their velocity or mass-to-charge ratio; lighter ions (higher velocity) reach the detector first.

fragment over long periods (2–20 μs). In a time-of-flight instrument if an ion fragments after leaving the ion source then the mass of the fragment can be determined using a technique called post-source decay analysis[5] (see later in this chapter). This technique offers a way to analyse the structure of the compound of interest and is usually applied to peptide sequencing.

1.2 Why Use the Time-of-Flight Analyser?

Analysis of ions formed by MALDI can also be done on other mass spectrometers, including magnetic sectors,[6] Fourier-Transform ion cyclotron resonance,[7,8] and quadrupole ion trap instruments.[9,10,11] However, it is the time-of-flight to which MALDI is most often coupled. In time-of-flight mass spectrometers, all ions are accelerated by a voltage, V, to the same final kinetic energy as they exit the ion source, i.e., for an ion of mass m:

$$eV = \frac{1}{2}mv^2, \qquad (1)$$

where v is the ion's final velocity as it exits the ion source and e is the unit of elementary charge. The ions enter a field free region where they separate according to their mass-to-charge ratio (see Figure 1.1A). The final velocity can be expressed as the length of the field free drift region, D, divided by the time, t, to traverse this region. Therefore, ion flight time, which is dependent on the square root of an ion's mass, can be expressed as:

$$t = \left(\frac{m}{2 \cdot e \cdot V}\right)^{1/2} D. \qquad (2)$$

A time-of-flight mass spectrometer does not measure ion current continually. Ions are pulsed out of the ion source in discrete packets. Measurement of their flight time requires that the start point be known. For convenience, the start time is the time that the push-out pulse is turned on. MALDI is an inherently pulsed ionisation method, i.e., pulsed lasers are used for ion desorption, thus defining the start point. A time-of-flight, equipped only with constant potential power supplies, provides a simple instrument for the analysis of MALDI formed ions.

Additionally, a time-of-flight is the only mass analyser with an unlimited mass range. MALDI generated ions greater than 1 MDa have been detected in time-of-flight analysers.[12,13] Also, time-of-flight instruments are highly sensitive mass spectrometers. With each laser pulse, all ions formed are detected, i.e., scanning the mass analyser, which reduces sensitivity, is not necessary.

Time-of-flight instruments are inexpensive to construct and operate. However, they often require expensive data collection systems. The data system, including, high speed amplifiers, digital oscilloscopes, and computers can often be one-half the cost of the instrument. Sometimes, the resolution of a time-of-flight can be limited by its detection system. Although, recent advances in electronics and the introduction of digital oscilloscopes with 1 ns/point or better temporal resolution have made this less likely. Time-of-flight instruments generate large data files (a spectrum collected at 1 ns/point out to a 50 μs flight time requires 100 kbytes of storage space). A good modern data handling and storage system can handle the quantity of data produced.

1.3 The Resolution Problem.

Time-of-flight analysers are generally seen as low resolution instruments. Ideally, all ions formed in the source would start from the same point, simultaneously, with the same initial kinetic energy. In reality, this does not happen. Depending upon the ion source used, the resolution can be limited by the uncertainty in the time of ion formation, the uncertainty in ion position, the uncertainty in an ion's initial kinetic energy, or a combination of these reasons. Ions formed in the gas phase, using electron impact ionisation, will have a spatial distribution equal to the width of the ionisation beam and an initial kinetic energy distribution equal to the thermal energy distribution of the gas phase neutrals. If two ions, with the same energy, are formed at different points in the source, then the ion formed closer to the repeller (further from the detector) will catch up to the ion further from the repeller at the space-focus plane. In a single-stage ion source (a repeller and exit plate or ground plate, as shown in Figure 1.1A), if an ion is formed at a position s, then the space-focus plane is at a position $2s$. Placing a detector so close to the source is usually inconvenient because ions of different mass will not have time to separate sufficiently. A method used to correct for

the initial spatial distribution was devised by Wiley and McLaren in 1955.[14] In their method a two-stage ion source was used, see Figure 1.1B. Adjusting the ratio of the electric field strengths in the second region, E_2, to the electric field strength in the first region, E_1, makes it possible to move the space-focus plane to the detector. The location of the space-focus plane is mass independent but ions of different mass reach it at different times.[15] Unfortunately, a low value of E_1 favours moving the space-focus plane toward the detector but high extraction potentials minimize the effect of the initial kinetic energy distribution. Therefore, simultaneous space and energy focusing is not possible; a compromise is usually made. In addition, ions may be formed with their initial velocity directed toward or away from the detector. These ions will be accelerated to the same final kinetic energy but reach the detector at different times, with the difference called the turnaround time.[15]

Ions desorbed from a surface are directed forward (away from the surface) and have a minimal spatial distribution. The spatial contribution to the decrease in resolution is usually ignored. Also, there is no effect of turnaround time. In MALDI, samples are usually deposited as thin films and desorbed from a probe inserted through an opening in the repeller plate (Figure 1.2). Pulsed lasers with 1 - 10 ns pulse widths are used for desorption. Thus, the temporal distribution of MALDI ions is low. The major contribution to low resolution in MALDI is the inherently broad initial kinetic energy distribution. Initial velocities are almost independent of mass; thus, initial kinetic energies increase approximately linearly with mass.[16] For example, an insulin ion has an initial kinetic energy of ~11 eV (1 eV = 1.60218×10^{-19} J) and a distribution of ~2 eV.[16] Fortunately, several methods have been devised to compensate for the initial kinetic energy distribution in time-of-flight instruments.

1.4 Solutions to the Resolution Problem

Compensation for the initial kinetic energy distribution can be accomplished in several ways. The techniques include time-lag focusing,[14] the ion mirror (or reflectron),[17,18] impulse-field focusing,[19] velocity compaction,[20] dynamic-field focusing,[21] and post-source pulse focusing.[22] Of these, time-lag focusing and impulse-field focusing are in-source techniques, whereas, the others are post-source methods.

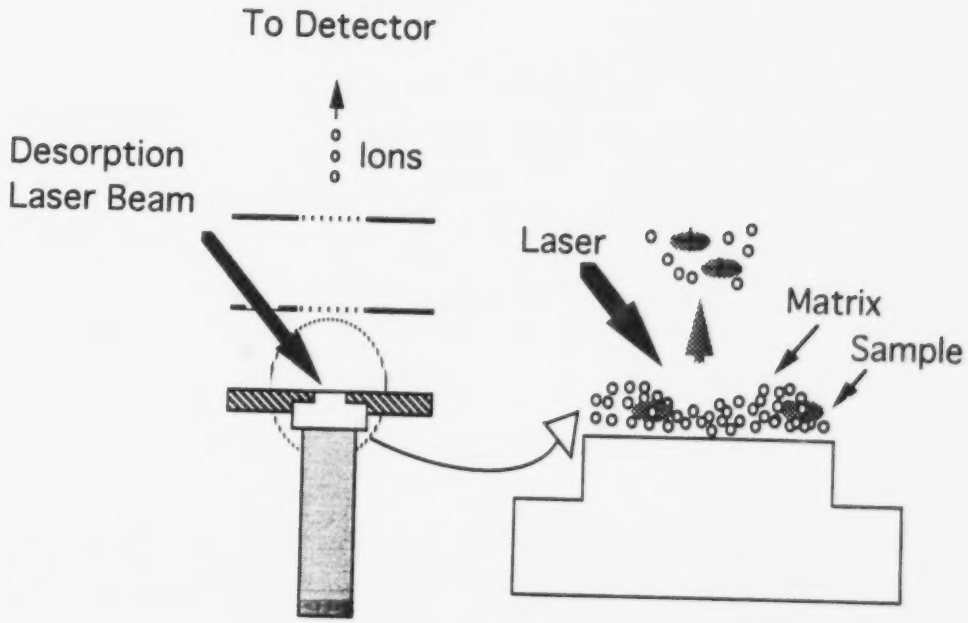

Figure 1.2 In MALDI, the sample probe is inserted through the repeller. The sample of interest is mixed with a matrix, whose electronic transition matches the wavelength of the laser. The laser desorbs/ionises the matrix along with the sample.

1.4.1 The Ion Mirror (Reflectron)

As discussed above, the adjustments for the initial spatial distribution may be done in the source. Additionally, if the space-focus plane is the focal point of an ion mirror, then the spatial distribution problem becomes an energy focusing problem. Ion mirrors, introduced in 1973 by Mamyrin, et al.,[17] are commonly used to compensate for the initial spatial distribution or the initial kinetic energy distribution or both. The Mamyrin ion mirror is a two-stage design, where two-thirds of an ion's energy is reduced in a short retarding region and the ion's direction is reversed in a reflecting region. The reflecting region consists of a series of parallel plates with gradually increasing potentials applied; the potential of the last plate is usually set to match the source potential. A single-stage ion mirror was developed by Standing, et al.,[18] at the University of Manitoba. In their instrument, ion energy is reduced gradually across the entire length of the ion mirror. This requires that the single-stage ion mirror be much longer than the dual-stage alternative. However, the energy compensation of the single-stage reflectron is mass independent and a simple linear relationship exists between the flight time of parent ions and their unimolecular decay product ions; this is not true for the dual-stage instrument.

The mechanism of kinetic energy compensation is easily understood. Ions with greater kinetic energy penetrate more deeply into the reflecting region than ions of lower energy. Thus, the more energetic ions spend more time in the reflecting region; all ions of the same mass reach the detector simultaneously; the resolution is greatly improved.[17,18]

A major reason to couple an ion mirror with a MALDI source is the application of the mirror to post-source decay analysis.[5] Unimolecular decay in the field-free region forms fragment ions with the same velocity (different kinetic energy) as the parent ion. The fragment ion can be analysed for its mass by reducing the potential applied to the ion mirror. The fragment ions penetrate the mirror and are brought to focus at the detector. The mass of the fragment is determined by the ratio of the source to ion mirror potential.[18] Cornish and Cotter recently introduced an ion mirror that does not require scanning to analyse the mass of fragment ions.[23] All fragment ions are focused at the detector with a constant potential setting on the ion mirror. The sensitivity of fragment ions is higher than for other ion

mirrors.

1.4.2 Impulse-Field Focusing

The theory for impulse-field focusing was developed by Marable and Sanzone in 1974, with experimental confirmation of the model following later.[24] Impulse-field focusing was used with electron-impact ionisation of gas phase neutrals. As discussed above, the resultant ions can be formed with their initial velocity directed toward or away from the detector. The idea behind impulse-field focusing was to apply a short duration intense pulse, forcing the ions closer to (and moving toward) the repeller to turnaround and then reduce the pulse amplitude to a characteristic value until all ions exit the source. This method is a variation of time-lag focusing. The method uses a two-stage ion source for space focusing and varies the time lag for energy focusing (see later in this chapter). Resolution improves from 280 to 450 in Sanzone's linear time-of-flight instrument using impulse-field focusing.

1.4.3 Velocity Compaction

The theory and initial testing of velocity compaction were done in 1987 by Muga. Velocity compaction is designed to give simultaneous space and energy focusing for all masses. The model describes a single-stage extraction source, where ions generated by an electron impact beam are extracted with a - 10 V potential, followed by a short field-free drift region. Ions of different mass will partially separate according to their mass-to-charge ratio. Ions of the same mass will be partially separated by their initial kinetic energy and spatial distributions. Following the drift region is another acceleration region. Here, the acceleration energy is increased with time such that the initially more energetic ions that first enter the second acceleration region receive less energy. The idea is to give ions of the same mass the same velocity upon passing into the second field-free region. Space focusing is accomplished similarly. Ions of the same mass that have the same energy but are spatially dispersed will be forced into focus at the detector by imparting more kinetic energy to the lagging ions. The author may have missed an important consideration in his velocity compaction model. The velocity compaction scheme will give ions of the same mass the same velocity (energy) upon reaching the second field-free region but these ions will have reached the grid at different times and thus arrive at the detector at different times (in fact the

model predicts tailing peaks). However, imparting more velocity (energy) to the slower ions will improve resolution. Experimental confirmation of the model showed a resolution of 1176 at m/z 173 for $[CHBr_2]^+$ ions.

1.4.4 Dynamic-Field Focusing

The model for dynamic-field focusing was developed in 1989 by Yefchak, Enke and Holland. Their model is designed to overcome a limitation of time-lag focusing and is a variation of the velocity compaction model. As mentioned previously, simultaneous space and energy focusing is not possible using time-lag focusing for gas phase generated ions. They proposed allowing the ions to pass the space-focus plane (using a single-stage source so that the space focus plane is at $2s$) in the field-free region. Past the space-focus plane there is a correlation between an ion's position and its velocity. Application of a pulse that decreases in amplitude (positive ions) with time (a dynamic pulse) allows ions of the same mass to arrive at the detector simultaneously. The ions of higher velocity receive less energy from the pulse than ions of lower velocity because the energy imparted by the pulse is increasing with time. Calculations showed that all ions, despite mass, could be brought into focus at the detector. Unfortunately, experimental confirmation of this model has not been reported.

1.4.5 Post-Source Pulse Focusing

The theory of post-source pulse focusing was developed in 1989 by Kinsel and Johnston with experimental confirmation following in 1991 for multiphoton ionisation[25] and in 1993 for MALDI.[26] This method is again similar to velocity compaction. A dual-stage source was used such that the space-focus plane could be moved to any place in the flight tube. Ions exiting the source, enter a field-free region. After the highest mass ion of interest has past the source exit grid, the grid is pulsed. The method provides energy focusing of the same mass ions that is mass independent. All ions that are between the source exit grid and second grid defining the end of the pulsed region are brought to focus at the detector. The disadvantage of this technique is that energy focusing comes at the expense of space focusing. Similar to time-lag focusing, simultaneous space and energy focusing cannot be achieved. However, for multiphoton ionisation of gas phase neutrals, a three-fold

improvement in resolution to 1500 fwhm is observed for chrysene (m/z 228). Also, for desorption techniques, spatial distributions are minimal. Application of post-source pulse focusing to MALDI generated ions gave a resolution of 2750 fwhm for angiotensin II (m/z 1046). Further work in this area by Grotemeyer, et al.,[27] has shown a resolution of 4600 fwhm for m/z 657. Grotemeyer also developed a method to calibrate the spectrum. However, the sensitivity of this method remains low.

All three of the above post-source focusing techniques suffer from a similar problem; the calibration is difficult. A simple relationship between flight time and mass does not exist.

1.4.6 Time-Lag Focusing

Wiley and McLaren developed an energy compensation technique called time-lag focusing in 1955. As mentioned earlier, they used a two-stage extraction source for gas phase generated ions that allows movement of the space-focus plane to the detector by selection of the proper ratio of E_2/E_1. Energy focusing was accomplished by varying the delay between the time of ion formation and ion extraction. Ions were generated in the centre of a field-free ion source and allowed to separate according to their initial energy (see Figure 1.3). If one considers only ions moving toward the detector then the initially more energetic ions move further from the repeller than the initially less energetic ions. Application of the extraction pulse imparts more energy to the ions closer to the repeller than to the extractor. The initially less energetic ions closer to the repeller catch up to the initially more energetic ions at the detector (see Figure 1.3 C). Of course, gas phase generated ions are moving in all directions, which gives a spatial distribution and turnaround time. However, the turnaround time is minimized in the same way as the kinetic energy distribution. Ions closer to the repeller during extraction receive more energy and catch up to ions initially closer to the extractor. A compromise is made between the best space and energy focusing. In addition the optimal delay time is mass dependent.

Equation (2) is a simplification of the true flight time of an ion. The equation only measures the time required to traverse the field-free region. In reality the time spent to accelerate the ion needs to be included. Therefore, for a two-stage source as shown in Figure

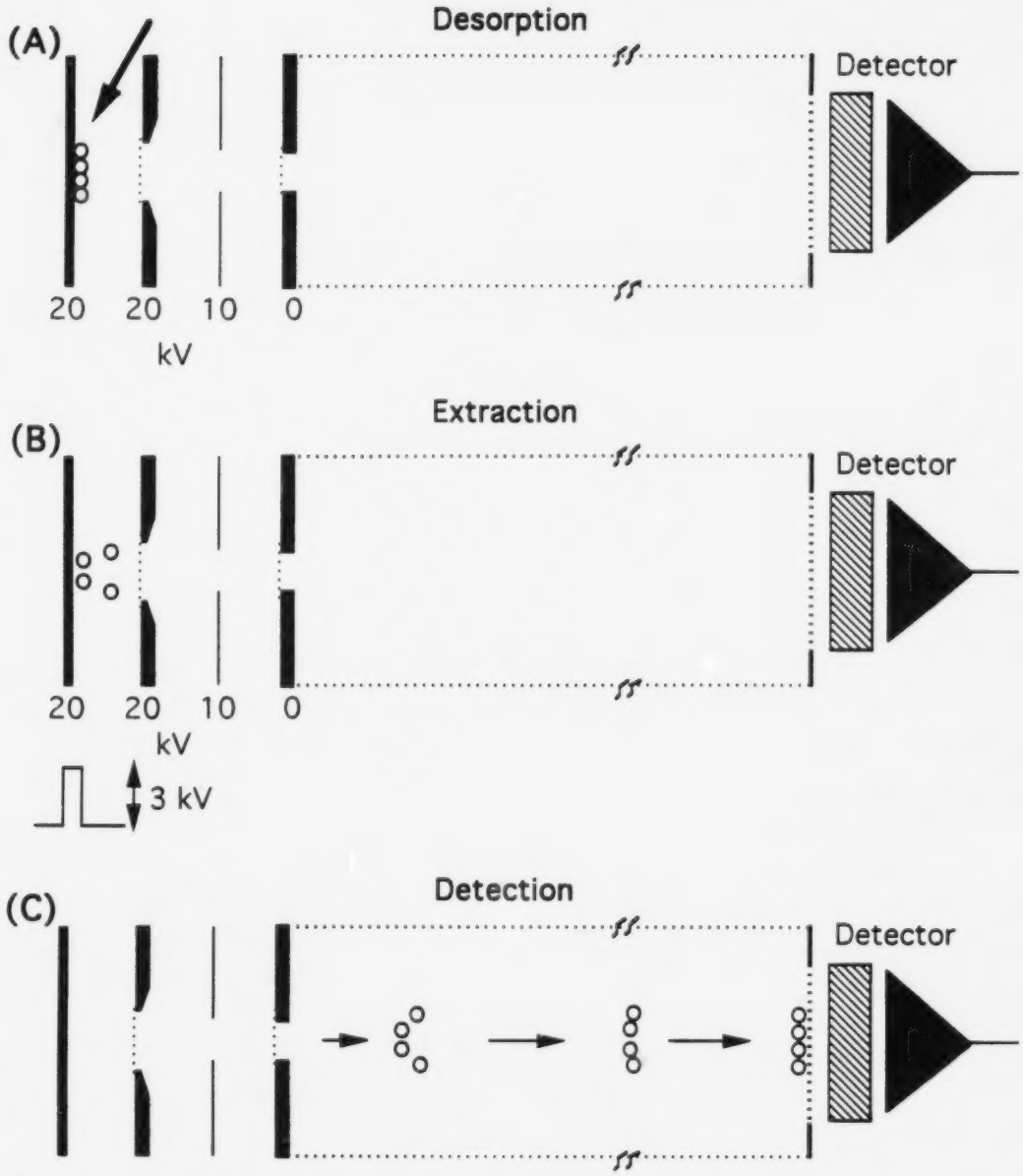

Figure 1.3 Time-Lag focusing in a time-of-flight mass spectrometer. (A) Ions are desorbed into a field-free region where they separate according to their initial velocity. Ions of the same mass with higher initial velocity (energy) move further from the repeller. (B) As the extraction pulse is applied, the initially more energetic ions receive less energy from the extraction pulse than the initially less energetic ions. (C) The initially less energetic ions catchup to the initially more energetic ions at the detector plane, greatly improving resolution.

1.1B, the total flight time, t, is the sum of the times spent in the first stage of the source, t_1, the second-stage, t_2, the field-free region, t_D, and the region between the field-free region and the detector surface known as the post-acceleration region, t_{pa}, i.e.,

$$t = t_1 + t_2 + t_D + t_{pa}. \tag{3}$$

The flight time through each region can be calculated from basic equations from mechanical and electrical physics. The time in the first-stage (or source) is given by

$$t_1 = \frac{v_f - v_0}{a}, \tag{4}$$

where v_f is the final velocity of the ion, v_0 is the initial velocity, and a is the acceleration of the ion. The acceleration can be expressed as

$$a = \frac{e \cdot E_1}{m}. \tag{5}$$

The final velocity and initial velocity can be expressed in energy, U_1, and U_0, respectively, i.e.,

$$v_f = \left(\frac{2U_1}{m}\right)^{1/2}, \quad v_0 = \left(\frac{2U_0}{m}\right)^{1/2}, \tag{6}$$

and U_1 can be written as

$$U_1 = U_0 + e \cdot s \cdot E_1, \tag{7}$$

where s is the ion's position at the time the extraction pulse is applied. Substituting equations (5), (6), and (7) into equation (4) gives the flight time through the first stage as follows:

$$t_1 = \frac{(2m)^{1/2}}{e \cdot E_1}\left[\left(U_0 + e \cdot s \cdot E_1\right)^{1/2} \pm U_0^{1/2}\right]. \tag{8}$$

In the first term containing U_0, the ion's energy as it exits the first region is independent of its initial direction. In the second term, the '+' and '−' sign represent ions that have an initial velocity directed away from and toward the detector, respectively.

The final velocity in the first region becomes the initial velocity of the ion in the second region. If d_2 is the distance the ion travels through the second stage, then the final kinetic energy that the ion receives as it exits the source is

$$U_2 = U_f = U_1 + e \cdot d_2 \cdot E_2. \tag{9}$$

Therefore, the flight time of the ion in the second stage is

$$t_2 = \frac{(2m)^{1/2}}{e \cdot E_2}\left[U_f^{1/2} - \left(U_0 + e \cdot s \cdot E_1\right)^{1/2}\right]. \tag{10}$$

The flight time in the field-free region, given in equation (2), can be restated as a function of the total kinetic energy, U_f, as follows:

$$t_D = \frac{(2m)^{1/2}}{2 \cdot U_f^{1/2}} D. \tag{11}$$

Finally, most time-of-flight instruments have a detector at the end of the field-free region that is negatively biased. Positive ions are post-accelerated through a short distance, d_{pa}, between the field-free region and the detector with a field strength E_{pa}, i.e.,

$$t_{pa} = \frac{(2m)^{1/2}}{e \cdot E_{pa}}\left[\left(U_f + e \cdot d_{pa} \cdot E_{pa}\right)^{1/2} - U_f^{1/2}\right]. \tag{12}$$

Equations (8), (10), (11), and (12) are substituted into equation (3) to give the total flight time. Space focusing is achieved when $dt/ds = 0$. Wiley and McLaren[14] showed that for given values of s_0, d, and D, a unique and mass independent value of E_2/E_1 exits if $U_0 = 0$. They also showed that the optimum time lag, τ, is proportional to $m^{1/2}$. The optimum τ is found when dt/ds is negative ($U_0 \neq 0$) but this violates the space focus condition; thus, energy

focusing requires some sacrifice in space resolution.

Time-lag focusing has been referred to in the literature since 1955 with various names, including pulsed extraction or pulsed ion extraction or delayed extraction or more recently, space/velocity correlation focusing. However, all of them are, in reality, time-lag focusing. Many research groups successfully apply the technique to several different ionisation sources. For example, Cotter et al. used time-lag focusing for spatial and energy focusing to study such compounds as tetraalkylammonium halides,[28] cyclosporin A,[29] peptides, glycosides,[30] and chlorophyll-a[31] by laser desorption; peptides by liquid secondary ion mass spectrometry;[32,33] and proteins by MALDI.[34] O'Malley and coworkers reported that time-lag focusing can be used to study metastable ion decomposition rates of ions formed by multiphoton ionisation.[35,36] Cotter, et al., also showed the use of time-lag focusing to study metastable ion decomposition, including applications to peptide sequencing.[30,32]

1.5 Time-Lag Focusing and MALDI

The application of time-lag focusing to MALDI by Cotter was done with the sample probe orthogonal to the flight axis. However, to minimize the spatial distribution, the probe should be placed in the more conventional (for MALDI) parallel configuration, i.e., with the probe inserted through the repeller. If there is no spatial distribution to consider, then energy focusing can be optimized without compromise, although the mass dependence of time-lag focusing remains.

In equation (8) the initial energy was considered for ions travelling toward and away from the detector. Ions desorbed from a surface travel forward toward the detector. Thus, the second initial energy term, U_0, is negative. For ions desorbed into a field-free region, a relationship exists between an ion's position and its energy (velocity) when the extraction pulse is applied.[37] Ions closer to the repeller have lower initial velocity than ions further from the repeller. Application of the extraction pulse imparts more energy to the initially less energetic ions, allowing them to catch up to the initially more energetic ions at the detector plane (see Figure 1.3). If d_1 is the entire width of the first-stage of a two-stage source, then the ion's position, s, when the extraction pulse is applied is

$$s = d_1 - v_0\tau. \tag{13}$$

Expressing the ion's position as a function of initial velocity and time lag makes it more convenient to express initial energy as a function of velocity. Studies of the initial velocity of MALDI formed ions have shown that all protein ions have approximately the same initial velocity, despite mass.[16,38] Therefore, initial kinetic energy of the protein ions increases approximately linearly with mass. Consequently, for protein ions, a linear dependence of extraction pulse energy on mass should exist.

To find the optimum pulse voltage for a given mass the total expression for flight time should be considered. Rewriting equations (8), (10), (11), and (12) and substituting them into equation (3) gives the overall expression for flight time as follows:

$$\begin{aligned} t = {} & \frac{(2m)^{1/2}}{e\cdot E_1}\left[\left(\frac{1}{2}mv_0^2 + e\cdot(d_1 - v_0\tau)\cdot E_1\right)^{1/2} - \left(\frac{1}{2}mv_0^2\right)^{1/2}\right] \\ & + \frac{(2m)^{1/2}}{e\cdot E_2}\left[\left(\frac{1}{2}mv_0^2 + e\cdot(d_1 - v_0\tau)\cdot E_1 + e\cdot d_2\cdot E_2\right)^{1/2} - \left(\frac{1}{2}mv_0^2 + e\cdot(d_1 - v_0\tau)\cdot E_1\right)^{1/2}\right] \\ & + \frac{(2m)^{1/2}\cdot D}{2\cdot\left(\frac{1}{2}mv_0^2 + e\cdot(d_1 - v_0\tau)\cdot E_1 + e\cdot d_2\cdot E_2\right)^{1/2}} \\ & + \frac{(2m)^{1/2}}{e\cdot E_{pa}}\left[\left(\frac{1}{2}mv_0^2 + e\cdot(d_1 - v_0\tau)\cdot E_1 + e\cdot d_2\cdot E_2 + e\cdot d_{pa}\cdot E_{pa}\right)^{1/2} - \left(\frac{1}{2}mv_0^2 + e\cdot(d_1 - v_0\tau)\cdot E_1 + e\cdot d_2\cdot E_2\right)^{1/2}\right]. \end{aligned} \tag{14}$$

Optimum velocity (energy) focusing is achieved as dt/dv approaches zero. Solving this formidable equation for the optimum extraction potential, E_1, or lag time, τ, is best accomplished iteratively for reasonable values of d_1, d_2, d_{pa}, E_2, E_{pa}, and D. The initial velocity of the ion has a range of values as given by Beavis and Chait.[16] For chosen values of E_1 and τ, equation (14) must be solved for t at each value of v_0. The value of E_1 or τ can be varied systematically, to minimize Δt.

Figure 1.4 shows the calculated difference in flight time (using equation (14)) for insulin ions (5734.6 Da) that have an initial velocity between 300 and 900 m s^{-1}. For each given delay, there is an optimum extraction pulse potential that minimizes the difference in flight time. A minimum difference in the flight time of ions of the same mass means the

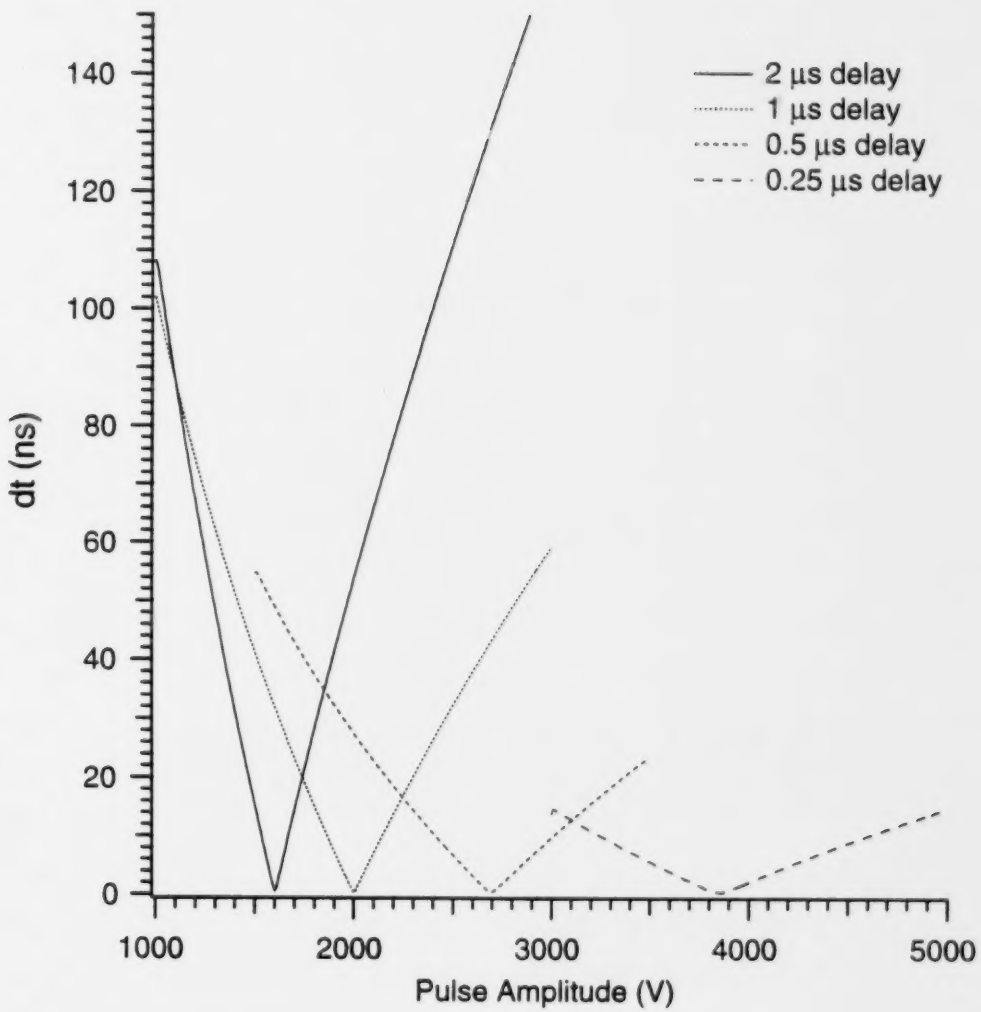

Figure 1.4 A simulated demonstration of time-lag focusing. Using equation (14), the difference in flight time of insulin ions desorbed from a surface was calculated assuming initial velocities ranging from 300 to 900 m s^{-1}. The smallest time difference (predicted < 1ns) represents the highest resolution. The effect of time lag and extraction voltage is shown. See text for details.

resolution is maximized. Figure 1.4 shows that a shorter time lag requires a higher extraction potential to bring the ions into focus.

Besides the improved resolution, several other reasons make time-lag focusing combined with MALDI attractive. Decoupling ion desorption from ion extraction reduces the number of collisions that would otherwise occur in a continuous extraction source. Excessive collisions can cause broadening of the peak. Collisions can ionise neutral molecules above the surface of the MALDI probe leading to an unanticipated spatial distribution.[39] Additionally, the number of collisions increases with laser power and signal intensity. This means that ion flight time is laser power dependent. At higher laser power ion flight times shift longer or ions receive less kinetic energy than anticipated. Ens, et al.,[39] showed that the kinetic energy deficit increases with mass. Time-lag focusing should largely eliminate this problem; post-source energy compensation methods cannot.

Ion mirrors are normally used with time-of-flight instruments to compensate for the initial kinetic energy distribution. However, improved resolution is limited to ~10 kDa. The metastable decomposition of MALDI formed ions reduces the sensitivity of the pseudomolecular ion. Loss of small neutral molecules, such as water, carbon dioxide, ammonia, etc., from the pseudomolecular parent ion leads to overlap of the parent ion with the fragment ion. In a linear instrument, metastable ions formed in the field-free region have the same velocity as the parent ion. If post-acceleration is low, then the fragment ions are indistinguishable from the parent ions; sensitivity and resolution are maintained. Time-lag focusing maintains good resolution at least up to ~30 kDa for proteins[40] and up to ~50 kDa for polymers.[41]

The analysis of metastable ions with short decay times or prompt fragmentation (collision induced) is possible with time-lag focusing but not in a continuous extraction instrument. Brown and Lennon have shown that fast metastable fragmentation analysis can be applied to peptide sequencing.[42] Unlike ion-mirror instruments, mass calibration of fragment ions is the same as for parent ions. A disadvantage of this technique is the requirement for very pure samples. In ion-mirror instruments, a mass gate can be used to select the parent ion of interest before metastable decay in the flight tube. Metastable decay

takes place over a longer time; the number of fragment ions is higher in ion-mirror instruments, possibly providing more comprehensive information.

As discussed above, time-lag focusing provides many benefits to MALDI analysis. Demonstrated in this thesis is improved resolution, mass accuracy, and improved tolerance of ion flight time to signal intensity (laser power). Also, the instrument developed was applied to several applications.

1.6 Literature Cited

(1) Tanaka, K.; Ido, Y.; Akita, S. In *Proceedings of the Second Japan-China Joint Symposium on Mass Spectrometry*; Matsuda, H.; Liang, X.-T., Eds.; Bando Press: Osaka, JP, 1987; pp 185-188.

(2) Tanaka, K.; Waki, H.; Ido, Y.; Akita, S.; Yoshida, Y.; Yoshida, T. *Rapid Commun. Mass Spectrom.* **1988**, *2*, 151-153.

(3) Karas, M.; Bachmann, D.; Bahr, U.; Hillenkamp, F. *Int. J. Mass Spectrom. Ion Processes* **1987**, *78*, 53-68.

(4) Karas, M.; Hillenkamp, F. *Anal. Chem.* **1988**, *60*, 2299-2301.

(5) Spengler, B.; Kirsch, D.; Kaufmann, R. *J. Phys. Chem.* **1992**, *96*, 9678-9684.

(6) Strobel, F. H.; Solouki, T.; White, M. A.; Russell, D. H. *J. Am. Soc. Mass Spectrom.* **1991**, *2*, 91-94.

(7) Hettich, R. L.; Buchanan, M. V. *J. Am. Soc. Mass Spectrom.* **1991**, *2*, 22-28.

(8) Castoro, J. A.; Wilkins, C. L. *Anal. Chem.*, **1993**, *65*, 2621-2627.

(9) Chambers, D. M.; Goeringer, D. E.; McLuckey, S. A.; Glish, G. L. *Anal. Chem.* **1993**, *65*, 14-20.

(10) Doroshenko, V. M.; Cotter, R. J. *Anal. Chem.* **1996**, *68*, 463-472.

(11) Qin, J.; Steenvoorden, R. J. J. M.; Chait, B. T. *Anal. Chem.* **1996**, *68*, 1784-1791.

(12) Schriemer, D. C.; Li, L. *Anal. Chem.* **1996**, *68*, 2721-2725.

(13) Nelson, R. W.; Dogruel, D.; Williams, P. *Rapid Commun. Mass Spectrom.* **1995**, *9*, 625.

(14) Wiley, W. C.; McLaren, I. H. *Rev. Sci. Instrum.* **1955**, *26*, 1150-1157.

(15) Cotter, R. J. In *Time-of-Flight Mass Spectrometry*; Cotter, R. J., Ed.; American Chemical Society: Washington, DC, 1994; Vol. 549; pp 16-48.

(16) Beavis, R. C.; Chait, B. T. *Chem. Phys. Lett.* **1991**, *181*, 479-484.

(17) Mamyrin, B. A.; Karataev, V. I.; Schmikk, D. V.; Zagulin, V. A. *Zh. Eksp. Teor. Fiz.* **1973**, *64*, 82-89.

(18) Tang, X.; Beavis, R.; Ens, W.; Lafortune, F.; Schueler, B.; Standing, K. G. *Int. J. Mass Spectrom. Ion Processes* **1988**, *85*, 43-67.

(19) Marable, N. L.; Sanzone, G. *Int. J. Mass Spectrom. Ion Phys.* **1974**, *13*, 185-194.

(20) Muga, M. L. *Anal. Instrum.* **1987**, *16*, 31-50.

(21) Yefchak, G. E.; Enke, C. G.; Holland, J. F. *Int. J. Mass Spectrom. Ion Processes* **1989**, *87*, 313-330.

(22) Kinsel, G. R.; Johnston, M. V. *Int. J. Mass Spectrom. Ion Processes* **1989**, *91*, 157-176.

(23) Cornish, T. J.; Cotter, R. J. *Rapid Commun. Mass Spectrom.* **1993**, *7*, 1037-1040.

(24) Browder, J. A.; Miller, R. L.; Thomas, W. A.; Sanzone, G. *Int. J. Mass Spectrom. Ion Phys.* **1981**, *37*, 99-108.

(25) Kinsel, G. R.; Mowry, C.D.; McKeown, P. J.; Johnston, M. V. *Int. J. Mass Spectrom. Ion Processes* **1991**, *104*, 35-44.

(26) Kinsel, G. R.; Grundwuermer, J. M.; Grotemeyer, J. *J. Am. Soc. Mass Spectrom.* **1993**, *4*, 2-10.

(27) Grundwürmer, J. M.; Bönisch, M.; Kinsel, G. R.; Grotemeyer, J.; Schlag, E. W. *Int. J. Mass Spectrom. Ion Processes* **1994**, *131*, 139-148.

(28) Van Breemen, R. B.; Snow, M.; Cotter, R. J. *Int. J. Mass Spectrom. Ion Phys.* **1983**, *49*, 35-50.

(29) Cotter, R. J.; Tabet, J. *Int. J. Mass Spectrom. Ion Phys.* **1983**, *53*, 151-166.

(30) Tabet, J.-C.; Cotter, R. J. *Anal. Chem.* **1984**, *56*, 1662-1667.

(31) Tabet, J.-C.; Jablonski, M.; Cotter, R. J. *Int. J. Mass Spectrom. Ion Processes* **1985**, *65*, 105-117.

(32) Olthoff, J. K.; Honovich, J. P.; Cotter, R. J. *Anal. Chem.* **1987**, *59*, 999-1002.

(33) Emary, W. B.; Lys, I.; Cotter, R. J.; Simpson, R.; Hoffman, A. *Anal. Chem.* **1990**, *62*, 1319-1324.

(34) Spengler, B.; Cotter, R. J. *Anal. Chem.* **1990**, *62*, 793-796.

(35) a) Martin, W. B.; O'Malley, R. M. *Int. J. Mass Spectrom. Ion Processes* **1984**, *59*, 277-294. b) Martin, W. B.; O'Malley, R. M. *Int. J. Mass Spectrom. Ion Processes* **1987**, *77*, 203-221.

(36) a) Zimmerman, J. A.; O'Malley, R. M.; Weinzierl, J. E. *Int. J. Mass Spectrom. Ion Processes* **1987**, *76*, 257-262. b) Zimmerman, J. A.; O'Malley, R. M. *Int. J. Mass Spectrom. Ion Processes* **1990**, *99*, 169-190.

(37) Colby, S. M.; Reilly, J. P. *Anal. Chem.* **1996**, *68*, 1419-1428.

(38) Verentchikov, A.; Ens, W.; Martens, J.; Standing, K. G. In *Proceedings of the 40th ASMS Conference on Mass Spectrometry and Allied Topics*; Washington, DC, 1992; pp 360-361.

(39) Zhou, J.; Ens, W.; Standing, K. G.; Verentchikov, A. *Rapid Commun. Mass Spectrom.* **1992**, *6*, 671-678.

(40) Vestal, M. L., Juhasz, P.; Martin, S. A. *Rapid Commun. Mass Spectrom.* **1995**, *9*, 1044-1050.

(41) Schriemer, D. C.; Whittal, R. M.; Li, L. In *Proceedings of the 44th ASMS Conference on Mass Spectrometry and Allied Topics*; Portland, OR, May 12-16, 1996; WPG 129.

(42) Brown, R. S.; Lennon, J. J.; *Anal. Chem.* **1995**, *67*, 3990-3999.

Chapter 2

High Resolution Matrix-Assisted Laser Desorption/Ionisation in a Linear Time-of-Flight Mass Spectrometer[a]

2.1 Introduction

Matrix-assisted laser desorption/ionisation (MALDI) has become an increasingly important technique for the detection of biopolymers.[1,2] Currently, the ions generated by the MALDI process are commonly analysed with the use of a time-of-flight mass spectrometer. A time-of-flight instrument is inexpensive to construct and easy to operate. It has no theoretical mass limit. The sensitivity can be very high due to its efficient ion transmission and ion extraction duty cycle with a pulsed-ionisation source.

A major drawback of the time-of-flight instrument is its low resolution for the detection of ions in MALDI. Low mass resolution can be attributed to several factors including the initial spatial, temporal, and kinetic energy distribution of the ions. Of these factors, the initial kinetic energy distribution is the major factor limiting resolution in a linear time-of-flight instrument. Metastable decay in the field-free drift region may also play a significant role.[3] Several approaches have been developed to reduce the contribution of one or more of these factors to enhance the mass resolution of MALDI in a time-of-flight spectrometer. For example, a time-of-flight equipped with an ion mirror (reflectron), for compensation of the kinetic energy distribution provides significantly improved resolution.[3] Resolution as high as 6000 fwhm (defined as $t/(2\Delta t)$, where t is the flight time of the ion and

---

[a] A form of this chapter has been published as an accelerated article: R.M. Whittal, L. Li "*High-Resolution Matrix-Assisted Laser Desorption/Ionization in a Linear Time-of-Flight Mass Spectrometer*" *Anal. Chem.* **1995**, *67*, 1950-1954.

In addition, part of this chapter is submitted for publication. Y. Dai, R. M. Whittal, L. Li, S. R. Weinberger "*Accurate Mass Measurement of Oligoneucleotides Using a Time-Lag Focusing MALDI Time-of-Flight Mass Spectrometer*"; *Rapid Commun. Mass Spectrom.* submitted. Ms. Y. Dai collected the oligonucleotide sample data.

Δt is the peak width at half the peak height) is reported for peptides with masses up to 3 kDa in a commercial system.[4] In contrast, a simple linear time-of-flight normally provides a mass resolution no greater than 1000 fwhm.

Mass resolution between 3000–6000 fwhm obtained on a linear time-of-flight is shown herein. To attain this resolution, a time-lag focusing method is used for ion extraction. With this resolution, isotopically resolved mass spectra are observed for peptides with masses up to 3 kDa.

In conventional MALDI instruments, the ions generated by the laser beam near the surface of the sample probe are extracted by a DC potential. In time-lag focusing, ions are allowed to expand into a field-free region between the repeller and first extractor plate during a short time delay (200 ns–2 μs) inserted between the laser desorption and ion extraction events. Following the delay, a voltage pulse is applied to the repeller. The initially less energetic ions closer to the repeller receive more energy (from the pulse) than the initially more energetic ions further from the repeller at the time the pulse is applied. Application of the appropriate pulse voltage provides the energy compensation necessary to detect all ions of the same mass-to-charge, despite their initial energy, simultaneously. The optimal pulse potential is mass dependent, higher pulse potentials are required for ions of higher mass.

Wiley and McLaren[5] first reported time-lag focusing to improve mass resolution in an electron impact ionisation time-of-flight instrument. Shortly after the report of the first MALDI experiment, Spengler and Cotter used time-lag focusing for MALDI in an orthogonal time-of-flight system.[6] Recently, Lennon and Brown[7] reported the use of pulsed ion acceleration in a conventional parallel ion-extraction design. Mass resolution up to 1600 fwhm is reported in their linear system. Reilly, et al.,[8] have developed a pulsed-spatial/velocity focusing instrument to achieve similar results. It is further noted, by Hillenkamp, et al.,[9] that the sensitivity of MALDI improves with pulsed-ion extraction. Herein, a study of time-lag focusing used to improve mass resolution in a linear MALDI time-of-flight is presented. It is shown that a simple linear system with time-lag focusing provides mass resolution similar to that obtained with an ion mirror. Because time-lag focusing is an in-source ion energy compensation method, observation of metastable decay

is reduced. Metastable decay reduces the resolution of ion mirror instruments especially for more fragile molecules such as deoxyribonucleic acids (DNA). Preliminary work on the analysis of oligonucleotides by time-lag focusing is presented.

2.2 Experimental

The MALDI time-of-flight was constructed at the University of Alberta. The ionisation region is housed in a 22 x 22 x 22-cm cubic stainless steel vacuum chamber pumped with a 15-cm diffusion pump (Varian). Additional pumping is provided by a 10-cm diffusion pump (Edwards) connected to the middle of the flight tube. The flight tube is made from 10-cm-diameter stainless steel tubing, providing a total flight path of ~1 m. The vacuum pressure of the instrument in the flight tube is 3-7 μPa. The ion optics design was facilitated with the SIMION ion trajectory simulation program. The ionisation and ion extraction regions consist of four stainless steel plates separated with 5-mm ruby balls that provide a plate separation of 4.5 mm. The ion repeller plate has a 4.2-mm hole in the centre for insertion of the sample probe. The two extraction plates are gridless with a 12-mm diameter hole. The ground plate has a 1-cm-diameter centre hole covered with a stainless steel grid. After the ground plate is a pair of ion deflectors. For all the experimental results shown here, the ion deflectors were grounded. The detector is a 1.8-cm-diameter Chevron multi-channel plate assembly (R. M. Jordan Co.) operated with the front plate set to -2 kV.

A nitrogen laser (Photochemical Research Associates LN1000) was used to generate the MALDI ions. The laser temporal width was not measured, but it is reported to be 800 ps by the laser manufacturer. The laser power used for each sample was adjusted to just above the threshold for ion production.

For continuous ion extraction, the voltage applied to the ion source is typically 12 kV, 8 kV, and 4 kV for the repeller and two extraction plates, respectively. For pulsed ion extraction, a custom-built power supply is used to power the repeller plate. This power supply can deliver a 5 kV pulsed potential with a rise and fall time of 30 ns and adjustable pulse width from 300 ns to 3 ms. The pulse potential used for ion extraction is typically 1 - 3 kV. This potential can be varied to achieve optimal ion focusing for the analyte of interest. Up to 20 kV can be applied as a DC offset to the pulse. The offset was adjusted to 12 kV DC

for all the peptide and protein spectra. An independent DC power supply was used to match the potential applied to the first extraction plate to that of the repeller voltage. The potential applied to the second extraction plate was 6 kV. Note that, this is essentially still a two-stage source, since the field strength in the second and third regions is identical. The timing sequence in the time-lag focusing experiment is as follows. A portion of the laser beam from the nitrogen laser strikes a photodiode to generate a trigger pulse. This pulse is used to trigger a pulse generator that in turn triggers the high voltage pulse power supply. An induction signal from the high voltage pulse is used to trigger the oscilloscope. The minimum time delay in the trigger circuit is 230 ns, which is set by the propagation delay time of triggering and pulsing circuitry. The time delay between the ionisation and ion extraction events was optimized at 280 ns and used for all of the peptide and protein spectra.

The ion signal is first amplified with a 500 MHz (3 dB), 20 dB amplifier (CLC 100, Comlinear Corp.). A spectrum is captured using either a LeCroy 9354M or 9350M digital oscilloscope. The major difference is the sampling rate. The 9354M oscilloscope provides a sampling rate of up to 2×10^9 samples/s or a time resolution of 0.5 ns/point whereas the 9350M oscilloscope has a time resolution of 1 ns/point. In most time-lag focusing experiments, the 9350M oscilloscope is adequate. However, single shot spectra may have peak widths as narrow as 2.0 ns; thus, undersampling is observed sometimes. All mass spectra, with exceptions noted, are the result of signal averaging of 100 laser shots. Signal averaging was done on the oscilloscope without selection. The averaged mass spectrum was then downloaded to a computer for processing.

2.2.1 Peptides and Proteins. Bradykinin, insulin, cytochrome *c*, and myoglobin were purchased from Sigma. The synthetic peptides were gifts from the Centre of Excellence in Protein Engineering at the University of Alberta. The matrices α-cyano-4-hydroxycinnamic acid and sinapinic acid were purchased from Aldrich. All solvents were purchased from BDH Laboratories Inc. Trifluoroacetic acid was purchased from Caledon Laboratories. Water used throughout the experiment was from a NANOpure water system (Barnstead/Thermolyne).

Standard preparation techniques were used to prepare samples.[10] A saturated solution

of a matrix was prepared in 30% methanol/0.1% trifluoroacetic acid (v/v) with the aid of vortex mixing. The matrix solution was then centrifuged to eliminate suspended solids. Peptide and protein samples were prepared at a concentration of 1-5 μM in 0.1% trifluoroacetic acid. A 1.0 μL drop of matrix and 1.0 μL drop of a sample were mixed on the probe tip and allowed to dry. Alternatively, the method of Vorm et. al.[11] was used. Here, matrix solutions were prepared in acetone at a concentration of 0.12 M. A 0.5 μL drop of matrix solution was applied to the probe tip. The droplet spreads and dries very quickly, leaving a thin layer of matrix crystals. Peptide samples were prepared in 0.1% trifluoroacetic acid at a concentration of 1.0 μM. A 1.0 μL drop of peptide solution was placed on top of the matrix layer and allowed to dry. The sample was then washed by placing 10 μL of room temperature water on the probe tip. After 20 s the water was absorbed by placing an absorbent tissue (Kimwipe) at the edge of the probe tip.

2.2.2 Oligonucleotides. The instrument was operated at 20 kV DC, a 1-μs time-lag was used between laser desorption and ion extraction. All extraction plates were powered with one power supply using a voltage divider. A grid was placed on the repeller side of the first extraction plate. The pulsed-extraction potential was varied according to the mass analysed. Each spectrum collected was the result of signal averaging of 50 to 60 laser shots.

Sample Preparation. The matrix 3-hydroxypicolinic acid was saturated in 33% acetonitrile/ water (v/v) with the aid of vortex mixing, centrifuged and the supernatant solution was transferred to another vial containing regenerated H^+ activated ion-exchange beads. Preparation of the ion-exchange beads was as follows. Dowex 50W-X8, 20-50 mesh beads were regenerated in a glass column by rinsing with 50 mL ultra-pure water, 50 mL 3M HCl, followed by rinsing with ultra-pure water until neutral pH was reached.[12] A few beads were added to the 3-hydroxypicolinic acid solution. To prepare the ammonium form of the ion-exchange beads, the regenerated H^+ form beads were placed in a column and washed with 50 mL of 3 M NH_4Cl and then rinsed until neutral pH was achieved. DNA was prepared by dissolution in pure water with the addition of NH_4^+ activated ion exchange beads.

The crushed crystal method, as described by Xiang and Beavis, was used to prepare the sample on the probe tip.[13] In brief, 1 μL of 3-hydroxypicolinic acid solution was loaded

on the probe tip and allowed to dry, the crystals were crushed, and then 0.7 to 1 μL of the second layer solution was applied on the top of the first layer. To prepare the second layer solution, 1 μL of ion-exchanged DNA solution, 0.75 μL of 0.3M diammonium citrate and 3.25 μL ion exchanged matrix solution were mixed. As the second layer was drying, the solution was stirred on the probe tip using a micro pipette tip until small crystals formed.[14]

The 17-mer (5'-GTAAAACGACGGCCAGT-3') was purchased from Sigma and the 23-mer (5'-CCCAGTCACGACGTTGTAAAACG-3') and the 35-mer (5'-CCCAGTCACGACGTTGTAAAACGTTACGCCCTCAT-3') were purchased from Integrated DNA Technologies, Inc. 3-Hydroxypicolinic acid was purchased from Aldrich.

2.3 Results and Discussion

Figure 2.1A shows a typical MALDI mass spectrum for 1 pmol of a synthetic peptide (exact mass of 2224.317 Da) acquired with the application of a DC potential. Figure 2.1B is the mass spectrum of the same peptide, obtained under the same experimental conditions except for the application of time-lag focusing. The molecular ion region of each spectrum is shown in the insert. The observed mass resolution for Figure 2.1A is ~600 fwhm. Figure 2.1B shows that the isotope peaks of this compound are well resolved with time-lag focusing MALDI. The mass resolution is 4700 fwhm. Using a two-point external mass calibration, the mass of the monoisotopic peak is 2224.790 Da, representing a mass measurement accuracy of +0.02%. With the use of a two-point internal calibration, the molecular ion mass is 2224.302 Da. This shows a mass accuracy of -7 ppm. The average mass accuracy value for three repeat internally calibrated spectra is -53 ppm. The internal calibrant peaks are the peaks at m/z 1569 Da and m/z 1959 Da corresponding to the synthetic peptides Ac-KLEALEAKLEALEA-Am and Ac-EAEKAAKEAEKGAKEAEK-Am, respectively.

Figures 2.2A through F show the molecular ion region of several peptides with molecular weights between 1-3 kDa. The observed mass resolution of each spectrum is listed in the figures and exceeds 3000 fwhm usually. The temporal peak width is generally between 3.0-4.5 ns fwhm. The theoretical minimum peak width is the combination of the detector response, oscilloscope and amplifier bandwidths and jitter in the trigger electronics.[15] A signal from a dual microchannel plate detector has a minimum pulse width

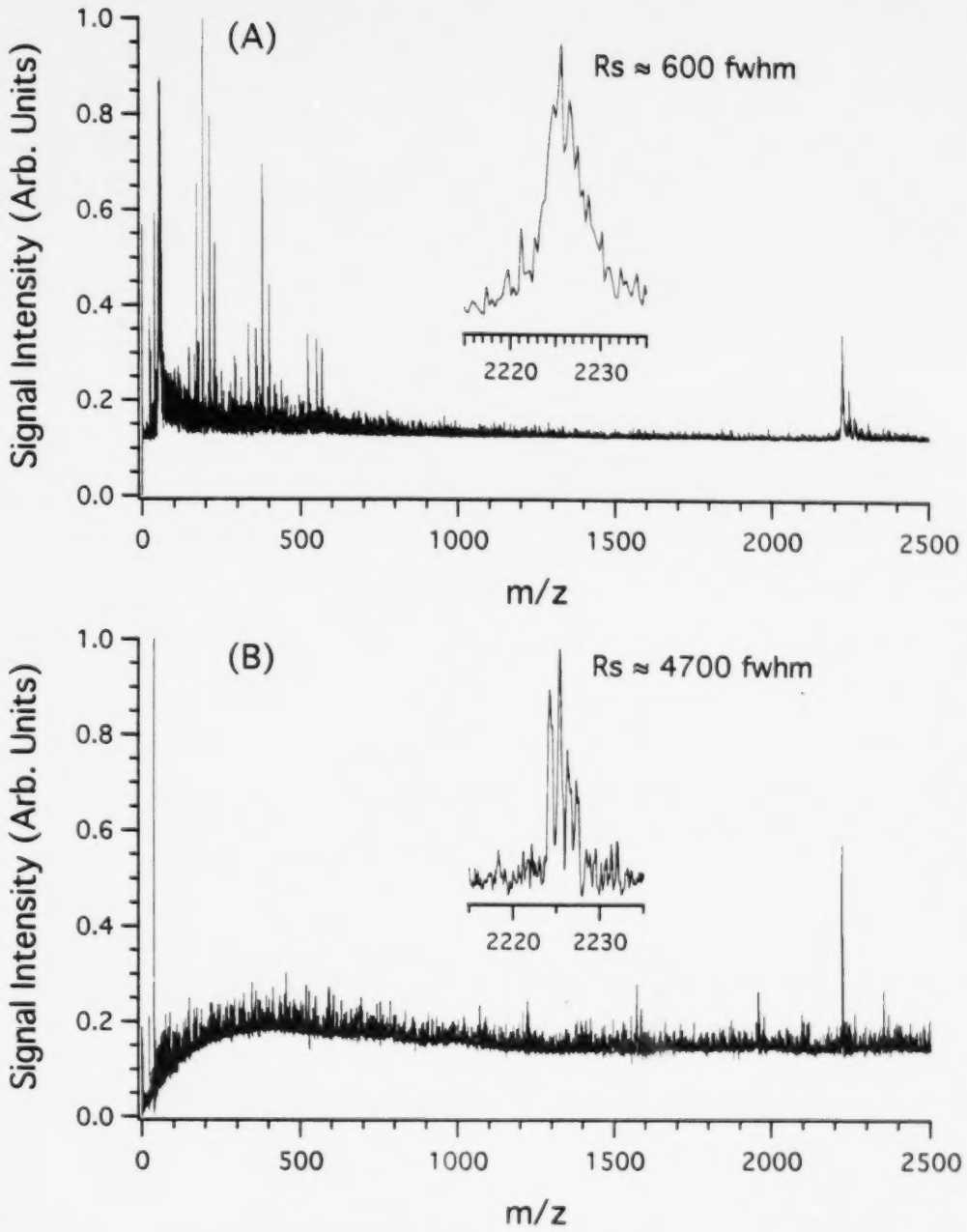

Figure 2.1 MALDI mass spectra for a total loading of 1 pmol of a synthetic peptide, Ac-ELEKLLKELEKLLKEAEK-Am (monoisotopic, $(M + H)^+ = 2224.317$ Da), obtained by using (A) DC ion extraction and (B) time-lag focusing ion extraction with a 2.00 kV pulse. Each spectrum is the result of signal averaging of 100 shots on the oscilloscope.

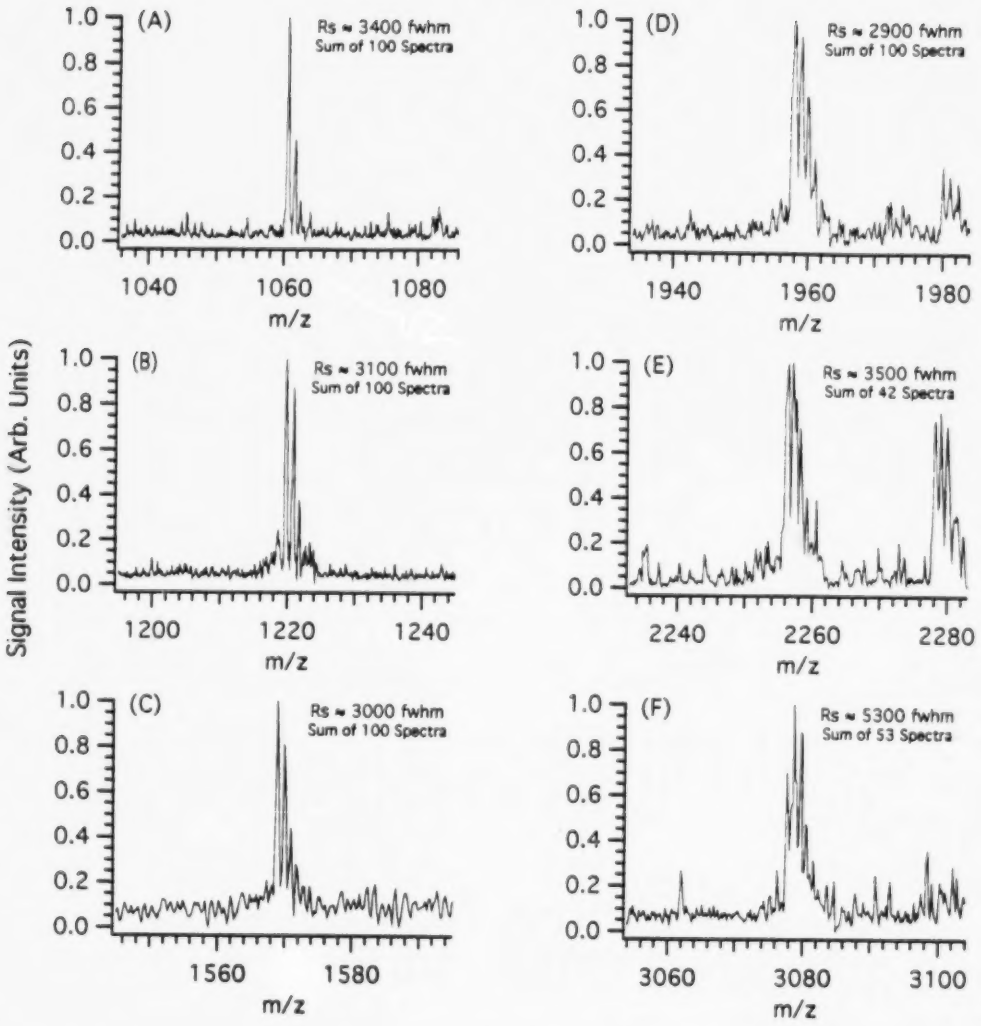

Figure 2.2 Time-lag focusing MALDI mass spectra for a total loading of 1 pmol of peptide for several peptides using α-cyano-4-hydroxycinnamic acid as matrix, the pulse potential used is given in brackets. (A) Bradykinin, $(M+H)^+$ = 1060.569 Da, (0.90 kV), (B) LYPVKLYPVK, $(M+H)^+$ = 1219.746 Da, (1.00 kV), (C) Ac- KLEALEAKLEALEA-Am, $(M+H)^+$ = 1568.290 Da, (1.30 kV), (D) Ac-EAEKAAKEAEKGAKEAEK-Am, $(M+H)^+$ = 1958.020 Da, (1.75 kV), (E) Ac-ELEKLLKECEKLLKELEK-Am, $(M+H)^+$ = 2256.289 Da, (2.05 kV), (F) Ac- KLEALEAKLEALEAKLEALEAKLEALEA-Am, $(M+H)^+$ = 3077.735 Da, (2.50 kV)

of ~2 ns. The LeCroy 9350M and 9354M oscilloscopes and Comlinear's CLC 100 preamplifier have a bandwidth of 500 MHz. A 500 MHz bandwidth should have an insignificant broadening effect upon a 2-ns peak. An electronic jitter in the acquisition starting point and trigger relays broadens peaks when summing spectra. The extent of jitter-induced peak broadening is not known for the system but one should expect it to be significant. As an example, Figure 2.3 shows the $(M+H)^+$=1958.02 Da and $(M+Na)^+$ molecular ions for a single shot mass spectrum of a synthetic peptide. The peak widths vary from 1.8 to 2.3 ns. Therefore, the calculated mass resolution for this single shot spectrum also varies from 5700 to 7300 fwhm. The inset in Figure 2.3 shows the theoretical isotopic distribution for this peptide. Note that although the mass accuracy is better than 33 ppm for all peaks, the isotopic distribution is not accurately represented in a single shot spectrum.

Further investigation of Figure 2.3 reveals that small peaks are observed on the high mass side of most of the peaks, preventing baseline separation. These small peaks cannot be due to an electronic jitter but must be the result of other experimentally induced parameters. Specifically, the major contribution to peak broadening for a summed spectrum may be the kinetic energy and spatial distribution of the ions at the time the potential pulse is applied. The initial kinetic energy distribution is converted into an energy and spatial distribution that can be compensated in the ion source.[5] Selection of the appropriate pulse voltage provides focusing such that the slower ions closer to the repeller collide with the detector at the same time as the faster ions further from the repeller. However, this compensation may not be perfect. If this is true, improvement in the ion optics design and the pulse shape, rise time etc. of the extraction pulse may be necessary. Further ion energy compensation for ions of the same mass-to-charge can only be done with the use of an instrument equipped with an ion mirror. While it is yet unknown what factor limits the observed peak width, isotopic resolution can be achieved, as shown in Figure 2.2, for small peptides with masses up to 3 kDa in a linear 1-m time-of-flight spectrometer using moderate acceleration voltages.

In achieving high mass resolution, the pulse applied to the repeller requires optimization to provide energy/spatial focusing at the detector plane. Although the pulse

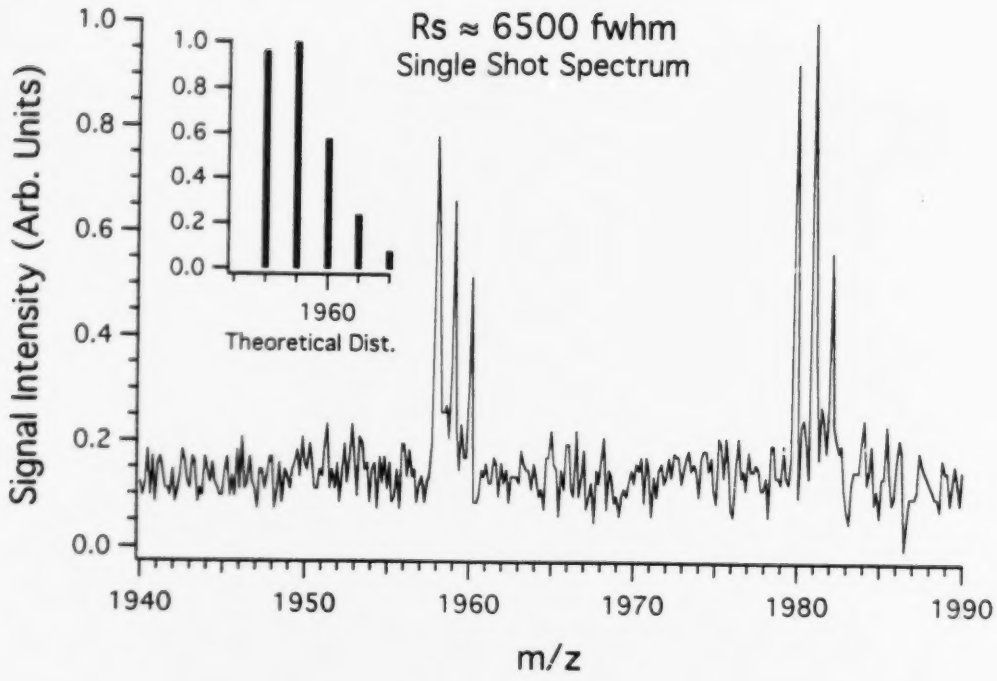

Figure 2.3 Single shot mass spectrum for a total loading of 1 pmol of synthetic peptide Ac-EAEKAAKEAEKGAKEAK-Am using α-cyano-4-hydroxycinnamic acid as matrix. The pulse potential used is 1.75 kV.

potential may not be optimal for each individual species, a given pulse potential is sufficient for a range of mass values. The width of the mass range where isotopically resolved peptide peaks can be achieved is dependent upon the delay time. Shorter delay times increase the range that is simultaneously focused. Figure 2.4 shows the mass spectrum of a mixture of bradykinin and two synthetic peptides. The molecular ion region of each peptide is shown in the insert. The mass resolution for each peptide is 1600, 2000, and 2600 fwhm for bradykinin, synthetic peptide 1 and synthetic peptide 2, respectively. As Figure 2.4 illustrates, the resolution obtained is adequate to resolve the isotopic peaks of each peptide.

Several larger peptides and proteins were examined using time-lag focusing. Figure 2.5 shows the mass spectra of bovine insulin, equine cytochrome *c* and equine apomyoglobin. Broader molecular ion peaks are observed. However, compared with DC ion extraction, time-lag focusing provides improved mass resolution. For example, the observed mass resolution is 1000 fwhm for insulin, 800 fwhm for cytochrome *c*, and 900 fwhm for apomyoglobin. The reduction of the apparent mass resolution for larger ions can likely be attributed to the increased kinetic energy distribution for ions of higher mass.[16,17] Increasing the pulse potential to compensate for the increased kinetic energy distribution does not appear to provide complete compensation. However, the mass measurement accuracy is good for proteins. Using a two point external calibration, the mass obtained for insulin, cytochrome *c*, and apomyoglobin is 5734.37 Da, 12362.6 Da and 16959.1 Da representing a mass measurement accuracy of -0.002%, +0.01% and +0.04%, respectively. The calibrants for bovine insulin were a synthetic peptide (ave. MW 3079) and equine cytochrome *c*. The calibrants for cytochrome *c* were bovine insulin chain B and bovine insulin. The calibrants for equine apomyoglobin were bovine insulin and equine cytochrome *c*. With internal calibration (spectra not shown), the mass obtained for cytochrome *c* and apomyoglobin is 12361.8 Da (+57 ppm) and 16954.7 Da (+130 ppm), respectively.

Analysis of DNA, an important class of biological compounds, benefits from the use of time-lag focusing in MALDI analysis. Metastable decay in the field-free drift region is important in the analysis of DNA by MALDI. Metastable decay is significant, often involving loss of small neutrals, such as water; loss, from the 5'-end, of a deoxynucleoside;

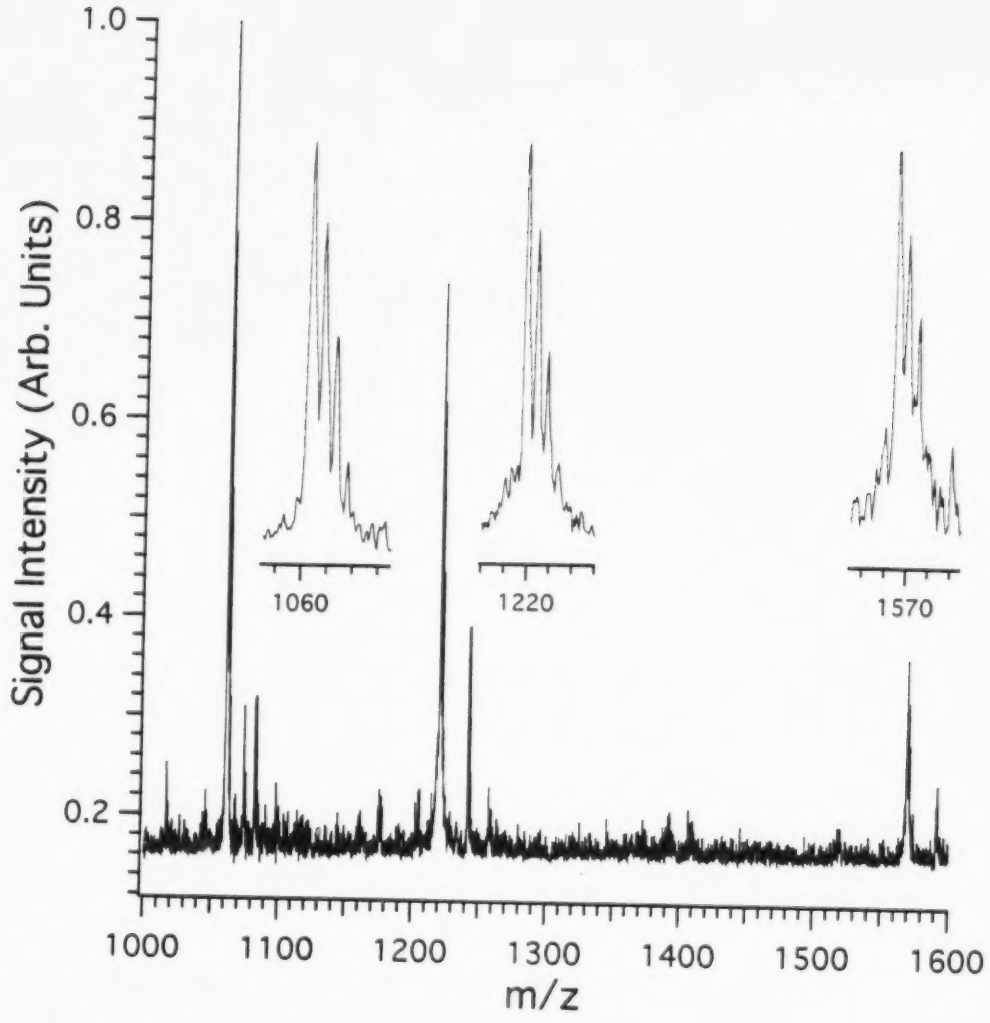

Figure 2.4 Time-lag focusing MALDI mass spectrum of a mixture of peptides (1 pmol of each peptide is loaded to the sample probe) using α-cyano-4-hydroxycinnamic acid as matrix. The pulse potential used is 1.20 kV. The peptide sequence of the two synthetic peptides is given in Figure 2.2.

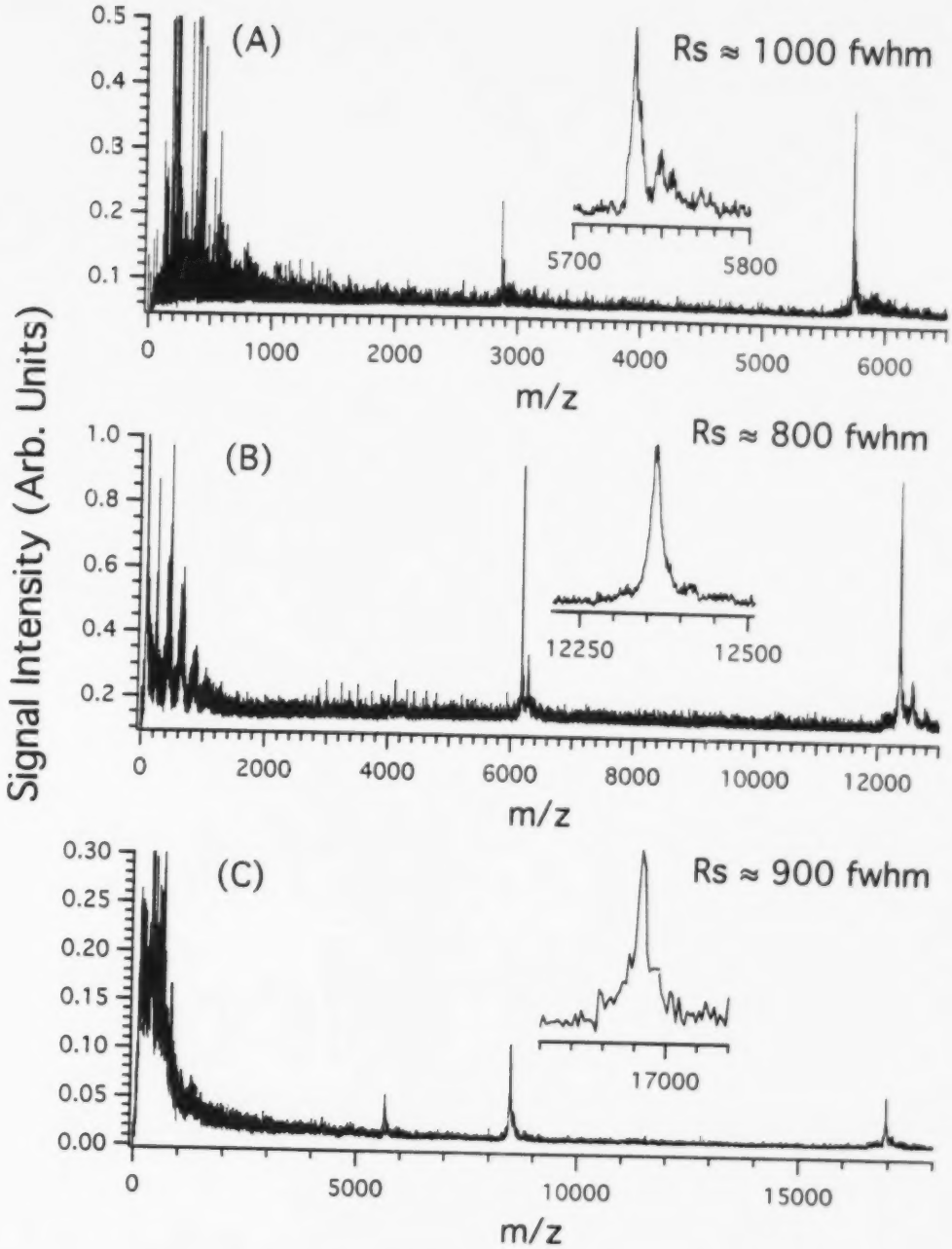

Figure 2.5 Time-lag focusing MALDI mass spectra for a total loading of 1 pmol of (A) bovine insulin $(M + H)^+ = 5734.37$ Da using α-cyano-4-hydroxycinnamic acid as matrix, pulse potential 2.75 kV (B) equine cytochrome *c* using sinapinic acid as matrix, pulse potential 3.50 kV (C) equine apomyoglobin using α-cyano-4-hydroxycinnamic acid as matrix, pulse potential 4.50 kV.

loss, from the 3'-end, of deoxynucleotide; and loss, from the backbone, of the bases adenine, guanine, or cytosine.[18] For instruments equipped with an ion mirror, ions spend about one-quarter of their total flight time in the field-free drift region before entering the mirror. From metastables, sensitivity is diminished and little, if any, gains in resolution are observed.[18] Perhaps what is more important, mass accuracy decreases in reflectron mode when the parent molecular ion cannot be distinguished from small mass loss.[18] In a linear time-of-flight, fragment ions formed due to metastable decay in the field-free drift region are not separated from their parent molecular ion; therefore, loss in resolution is minimal (if post acceleration is minimal).[3] Energy correction in the source combined with a linear time-of-flight offers an attractive alternative. The excellent sensitivity of the linear system is maintained; the observation of metastable decay is minimized. Preliminary study shows higher resolution, mass accuracy, and sensitivity with time-lag focusing than with the use of an ion mirror.

Figure 2.6 shows the MALDI spectrum of a DNA 35-mer using time-lag focusing. The resolution is (A) 1210 fwhm in positive ion and (B) 1300 fwhm in negative ion operation. The molecular weight of the 35-mer is 10636.01. The observed mass, using external standards, (A) 10636.40 $(M+H)^+$ and (B) 10634.04 $(M-H)^-$ represents a mass measurement accuracy of -58 ppm and -91 ppm, respectively. The external calibrants were a DNA 17-mer and 23-mer prepared with the same matrix, 3-hydroxypicolinic acid, as was used for the 35-mer. Accuracy using the external calibration depends upon the reproducibility of sample preparation as well as the electronic and mechanical stability of the instrument. The formation of densely packed uniform microcrystals improves sensitivity and mass accuracy.[19] The flight time of an ion is strongly dependent upon its flight distance and thus upon its starting position. Microcrystals provide a uniform thin layer that combined with good mechanical stability, ensure a reproducible starting position for ions inside the source.

Table 2.1 shows the accuracy and reproducibility of measurement of a DNA 35-mer using the microcrystal method in positive ion mode. The observed $(M+H)^+$ mass for the 35-mer was 10636.06±0.56 Da (for seven trials) giving a relative error of -90 ppm, a significant improvement over continuous extraction where mass errors are typically >1000

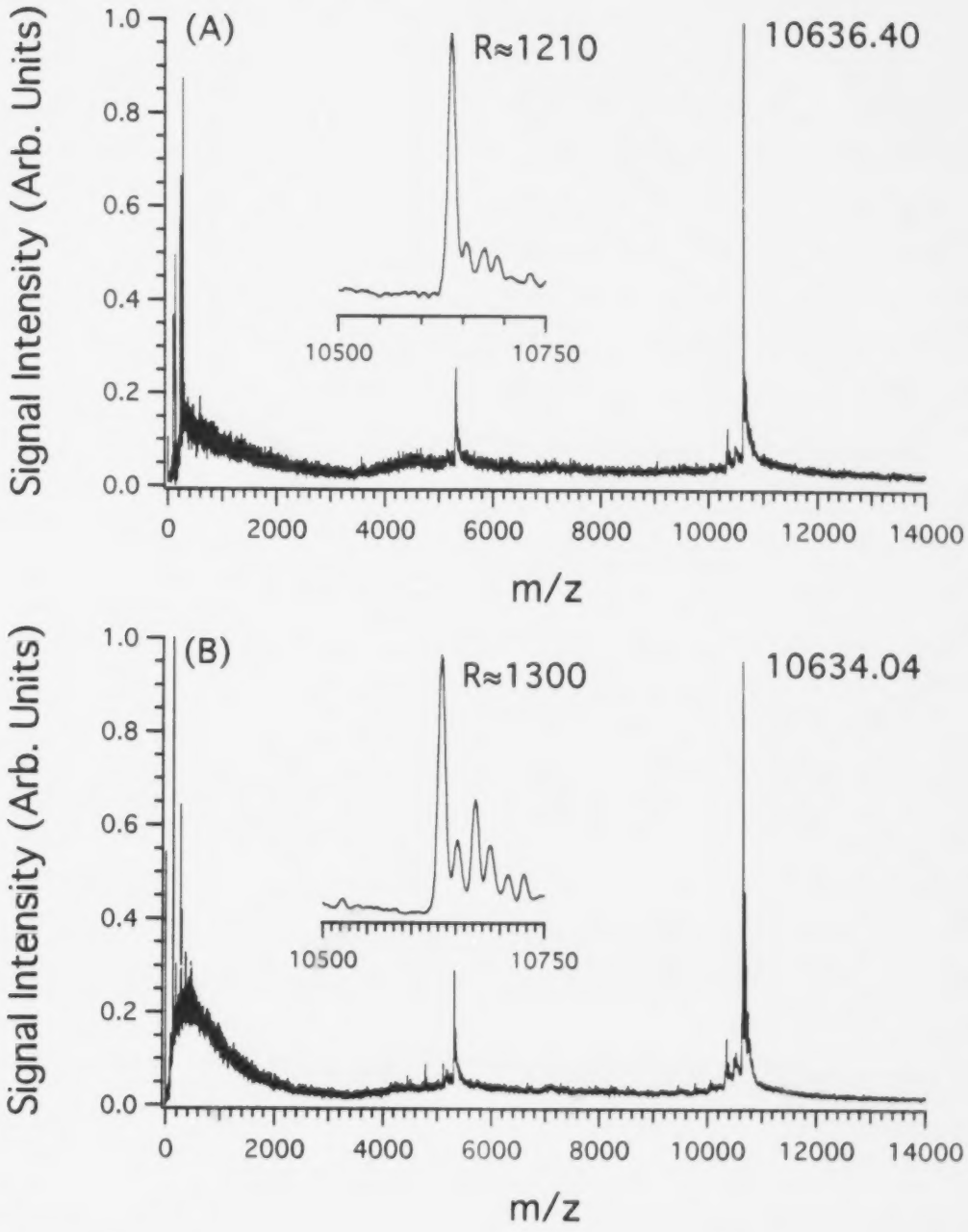

Figure 2.6 MALDI mass spectra of 7 pmol of a DNA 35-mer analysed in (A) positive-ion and (B) negative-ion modes using a 1-μs time-lag and (A) 2.95 kV, (B) −3.15 kV pulsed-extraction potential

ppm for an external measurement.

Table 2.1 Mass Accuracy and Reproducibility of a DNA 35-mer $(M+H)^+$ with a mass of 10637.02 Da

Trial #	Measured $(M + H)^+$ External standard
1	10635.26
2	10636.40
3	10636.59
4	10636.36
5	10636.38
6	10636.18
7	10635.24
Average ($\bar{x}$)	10636.06
Rel. error (ppm)	-90
$s/\bar{x}$ (ppm)	53

Note: $s/\bar{x}$ represents the relative standard deviation for 7 trials.

In summary, with a standard 1-m flight tube time-of-flight instrument, a linear system can be used to achieve unit mass resolution for peptides up to 3 kDa. High resolution and mass measurement accuracy are also obtained for larger peptides, DNA and proteins with masses up to ~17 kDa. This simple system should be useful for many applications.

2.4 Literature Cited

(1) Chait, B. T.; Kent, S. B. H. *Science* **1992**, *257*, 1885-1894.

(2) Hillenkamp, F.; Karas, M.; Beavis, R. C.; Chait, B. T. *Anal. Chem.* **1991**, *63*, 1193-1203.

(3) Cotter, R. J. In *Time-of-Flight Mass Spectrometry*; Cotter, R. J. Ed.; ACS Symposium Series 549; American Chemical Society: Washington DC, 1994; pp 16-48.

(4) Ingendoh, A.; Karas, M.; Hillenkamp, F.; Giessmann, U. *Int. J. Mass Spectrom. Ion Processes* **1994**, *131*, 345-354.

(5) Wiley, W. C.; McLaren, I. H. *Rev. Sci. Instr.* **1955**, *26*, 1150-1157.

(6) Spengler, B.; Cotter, R. J. *Anal. Chem.* **1990**, *62*, 793-796.

(7) Lennon, J. J.; Brown, R. S. In *Proceedings of the 42nd ASMS Conference on Mass Spectrometry and Allied Topics*; Chicago, IL, May 29–June 3, 1994; p 501.

(8) Colby, S. M.; King, T. B.; Reilly, J. P. *Rapid Commun. Mass Spectrom.* **1994**, *8*, 865-868.

(9) Wang, B. H.; Dreisewerd, K.; Bahr, U.; Karas, M.; Hillenkamp, F. *J. Am. Soc. Mass Spectrom.* **1993**, *4*, 393-398.

(10) Karas, M.; Bahr, U.; GieBmann, U. *Mass Spectrom. Rev.* **1991**, *10*, 335-357.

(11) Vorm, O.; Roepstorff, P.; Mann, M. *Anal. Chem.* **1994**, *66*, 3281-3287.

(12) Nordhoff, E.; Cramer, R.; Karas, M.; Hillenkamp, F.; Kirpekar, F.; Kristiansen, K.; Roepstorff, P. *Nucleic Acids Res.* **1993**, *21*, 3347-3357.

(13) Xiang, F.; Beavis, R. C. *Rapid Commun. Mass Spectrom.* **1994**, *8*, 199-204.

(14) Benner, W. H.; Horn, D.; Katz, J.; Jaklevic, J. *Rapid Commun. Mass Spectrom.* **1995**, *9*, 537-540.

(15) Guilhaus, M. *J. Am. Soc. Mass Spectrom.* **1994**, *5*, 588-595.

(16) Beavis, R. C.; Chait, B. T. *Chem. Phys. Lett.* **1991**, *181*, 479-484.

(17) Pan, Y.; Cotter, R. J. *Org. Mass Spectrom.* **1992**, *27*, 3-8.

(18) Nordhoff, E.; Kirpekar, F.; Karas. M.; Cramer, R.; Hahner, S.; Hillenkamp, F.; Kristiansen, K.; Roepstorff, P.; Lezius, A. *Nucleic Acids Res.* **1994**, *22*, 2460-2465.

(19) Dai, Y.; Whittal, R. M.; Li, L. *Anal. Chem.* **1996**, *68*, 2494-2500.

Chapter 3

Functional Wave Time-Lag Focusing Matrix-assisted Laser Desorption/Ionisation in a Linear Time-of-Flight Mass Spectrometer; Improved Mass Accuracy[a]

3.1 Introduction

Matrix-assisted laser desorption/ionisation (MALDI) has been applied to the analysis of many organic and biomolecules, since its introduction in 1988 by Tanaka et al.,[1] and Karas and Hillenkamp.[2] MALDI, a pulsed ion source, is most often coupled to time-of-flight mass spectrometers. In a linear time-of-flight mass spectrometer the observed resolution is low due mainly to the inherent energy spread of the desorption plume. Compensation of the inherent energy spread can be accomplished with an ion mirror (or reflectron)[3,4] or by the technique developed by Wiley and McLaren called time-lag focusing.[5]

Major differences in these two methods of kinetic energy compensation exist. The ion mirror is post-source while time-lag focusing is an in-source energy compensation method. Single-stage ion-mirror[4] energy compensation is mass independent; whereas, the time-lag focusing method is mass dependent.[5] The post-source-decay method requires a reflectron for the analysis of the fragment ions formed due to metastable decay in the field-free drift region.[6,7] Time-lag focusing can be used to analyse the fragment ions formed in the source, as prompt fragmentation ions or metastable ions with short decay times.

---

[a] A form of this chapter is in preparation for publication: R. M. Whittal, L. R. Russon, S. R. Weinberger, L. Li "Functional Wave Time-Lag Focusing Matrix-Assisted Laser Desorption/Ionization in a Linear Time-of-Flight Mass Spectrometer; Improved Mass Accuracy" Dr. S. R. Weinberger collected the continuous extraction data comparing the dependence of ion flight time with laser flux with and without capacitance added to the source.

For MALDI formed ions, prompt fragmentation and improved resolution were first demonstrated by Brown et al.[8,9,10] Resolution enhancement using time-lag focusing was also reported by Reilly et al. for proteins[11] and oligonucleotides;[12] and by Li et al. for peptides, proteins,[13] oligosaccharides,[14] modified organic polymers,[15,16] and oligonucleotides.[17] Coupling of time-lag focusing extraction to an ion mirror, as proposed by Cotter in 1989,[18] has been shown by Vestal et al.[19] for peptides and proteins, and by Juhasz and coworkers[20] for oligonucleotides.

Early studies of the initial velocity of MALDI formed ions show that all protein ions have the same initial velocity, independent of their mass.[21,22] Therefore, initial kinetic energy of the protein ions increases approximately linearly with mass. If imparted kinetic energy (from the power supply) is fixed then total kinetic energy increases with mass. In a time-lag focusing MALDI experiment where desorption of proteins is in parallel to the flight axis, there are obvious effects on the calibration curve. If one plots the second power of flight time versus mass (Figure 3.1) then higher mass ions have flight times that are less than expected.[23] If the instrument is calibrated using ions of higher mass, then ions of lower mass will have flight times that are less than predicted. Calibration using one low mass and one high mass ion would predict flight times less than that observed for all points between. This phenomenon, reported by Juhasz et al.[19] in the analysis of DNA by delayed extraction, limits the utility of MALDI for analysis of unknown compounds when accurate mass assignment is needed. Nevertheless, superior mass accuracy over continuous extraction MALDI is shown using time-lag focusing.[9,13-17,19,20]

In conventional continuous extraction MALDI, accurate mass calibration is more difficult and dependent upon signal intensity. Ens, et al.,[24] showed that there exists an energy deficit for MALDI ions formed in an electric field that increases with ion mass and signal intensity. The energy deficit is the difference in energy between the expected imparted energy and the observed ion energy, the observed ion energy being less. Thus, in continuous extraction MALDI, total kinetic energy decreases with ion mass, opposite to the effect observed in time-lag focusing MALDI.[20] The study by Ens and coworkers was completed to explain the observed difference in the width of an energy distribution for ions produced

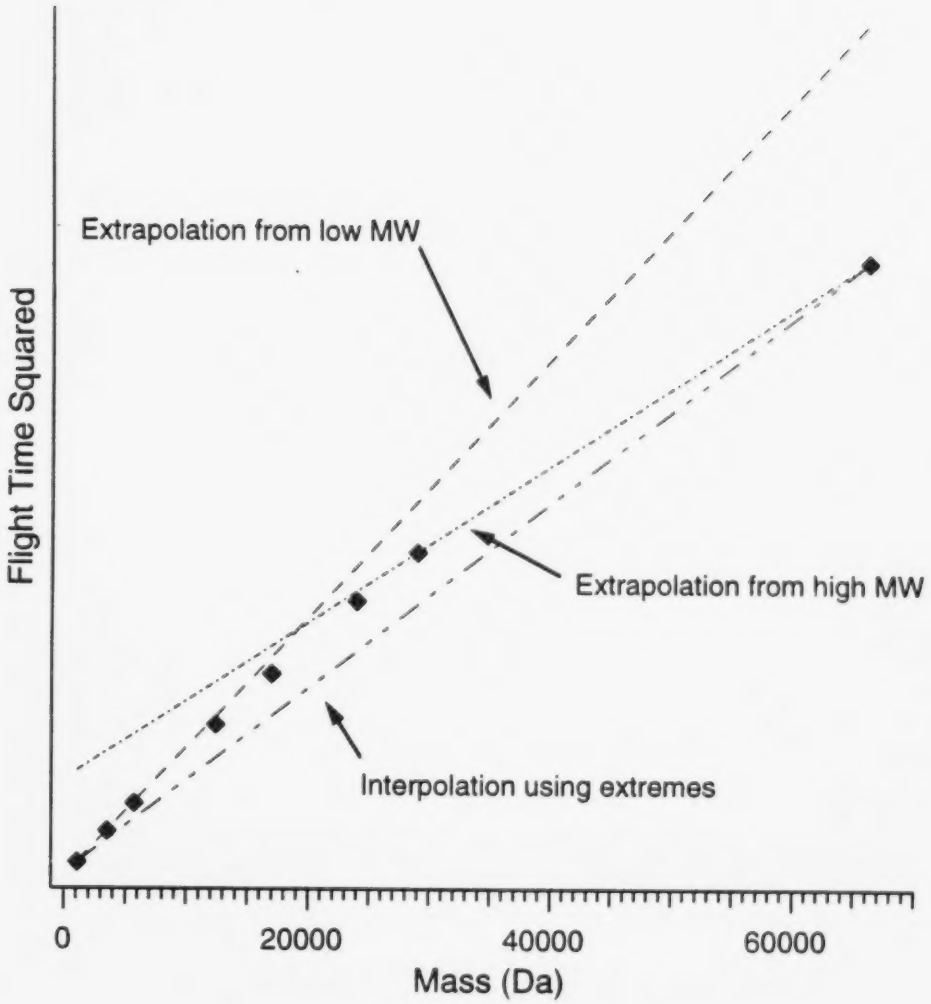

Figure 3.1 In time-of-flight instruments calibrations are done assuming there is a linear relationship between (flight time)^2 and m/z. This does not account for the initial energy of an ion. If an initial ion velocity of 500 m/s is assumed for all MALDI ions, then a linear relationship no longer holds. The effect upon the calibration is shown.

in a field-free environment[21,22] versus ions formed in an extraction field.[25] They propose a collisional model to explain the difference, i.e., ions are slowed due to collisions with other molecules in the desorption plume or neutral molecules are ionised, due to collisions, at a lower extraction potential.

In time-lag focusing, total kinetic energy increases with mass; thus, proposed herein is the use of a modified pulse that decreases in amplitude with time. Ions of higher mass spend more time in the source. If the pulse amplitude decreases, then higher mass ions would receive less imparted kinetic energy from the pulse than ions of lower mass, compensating for the difference in initial kinetic energy; total kinetic energy remains constant.

3.1.1 Model. The modified pulse requires that correction of the total kinetic energy be done in the source region between the repeller and extraction plate. The amount that the potential of the repeller must decrease with time is proportional to the increase in initial kinetic energy for ions of mass m_1 and m_2. Thus, there exists some function, $V(t)$, which describes the pulse shape that is necessary to maintain constant total kinetic energy for all ions:

$$V(t) = V_0 - \frac{dV}{dt} t, \qquad (1)$$

where V_0 = the initial pulse potential,
and $V(t)$ = the pulse potential at any time t.

Equation (1) can be rewritten as the electric field strength, E. Equation (1) becomes

$$E(t) = E_0 - \frac{dE}{dt} t. \qquad (2)$$

If the total kinetic energy for an ion of mass m is U_T, then

$$U_T = \frac{1}{2} m v_0^2 + eV_{DC} + e\bar{V}_p \,, \tag{3}$$

where v_0 = the initial velocity of an ion of mass m,
eV_{DC} = the imparted kinetic energy between the extraction plate and ground,
$e\bar{V}_p$ = the imparted kinetic energy from the TLF pulse,
$\bar{V}_p$ = the average potential an ion receives from the TLF pulse,
and e = the unit of elementary charge.

If total kinetic energy is to remain constant for all m, then for an ion of mass m_1 and an ion of mass m_2, $U_{T1} = U_{T2}$. Therefore,

$$\bar{V}_{p_1} - \bar{V}_{p_2} = \frac{m_2 v_2^2 - m_1 v_1^2}{2 \cdot e} \,, \tag{4}$$

where v_2 = the initial velocity of an ion of mass m_2
and v_1 = the initial velocity of an ion of mass m_1.

Equation (4) can be rewritten as the average electric field strength, E, that an ion experiences during its time in the source; thus,

$$\bar{E}_1 - \bar{E}_2 = \frac{m_2 v_2^2 - m_1 v_1^2}{2 \cdot e \cdot d_1} \,, \tag{5}$$

where d_1 = the distance from the repeller to the first extraction plate
and $\Delta\bar{E} = \bar{E}_1 - \bar{E}_2$.

Therefore, one can determine the difference in the average electric field strength that must exist between two ions of mass m_1 and m_2. The rate of change is dependent upon the difference in time that the two ions spend in the source. The time an ion of mass m spends in the source for an ion desorbed from a surface and travelling forward and parallel to the electric field (as in MALDI in its normal parallel extraction geometry) is given by the following equation:[26]

$$t_s = \frac{(2m)^{1/2}}{e \cdot \bar{E}} \left[(U_0 + e \cdot \bar{E} \cdot s)^{1/2} - U_0^{1/2} \right], \quad \textbf{(6)}$$

where $s = d_1 - v_0 \cdot \tau$

and τ = the delay time or time lag.

The time in the source can be determined for an ion of mass m_1 and an ion of mass m_2. The difference in time is $\Delta t = t_{s2} - t_{s1}$. However, on the function $E(t)$ (equation (2)) the points t_{s2} and t_{s1} correspond to the points E_2 and E_1 not $\bar{E}_2$ and $\bar{E}_1$. An approximation can be made if one assumes $E(t)$ is a nearly linear function

$$\bar{E}_1 = \frac{E_0 + E_1}{2} . \quad \textbf{(7)}$$

An iterative approach can be used to solve this equation and find $E(t)$ at t_{s2} and t_{s1}. Equation (5) can be solved to find $\Delta\bar{E}$; this need be done only once for each pair of m under consideration. Although $\Delta\bar{E}$ is a known and fixed value, an initial guess must be made for $\bar{E}_1$. A reasonable guess is to use the initial value of the pulse potential, i.e., E_0. Equation (6) is then solved and Δt determined. Using equation (2) E_1 can be found and substituted into equation (7). Since, $\Delta\bar{E}$ is known $\bar{E}_2$ can be found. $\bar{E}_1$ and $\bar{E}_2$ are substituted into equation (6) and the cycle is repeated. After four iterations further changes occur only in the 16th significant figure. For each value of m, one value of $E(t)$ is determined. An iterative increase in the value of m allows the determination of the entire $E(t)$ function. Figure 3.2 shows the ideal pulse shape predicted by the iterative analysis.

3.2 Experimental

3.2.1 Instrument. Most of the spectra and data were collected on the previously described MALDI instrument, modified for operation up to 30 kV (see Chapter 2).[13] The modification was undertaken to optimize the source for operation under either continuous extraction or time-lag focusing extraction conditions. The first extraction plate was redesigned and a grid was placed on the repeller side. One DC power supply was used to set the potential on the repeller and first extraction plate and to set the potential on the second extraction plate

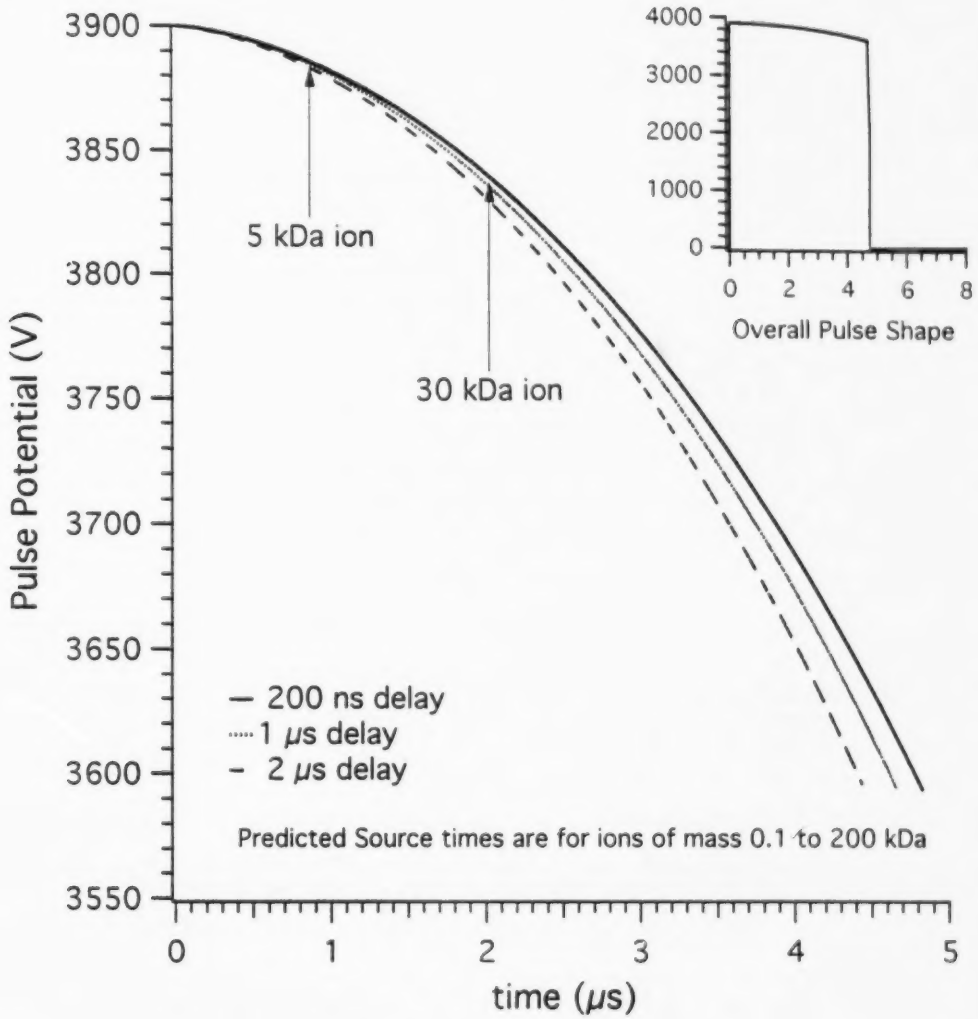

Figure 3.2 The predicted pulse shape that is required to maintain constant total kinetic energy for all ions by delivering less imparted kinetic energy to ions of higher mass. The times at which a 5 kDa and a 30 kDa ion exit the region between the repeller and the first extraction plate are labelled on the graph. The effect of a change in the time lag is shown. The inset figure shows the overall pulse shape between 0 and 3.9 kV. See the text for details.

through a voltage divider. A mass filter was added to the system. The mass filter can prevent saturation of the microchannel plate detector by deflecting matrix ions out of the ion trajectory, reducing the ion current from low mass ions. A nitrogen laser (VSL-337ND, Laser Science, Inc.) with a 3-ns pulse width was used for desorption. Desorption was at 67.5° to the probe surface normal. The laser energy was measured using a laser energy meter (Molectron; Portland, OR). The energy can be determined with good precision (<2%). The laser spot size was measured and the laser energy was converted to laser flux with consideration of the pulse width. Determining the desorption area accurately and precisely is difficult. The measured area was $8\pm3\times10^{-5}$ cm^{-2} for five measurements.

The instrument used to measure the flight times of human insulin ions at various laser powers in continuous extraction was a Linear Scientific LDI 1700 XP (now a Hewlett Packard G-2025A). The laser flux was measured in the same manner as previously described.

3.2.2 Sample Preparation. Sinapinic acid (matrix) was purchased from Aldrich and used without further purification. Bovine insulin, human insulin, equine cytochrome *c*, equine myoglobin, bovine trypsinogen, and bovine carbonic anhydrase II were purchased from Sigma and used without purification. Proteins were dissolved in water to generate stock solutions. The stock solutions were frozen at –20°C. A solution containing a mixture of proteins was prepared fresh daily.

Samples were prepared using a two-layer method,[27] a modification of the crushed crystal and fast evaporation methods.[28,29] To prepare the first layer, sinapinic acid was dissolved in 60%methanol/acetone (v/v) at a concentration of 5 mg mL^{-1}. To prepare the second layer, sinapinic acid was saturated (~15 mg mL^{-1}) in 50% acetonitrile/water (v/v) and mixed 1:1 (v/v) with the protein solution. The stainless steel MALDI probe was successively polished with aluminum oxide particles to a final particle size of 0.3 μm. Onto to this surface, 1.0 μL of the first-layer solution was added and allowed to dry. The first layer spreads across the entire probe surface and dries quickly, without the aid of heat or vacuum, to form a thin layer of the matrix. To the first layer, 0.5 μL of the second-layer solution was added and allowed to dry at room temperature and without the aid of a vacuum. The total

amount of each protein loaded to the MALDI probe was 0.12 pmol insulin, 1.2 pmol cytochrome *c*, 2.2 pmol myoglobin, 2.5 pmol trypsinogen and 3 pmol carbonic anhydrase II.

Samples prepared for the measurements on the Linear Scientific instrument were prepared using the vacuum preparation method.[30] A 50-μM solution of sinapinic acid in 60% acetonitrile, 36% methanol, and 4% water was mixed 1:1 with a 10-μM aqueous solution of human insulin. A 1.0 μL aliquot was loaded to the sample probe and dried under a vacuum.

3.3 Results and Discussion

In a time-of-flight instrument, desorption of matrix and entrained analyte results in ions directed forward (away from the probe), usually parallel to the electric field. One expects the total kinetic energy of an ion that is formed travelling in a direction parallel to the electric field to be the sum of the imparted kinetic energy and the ion's initial kinetic energy from the desorption process. Thus, total kinetic energy should increase with ion mass; since, initial kinetic energy increases with ion mass.[21,22] In Figure 3.1 it was shown that a positive mass error would result for ions whose mass is between the two calibrant ions if total kinetic energy increases with mass. Table 3.1 shows the mass accuracy observed for protein ions analysed under time-lag focusing MALDI conditions. As expected, the total kinetic energy increases with ion mass. The results for square-wave time-lag focusing show a positive mass error for all ions between the calibration points. The column in Table 3.1 listing calculated error was determined assuming that each ion receives equal imparted kinetic energy and that each ion has the same initial velocity of 500 m s^{-1}.[31] The calculated mass error compares well with the observed error for square-wave time-lag focusing proving that an energy excess not a deficit exists in time-lag focusing extraction MALDI.

The shape of the time-lag focusing pulse affects the observed mass accuracy. The pulse shape was adjusted to provide constant total kinetic energy to all protein ions by delivering less imparted energy to ions of higher mass. To obtain the desired pulse shape shown in Figure 3.2, the iterative approach outlined above was used. An estimate of the initial velocity of the MALDI ions of interest must be made to find the pulse shape. Based upon recent work in this laboratory an approximate value of 500 m s^{-1} was used.[31] The pulse shape was fine tuned experimentally through observation of the resultant error in mass

accuracy. Referring to Figure 3.1, a two-point calibration using the highest and lowest mass in a mixture of proteins results in a positive mass error for the points between if a square pulse is used or if the pulse slope is too shallow. Similarly, if the slope is too steep then negative mass errors would result. The optimal pulse shape provides higher mass accuracy than is observed for time-lag focusing with a square pulse. Contrary to square-wave time-lag focusing, the modified pulse shows no regular mass error; the mass error is scattered about both sides of the calibration line.

Table 3.1 Internal Mass Accuracy for Time-Lag Focusing (TLF) MALDI Using a Square Wave and a Modified Wave Shape

Protein	Calculated $(M+H)^+$ (Da)	Error (ppm) Calc.*	Square Pulse TLF**	Modified Pulse TLF**
Bovine Insulin	5734.58	—	—	—
Equine Cytochrome *c*	12361.18	+460	+470	-26
Equine Apomyoglobin	16952.52	+430	+460	+9
Bovine Trypsinogen	23981.97	+210	+170	-5
Bovine Carbonic Anhydrase II	29024.72	—	—	—

* The calculated mass error represents the expected mass accuruacy based upon an initial velocity of 500 m/s using insulin and carbonic anhydrase as calibrants.
** The average mass of three spectra was used to determine the relative error

The difference in voltage, ΔV, that the extraction pulse must deliver to ions of mass m_1 and m_2 is fixed based on their initial velocity. However the rate at which the difference must be delivered, $\Delta V/\Delta t$, is dependent upon the residence time of the ion between the repeller and extractor. The time required to traverse this region is dependent on the extraction potential and the time lag. In Figure 3.2, the dependence of the pulse shape on the time lag is shown. As the time lag increases the slope of the pulse becomes more steep. At

longer delays the ions move further from the repeller before the extraction pulse is turned on; thus, their residence time between the repeller and the extractor is shorter and the energy compensation must take place in a shorter period. Likewise, as the repeller voltage is increased, the slope of the pulse becomes more steep.

Designing a voltage pulser to deliver the ideal pulse shape shown in Figure 3.2 presents an engineering difficulty. The pulser used herein, gave a nearly linear slope over the time scale shown. Therefore, perfect energy compensation is not achieved. If the ideal pulse could be delivered, then one could expect energy compensation over a larger mass range. However, in a normal MALDI experiment matrix ions dominate the low mass region when analysing proteins up to 30 kDa. Thus, energy compensation between 3 and 30 kDa is sufficient. Although, perfect energy compensation is not achieved, partial compensation is better than no compensation, i.e., for square-wave time-lag focusing or continuous extraction MALDI.

Figure 3.3 shows the dependence of ion flight time on laser power. It was found that as the laser flux increased, flight times increased. This observation is also noted by Ens et al.[24] Attempts to monitor changes in flight time with signal strength at a fixed laser power, similar to the method of Ens et al., gave no observable difference in flight time. A neutral-density filter wheel was used to attenuate the laser power. The normal working laser flux range for sinapinic acid is between 9 and 20 MW cm^{-2} and the desorption threshold was 6 MW cm^{-2}. For insulin, the signal intensity increased steadily with laser flux up to a flux of 26 MW cm^{-2}. At 33 MW cm^{-2} and beyond the signal intensity decreased and resolution decreased sharply. Twenty laser shots were summed to produce a spectrum. Only laser shots with an analyte peak that exceeded a given threshold intensity, but did not exceed the maximum full-scale setting of the digitizer, for each laser power were summed. The threshold was set to one-quarter the average analyte intensity at each laser power. Four spectra were collected at each laser power. The average flight time is shown in Figure 3.3. The error bars represent the standard deviation of the analyte flight time of the four spectra. If the change in flight time is converted to a change in energy then at a laser flux of 26 MW cm^{-2}, the energy deficit is 7.7 eV for insulin and 6.8 eV for carbonic anhydrase, e.g., the

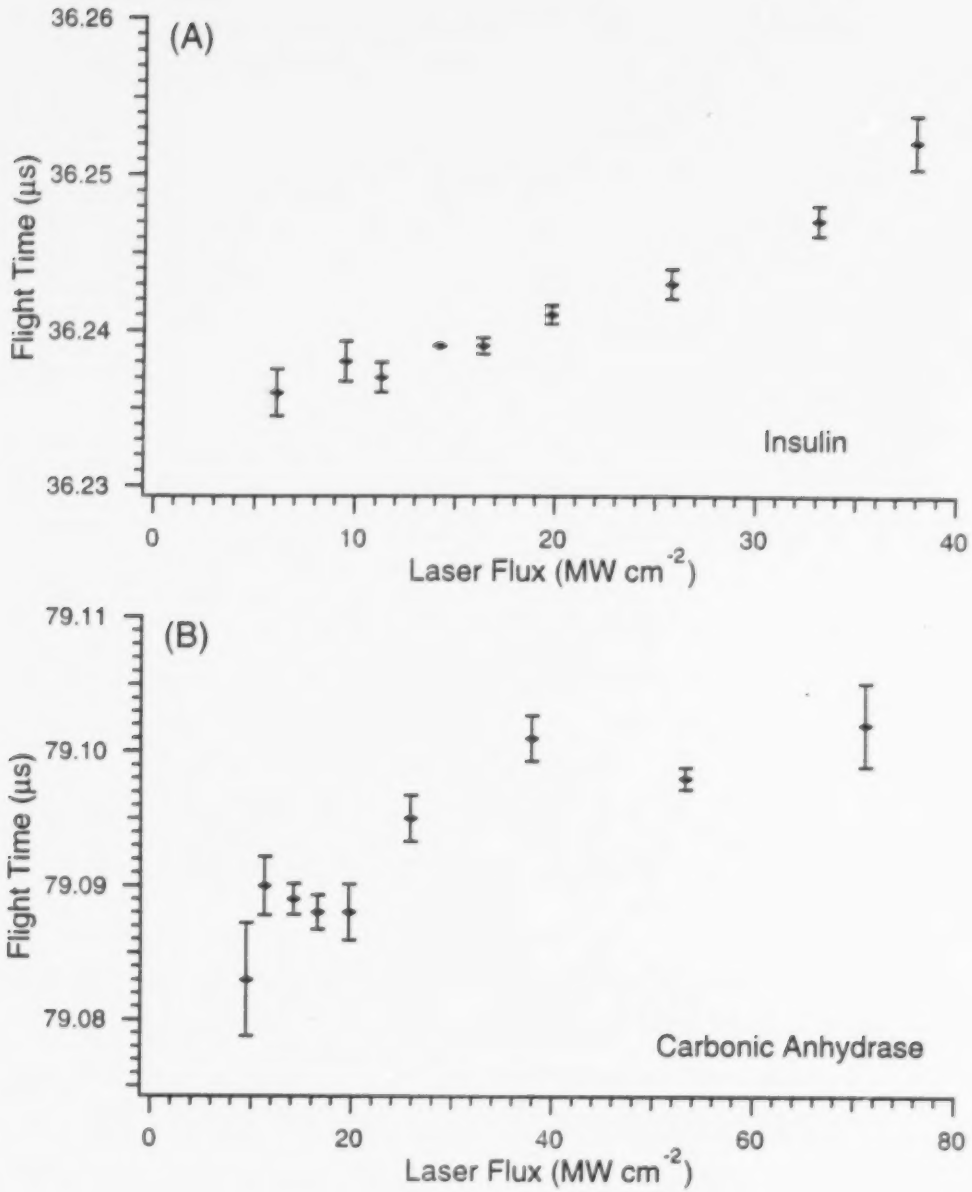

Figure 3.3 Changes in ion flight time with laser power for (A) bovine insulin and (B) bovine carbonic anhydrase II. Four spectra were averaged for each point. The error bars represent one SD in the observed flight time. Charge depletion on the repeller is proposed for the time shift with increasing laser power. See text for details.

protein ions have less energy than expected and thus their flight times increase. At a laser flux of 38 MW cm^{-2}, the energy deficit increases to 16 eV for insulin and 10 eV for carbonic anhydrase. Clearly, the trend differs from continuous extraction. A probable cause of the energy deficit is charge depletion on the repeller. Total ion current increases as the laser flux increases. Since both positive and negative ions are produced, the negative ions discharge on the repeller and the positive ions on the extraction plate when the extraction pulse is switched on. This discharge, which increases with ion current, reduces the source potential and thus the ion energy.

The effect of ion discharge decreases if the capacitance of the ion source increases. Figure 3.4 shows the dependence of the flight time of insulin ions upon laser power. The data was collected using continuous extraction on a Linear Scientific LDI 1700 XP. A sharp increase in flight time with laser power was observed if no capacitance was added to the ion source (30 pF inherent capacitance). Adding a 1-nF capacitor to the repeller reduces the effect of laser flux on ion flight time.

Figure 3.5 shows the MALDI spectra for a mixture of five proteins in continuous extraction and modified-wave time-lag focusing extraction with focusing centred at carbonic anhydrase using a 1-μs time delay. The observed resolution is listed in Table 3.2. As expected under time-lag focusing conditions the observed resolution is mass dependent. However, mass-dependent focusing should not be seen as a detraction. While time-lag focusing offers no improvement in resolution for insulin when the time lag or pulse amplitude is optimized for carbonic anhydrase, it does provide higher resolution between 8 and 29 kDa than is observed in continuous extraction. The key advantage to decoupling ion formation from ion extraction under most MALDI conditions, despite the mass range, is the improved mass accuracy, due both to improved resolution and the ability to compensate for the increase in initial kinetic energy as mass increases. Additionally, the energy deficit is much smaller in time-lag focusing than in continuous extraction MALDI. The small laser-power dependent kinetic energy deficit, while observed, is easily controlled. All measurements can be done using one laser flux for a given matrix.

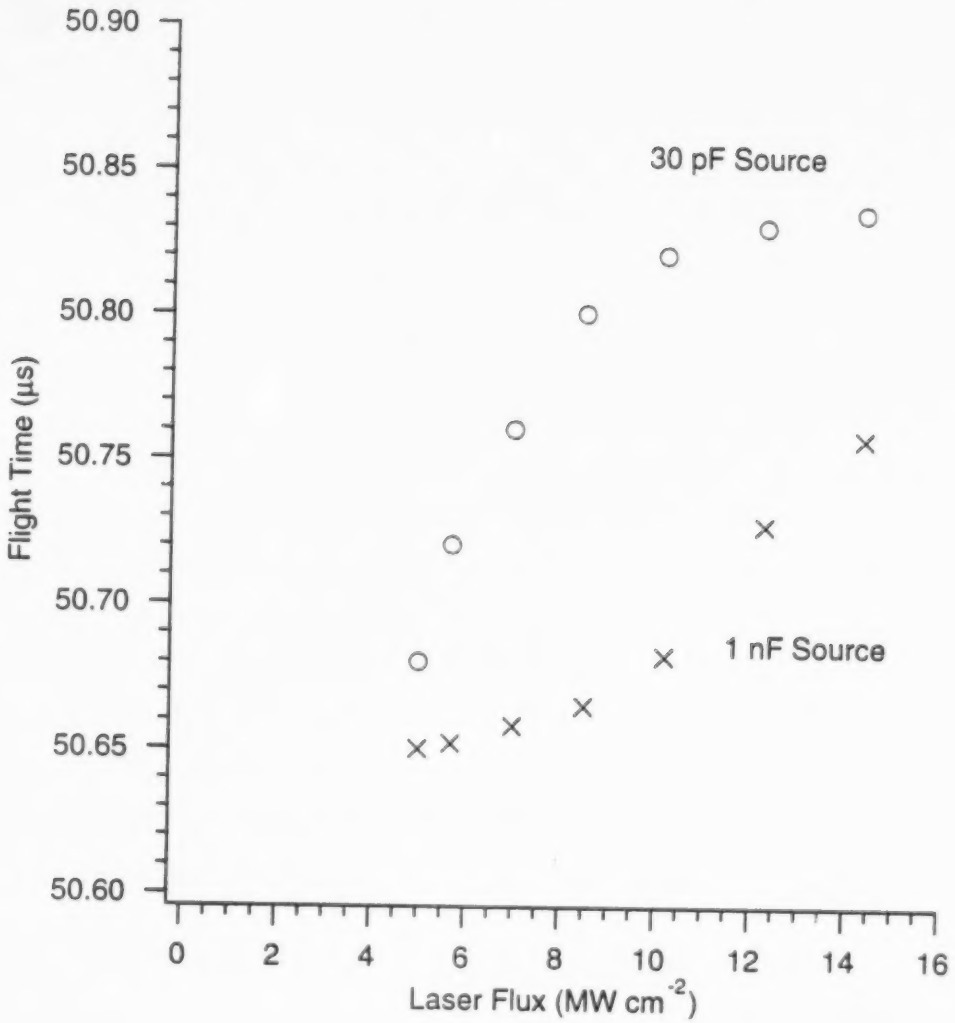

Figure 3.4 The dependence of the flight time of human insulin ions on the laser energy used for desorption in continuous extraction MALDI. Increasing the source capacitance decreases the effect of laser energy. See the text for details.

Table 3.2 Resolution of Proteins in Continuous Extraction and Time-Lag Focusing Extraction MALDI

Protein		Resolution (fwhm) Continuous Extraction	Time-lag Extraction
Bovine Insulin	$(M+H)^+$	340	280
Equine Cytochrome *c*	$(M+2H)^{2+}$	320	270
	$(M+H)^+$	280	460
Equine Apomyoglobin	$(M+2H)^{2+}$	300	320
	$(M+H)^+$	230	620
Bovine Trypsinogen	$(M+2H)^{2+}$	270	400
	$(M+H)^+$	210	1110
Bovine Carbonic Anhydrase II	$(M+2H)^{2+}$	200	510
	$(M+H)^+$	170	1330

As one may expect, with improved resolution and good internal mass accuracy, external mass accuracy is also improved. Table 3.3 lists the external mass accuracy and reproducibility for insulin, cytochrome *c*, myoglobin, trypsinogen and carbonic anhydrase II. The pulse voltage was set to maximize the resolution of carbonic anhydrase II. Reproducibility of sample thickness, sample position, and mechanical and electrical stability become limiting factors in external mass measurements. For example, an uncertainty of 10 μm in an insulin ion's initial starting position contributes a mass error of 145 ppm. This error would increase as the magnitude of the extraction pulse is increased.[26] A 10-V change in the DC power supply operating at 20 kV gives a mass error of 430 ppm. These values are calculated for the time-lag focusing instrument described herein with the pulse potential set to maximize the resolution of insulin. This emphasizes the need to prepare samples with a consistent thickness (see Chapter 4).[27] Small densely-packed matrix crystals provide better external mass accuracy than large crystals.

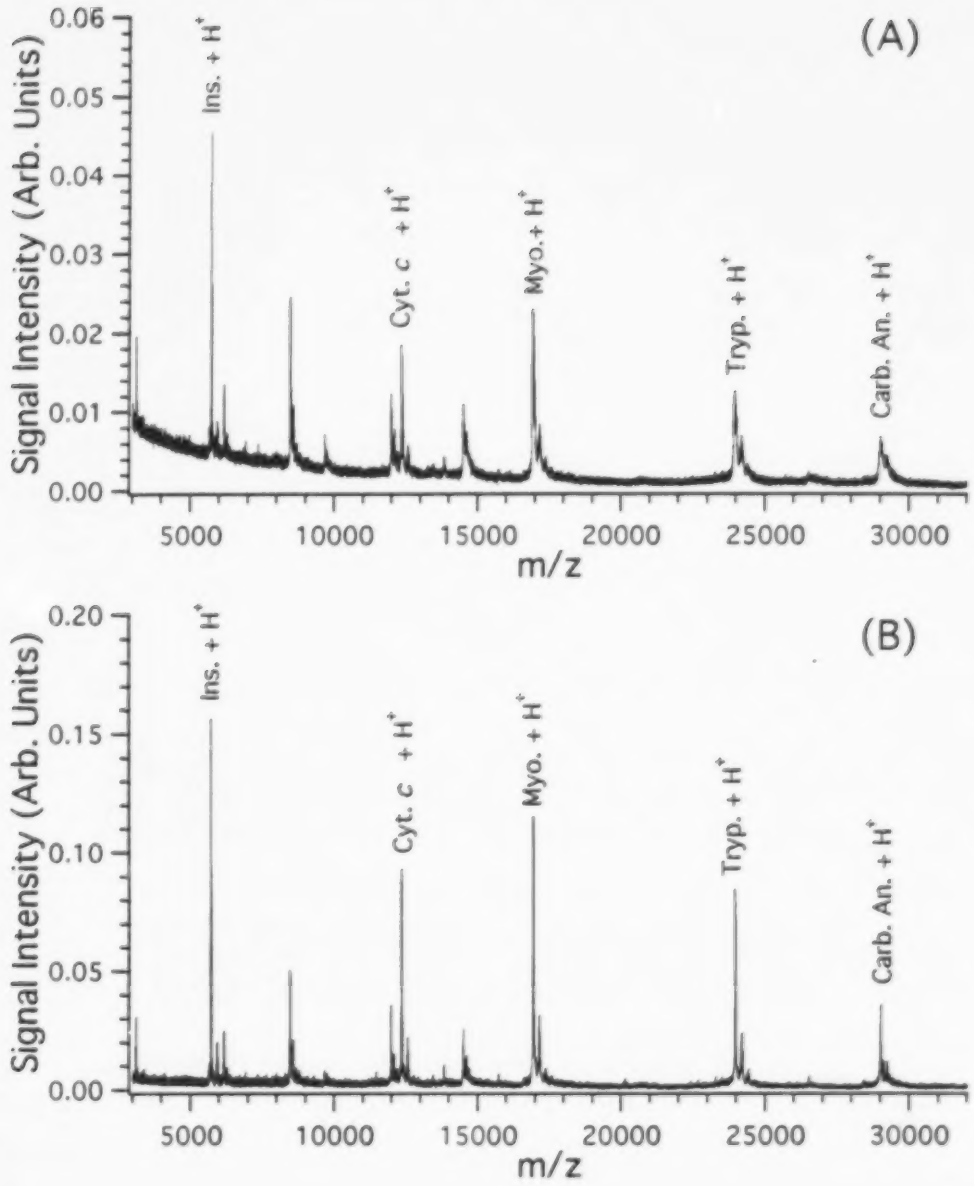

Figure 3.5 MALDI spectra of a mixture of insulin, cytochrome *c*, myoglobin, trypsinogen and carbonic anhydrase II in (A) continuous extraction and (B) time-lag focusing extraction with focusing centred at carbonic anhydrase using a 1-μs time lag.

Table 3.3 External Mass Accuracy and Reproducibility of Modified Pulse Time-Lag Focusing MALDI

	$(M + H)^+$ (Da)			
Protein	Calculated	Experimental	Average and Std. Dev.	Error (ppm)
Bovine Insulin	5734.58	5733.54 5736.22 5735.61 5735.52 5736.29 5734.28 5733.34	5734.97 ±1.24	+68
Equine Cytochrome *c*	12361.18	12359.54 12364.60 12363.56 12362.79 12362.61 12360.39 12359.72	12361.89 ±2.00	+57
Equine Apomyoglobin	16952.52	16952.01 16955.01 16954.61 16953.45 16953.05 16952.03 16951.76	16953.13 ±1.29	+36
Bovine Trypsinogen	23981.97	23981.49 23984.75 23983.26 23981.58 23980.82 23982.14 23980.33	23982.05 ±1.50	+4
Bovine Carbonic Anhydrase II	29024.72	29025.74 29027.89 29027.03 29024.06 29023.49 29025.72 29023.25	29025.31 ±1.77	+20

It was shown that both internal and external mass accuracies were improved over a 25-kDa mass range using modified pulse time-lag focusing for energy compensation. The modified pulse allows total kinetic energy to remain constant. Ion flight time is laser power dependent. An increase in ion current at higher laser power increases charge depletion on the repeller and extraction plate, reducing ion energy, and increasing flight time. Future work in this area could include changing the shape of the extraction pulse to extend focusing to all ions, despite mass. Normally time-lag focusing is a mass dependent energy compensation technique. The extraction pulse or time lag must be increased to focus ions of higher mass. If an extraction pulse that increases in amplitude with pulse width were used, then having mass independent focusing would be possible. The model for mass independent focusing would be similar to the dynamic post-source acceleration technique used by Yefchak, et al.,[32] and the post-source pulse focusing model of Kinsel and Johnston,[33] except that it would be an in-source method.

3.4 Literature Cited

(1) Tanaka, K.; Waki, H.; Ido, Y.; Akita, S.; Yoshida, Y.; Yoshida, T. *Rapid Commun. Mass Spectrom.* **1988**, *2*, 151-153.

(2) Karas, M.; Hillenkamp, F. *Anal. Chem.* **1988**, *60*, 2299-2301.

(3) Mamyrin, B. A.; Karataev, V. I.; Schmikk, D. V.; Zagulin, V. A. *Zh. Eksp. Teor. Fiz.* **1973**, *64*, 82-89.

(4) Tang, X.; Beavis, R.; Ens, W.; Lafortune, F.; Schueler, B.; Standing, K. G. *Int. J. Mass Spectrom. Ion Processes* **1988**, *85*, 43-67.

(5) Wiley, W. C.; McLaren, I. H. *Rev. Sci. Instrum.* **1955**, *26*, 1150-1157.

(6) Spengler, B.; Kirsch, D.; Kaufmann, R. *J. Phys. Chem.* **1992**, *96*, 9678-9684.

(7) Cornish, T. J.; Cotter, R. J. *Rapid Commun. Mass Spectrom.* **1993**, *7*, 1037-1040.

(8) a) Lennon, J. J.; Brown, R. S. In *Proceedings of the 42nd ASMS Conference on Mass Spectrometry and Allied Topics*; Chicago, IL, 1994; p 501. b) Brown, R. S.; Lennon,

J. J. *Anal. Chem.* **1995**, *67*, 1998-2003.

(9) Brown, R. S.; Lennon, J. J. *Anal. Chem.* **1995**, *67*, 3990-3999.

(10) Brown, R. S.; Carr, B. L.; Lennon, J. J. *J. Am. Soc. Mass Spectrom.* **1996**, *7*, 225-232.

(11) Colby, S. M.; King, T. B.; Reilly, J. P. *Rapid. Commun. Mass Spectrom.* **1994**, *8*, 865-868.

(12) Christian, N. P.; Colby, S. M.; Giver, L.; Houston, C. T.; Arnold, R. J.; Ellington, A. D.; Reilly, J. P. *Rapid Commun. Mass Spectrom.* **1995**, *9*, 1061-1066.

(13) Whittal, R. M.; Li, L. *Anal. Chem.* **1995**, *67*, 1950-1954.

(14) Whittal, R. M.; Palcic, M. M.; Hindsgaul, O.; Li, L. *Anal. Chem.* **1995**, *67*, 3509-3514.

(15) Whittal, R. M.; Li, L.; Lee, S.; Winnik, M. A. *Macromol. Rapid Commun.* **1996**, *17*, 59-64.

(16) Lee, S.; Winnik, M. A.; Whittal, R. M.; Li, L. *Macromolecules* **1996**, *29*, 3060-3072.

(17) Dai, Y.; Whittal, R. M.; Li, L.; Weinberger, S. R. *Rapid Commun. Mass Spectrom.* Submitted.

(18) Cotter, R. J. *Biomed. Environ. Mass Spectrom.* **1989**, *18*, 513-532.

(19) Vestal, M. L.; Juhasz, P.; Martin, S. A. *Rapid Commun. Mass Spectrom.* **1995**, *9*, 1044-1050.

(20) Juhasz, P.; Roskey, M. T.; Smirnov, I. P.; Haff, L. A.; Vestal, M. L.; Martin, S. A. *Anal. Chem.* **1996**, *68*, 941-946.

(21) Beavis, R. C.; Chait, B. T. *Chem. Phys. Lett.* **1991**, *181*, 479-484.

(22) Verentchikov, A.; Ens, W.; Martens, J.; Standing, K. G. In *Proceedings of the 40th ASMS Conference on Mass Spectrometry and Allied Topics*; Washington, DC, 1992; pp 360-361.

(23) Guilhaus, M. *J. Mass Spectrom.* **1995**, *30*, 1519-1532.

(24) Zhou, J.; Ens, W.; Standing, K. G.; Verentchikov, A. *Rapid Commun. Mass Spectrom.* **1992**, *6*, 671-678.

(25) Ens, W.; Mao, Y.; Mayer, F.; Standing, K. G. *Rapid Commun. Mass Spectrom.* **1991**, *5*, 117-123.

(26) Cotter, R. J. In *Time-of-Flight Mass Spectrometry*; Cotter, R. J.; Ed.; American Chemical Society: Washington, DC, 1994; Vol. 549; pp 16-48.

(27) Dai, Y.; Whittal, R. M.; Li, L. *Anal. Chem.* **1996**, *68*, 2494-2500.

(28) Xiang, F.; Beavis, R. C. *Rapid Commun. Mass Spectrom.* **1994**, *8*, 199-204.

(29) Vorm, O.; Roepstorff, P.; Mann, M. *Anal. Chem.* **1994**, *66*, 3281-3287.

(30) Weinberger, S. R.; Börnsen, K. O.; Finchy, J. W.; Robertson, V.; Musselman, B. R. In *Proceedings of the 41st ASMS Conference on Mass Spectrometry and Allied Topics*; San Francisco, CA, May 30-June 4, 1993; pp775a-775b.

(31) Russon, L. M.; Whittal, R. M.; Li, L., submitted.

(32) Yefchak, G. E.; Enke, C. G.; Holland, J. F. *Int. J. Mass Spectrom. Ion Processes* **1989**, *87*, 313-330.

(33) Kinsel, G. R.; Johnston, M. V. *Int. J. Mass Spectrom. Ion Processes* **1989**, *91*, 157-176.

Chapter 4

Confocal Fluorescence Microscopic Imaging for Investigating the Analyte Distribution in MALDI Matrices[a]

4.1 Introduction

In matrix-assisted laser desorption/ionisation (MALDI), sample and matrix preparation play a central role in achieving optimal performance. Sensitivity, selectivity, mass resolution, and mass accuracy are strongly dependent on the sample and matrix preparation. Understanding the chemical and physical phenomena underlying the sample preparation process is very important. A major objective of sample preparation studies is to identify sample properties, such as crystal size and shape, analyte distribution, matrix-to-analyte ratio, etc., that are relevant to the success and optimization of MALDI. By controlling these properties, improved sample preparation methods can be achieved for a wide range of applications. Because of the involvement of macromolecules and the complexity of the crystal formation process, few physical measurement techniques can be used to study sample preparation.

In chapter three, the discussion of mass accuracy shows the effect of sample preparation upon mass accuracy. Small axial spatial differences, as little as 10 μm, can introduce errors in mass accuracy of 145 ppm for insulin. Clearly, careful attention must be paid to sample preparation to achieve good mass accuracy and resolution in time-lag focusing MALDI.

Microscopic methods are commonly used to inspect the crystal morphology.[1] Most of these techniques, however, do not provide information about the analyte distribution.

---

[a] A form of this chapter is published as: Y. Dai, R. M. Whittal, L. Li "*Confocal Fluorescence Microscopic Imaging for Investigating the Analyte Distribution in MALDI Matrices*" *Anal. Chem.* **1996**, *68*, 2494-2500. The confocal images were collected by Ms. Y. Dai.

Knowledge of the analyte distribution in matrices is important for understanding the fundamental role of matrices in the overall MALDI process. For analytical applications, it is expected that uniform analyte distribution is desirable in achieving better signal reproducibility and improving quantitation.[2] Thus, any techniques that can provide analyte distribution information would be highly valuable while developing new and improved sample/matrix preparation protocols. Besides the microscopic studies, a paucity of reports show that spectroscopic techniques can be used, including X-ray crystallography,[3] Raman spectroscopy,[1c)] and X-ray photoelectron spectroscopy,[4] to study how the analyte is distributed in the MALDI crystals. The distribution of the analyte in the matrix is needed to develop new sample deposition methods for handling very small analyte volumes, such as cellular fluids.[5]

King and Owens[6] showed that fluorescence microscopy provides analyte distribution information. The authors use fluorescence microscopy to study the distribution of fluorescently-labelled proteins in MALDI matrices. However, the information gained from conventional fluorescence microscopy can present some ambiguity in mapping the true distribution of the analyte in matrix crystals. This is due to the presence of strong internal reflectance and transmission of fluorescence light emitted from the analyte within, or near the surface, of a crystal. The fluorescence emission from one region (e.g., the surface) can be readily transmitted or reflected throughout the crystal.

Herein laser confocal microscopy was used to map the distribution of fluorescently-labelled analyte in MALDI matrices. Some advantages and disadvantages of applying confocal microscopy to the study of MALDI samples are discussed. In addition, the potential to get new information on MALDI sample preparation by examining the analyte distribution with the confocal imaging method is illustrated.

In laser confocal microscopy, a laser beam is focused onto a small three-dimensional volume element, termed a voxel, in an object. The voxel size is typically 200 × 200 nm laterally and 800 nm axially and is dependent on the excitation and detection wavelengths used and the optical collection parameters.[7] The illuminated voxel is viewed with a specially designed optical system consisting of several lenses and apertures such that only signals

emanating from this voxel are detected, i.e., signal from outside the probed voxel is not detected. This is in contrast to conventional microscopy where signal from above or below the focal plane is also detected, resulting in poor specimen imaging.[8] By rastering the light beam (or mechanically scanning the specimen through the confocal point), an image of the complete specimen on the laser focal plane is obtained. By adjusting the vertical position of the laser focal point, the voxel is moved to another lateral plane where the beam is again rastered across the entire plane to produce an image. Thus, a three-dimensional image of the specimen can be readily constructed by stacking these "planar" images.

The three-dimensional image of the MALDI matrix crystal can be obtained by stacking planar images produced from the light reflected from the surface after laser illumination (reflection-mode) or from the transmitted light (transmission-mode). Since the MALDI matrix crystals do not fluoresce at the wavelength used for excitation, the analyte image can be obtained by operating the instrument in fluorescence-mode. Finally, the colour-coded analyte image and the overall sample image can be superimposed. The analyte distribution on the surface and within the sample crystals can then be examined.

4.2 Experimental

4.2.1 MALDI and Sample Preparation. The MALDI mass spectra were obtained in a time-lag focusing linear time-of-flight mass spectrometer,[9] as described in Chapters 2 and 3. The desorption laser spot size is an ~50×100μm oval. The tetramethylrhodamine (TMR)-labelled trisaccharide αGal(1→3)[αFuc(1→2)]βGal-TMR was a gift from Dr. O. Hindsgaul; its preparation has been described.[10] The fluorescein isothiocyanate-labelled insulin (insulin-FITC) was purchased from Sigma. The purity of the samples was checked with the use of capillary electrophoresis equipped with a laser induced fluorescence detector. The presence of free dye was less than 1%. Thus, the contribution of the free dye signal to the overall fluorescence signal observed in the microscopic imaging work is negligible for low concentration samples.

Samples were prepared using the dried-droplet,[11] crushed crystal,[1e] and fast evaporation[12] methods and the uniform submicron-crystal formation method described in this work. The insulin-FITC and tetramethylrhodamine-labelled trisaccharide were dissolved in

water at the concentration listed in the figure captions. To prepare matrix solution for the dried droplet method 2,5-dihydroxybenzoic acid was dissolved at a concentration of 20 mg mL^{-1} in 5% acetonitrile/water (v/v). Sinapinic acid matrix solution was prepared at a concentration of 11 mg mL^{-1} in 50% acetonitrile/water (v/v). The analyte solution was then premixed 1:1 with the matrix solution and 1 μL of matrix/analyte solution was placed on a stainless steel probe tip for both MALDI and microscopic examination. The matrix solution for the crushed crystal method was prepared as a saturated solution (~11 mg mL^{-1}) of sinapinic acid in 33% acetonitrile/water (v/v). The solution was mixed on a vortex mixer for ~1 min followed by centrifugation for 5 min. A 1.0 μL aliquot was applied to the probe, allowed to dry and crushed as described.[1e)] Analyte solution was then premixed 1:1 with matrix solution and 1.0 μL was applied on top of the crushed first layer. To prepare matrix solution for the fast evaporation method sinapinic acid was dissolved in 99% acetone/water (v/v) at a concentration of 27 mg mL^{-1}. A 1.0 μL aliquot of this solution was applied to the probe, followed by the independent delivery of 0.5 μL of analyte solution. To prepare matrix solution for the uniform submicron-crystal formation method, sinapinic acid was dissolved at a concentration of 6 mg mL^{-1} in 60% methanol, 39% acetone, 1% of a 0.1% trifluoroacetic acid solution (v/v). A 1.0 μL aliquot was applied to the stainless steel probe. A second matrix solution was prepared as a saturated solution of sinapinic acid in 30% acetonitrile, 20% methanol, 50% water (v/v). The matrix solution was premixed 1:1 with analyte solution and 0.5 μL was applied on top of the first layer. For all preparations, the stainless steel probe used was successively polished with aluminum oxide particles to a final particle size of 0.3 μm to give a polished surface with only minor micro-sized scratches on the probe surface.

To grow larger crystals, sinapinic acid mother liquor was prepared at a concentration of 11 mg mL^{-1} using 33% acetonitrile/water (v/v) with the aid of ~50°C water bath and vortex mixing for 5–10 min. The analyte solution was added to the matrix mother liquor and mixed well to yield a final concentration of 0.5 pmol μL^{-1} for bovine insulin-FITC. The solution mixture was kept in the refrigerator overnight with a half-open vial mouth.

4.2.2 Confocal Microscopy. A Molecular Dynamics' Multiprobe 2001 Confocal Laser Scanning Microscope was used for the generation of all the images reported here. An

Argon/Krypton laser operating at 488 nm was used for the excitation of insulin-FITC whereas the 568 nm line was used for the excitation of the tetramethylrhodamine-labelled trisaccharide.

To generate a sample image, the sample is deposited onto a stainless steel MALDI probe. The probe is then placed in the specimen holder in the microscope. The fluorescence image of the analyte is first constructed from five to thirty planar images spaced about 0.2 to 2 μm apart (dependent upon the crystal size) along the axis normal to the surface of the probe. The reflectance image of the sample is constructed in the same manner as in the fluorescence mode operation. These two three-dimensional images stored in the computer are then superimposed to produce an overall sample and analyte image. The overall image and individual layers of images can be readily viewed from different directions to inspect the details of the analyte distribution.

4.2.3 Application Notes. Confocal microscopy is currently used primarily for studying biological specimens, such as cells. The following points are noted from experience in the examination of MALDI samples using confocal microscopy.

1). The purity of the analyte should be checked to ensure that it is not contaminated with a significant amount of free fluorescent molecules.

2). The use of a high concentration of analyte should be avoided to reduce the possibility of detector saturation. The concentration range used in typical MALDI experiments, i.e., low fmol to low pmol/μL, is appropriate for confocal fluorescence measurement.

3). If multiple images are to be superimposed (e.g., fluorescence image plus reflection image), these images should be recorded with similar intensity. The signal intensity can be adjusted by controlling the laser power, detector amplifiers, and other operational parameters.

4). Sample thickness may be determined by stacking images in the vertical plane or by vertical scanning. The determination of sample thickness is constrained by the physical limitations of the confocal instrument itself. The instrument used was limited to depth profiling through a 300 μm range, which is adequate for most crystals.

4.3 Results and Discussion

Since most native proteins and oligosaccharides are nonfluorescent at the wavelength used for excitation in confocal microscopy, analyte molecules tagged with fluorescent labels are used in this work. Insulin-FITC exhibits a lower signal-to-noise ratio (the label is attached to lysine residues[13]) while the tetramethylrhodamine-labeiled trisaccharide shows an enhanced signal-to-noise when analysed via MALDI compared with their unlabelled counterparts. Other MALDI parameters and observations remain the same, such as the required matrix-to-analyte ratio and the shot-to-shot spectral reproducibility during MALDI analysis. For analyte molecules such as insulin-FITC, the labelling group mass is small, compared with the mass of the intact molecule. Figure 4.1 shows the MALDI mass spectrum of the labelled insulin, revealing that the major components of the insulin sample are the unlabelled insulin and insulin with one FITC group attached. In this chapter, all confocal microscope images, except those noted, were collected using bovine insulin-FITC as the analyte. Other labelled species give essentially the same results.

As in conventional light microscopy, the confocal system can generate phase-contrast images for studying the morphology of the MALDI crystals. Depending upon the type of material used as the sample substrate, either transmission or reflection mode of operation or both can be used. To operate the confocal system in transmission mode, the MALDI sample can be prepared on a glass microscope slide. The reflection mode of operation is useful for direct imaging of samples prepared on the MALDI probe made of stainless steel or other nontransparent materials. Figures 4.2A and 4.2B show two images of the samples prepared using 2,5-dihydroxybenzoic acid and sinapinic acid as matrices, respectively, on a glass slide with the dried-droplet sample preparation method. The insulin-FITC analyte image is shown in green and the phase-contrast image of the crystals is presented in red background.[b] As noted above, the two images were recorded using a similar light intensity. These colours are used for presentation only and do not represent the actual colours of the objects. For

[b] If these images are being viewed in black and white then please refer to the original publication as given in footnote [a].

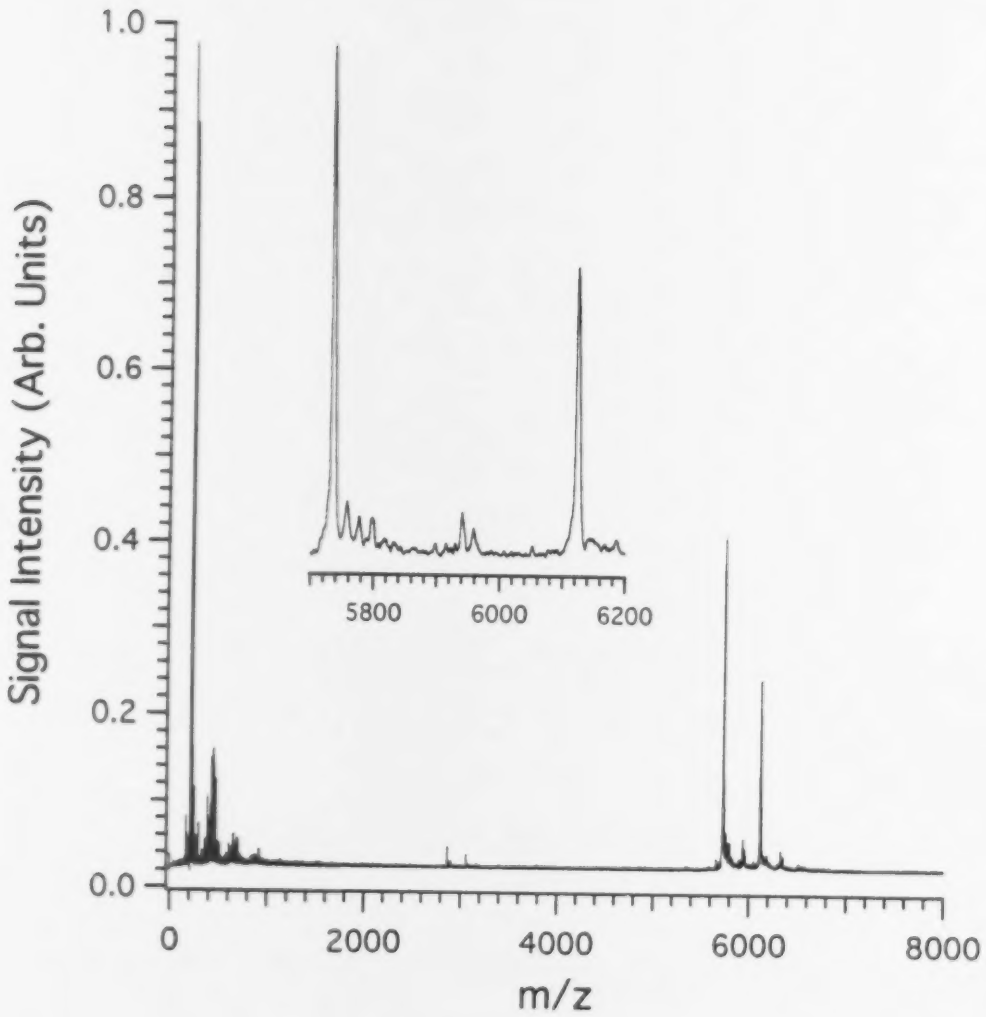

Figure 4.1 MALDI mass spectrum of 1 pmol bovine insulin-FITC using sinapinic acid as the matrix.

The Caption below refers to the figure on the next page.

Figure 4.2 Confocal microscopic images (scale bars in μm) of bovine insulin-FITC in: (A) 2,5-dihydroxybenzoic acid matrix crystals and (B) sinapinic acid matrix crystals, obtained by superimposing the transmission phase-contrast images of crystals (in red background) and the analyte fluorescence images (in green),prepared on a glass slide using the dried-droplet method. (C) 2,5-Dihydroxybenzoic acid matrix crystals and (D) sinapinic acid matrix crystals, obtained by superimposing the phase-contrast reflectance images of crystals (in red background) and the analyte fluorescence images (in green), prepared on a MALDI probe using the dried-droplet method. (E) A sinapinic acid matrix crystal prepared by a controlled slow-growth process. Sinapinic acid matrix crystals prepared by (F) the fast solvent evaporation method, (G) the crushed-crystal method, and (H) the uniform submicron-crystal formation method described in this work. Colour-coded confocal fluorescence images of bovine insulin-FITC (in green) and αGal(1→3)[αFuc(1→2)]βGal-TMR (in blue), see text for details. The sample is prepared by (I) the dried-droplet method with 2,5-dihydroxybenzoic acid as the matrix and (J) the fast evaporation method with sinapinic acid as the matrix. Note that the MALDI desorption laser is typically 50–100 μm.

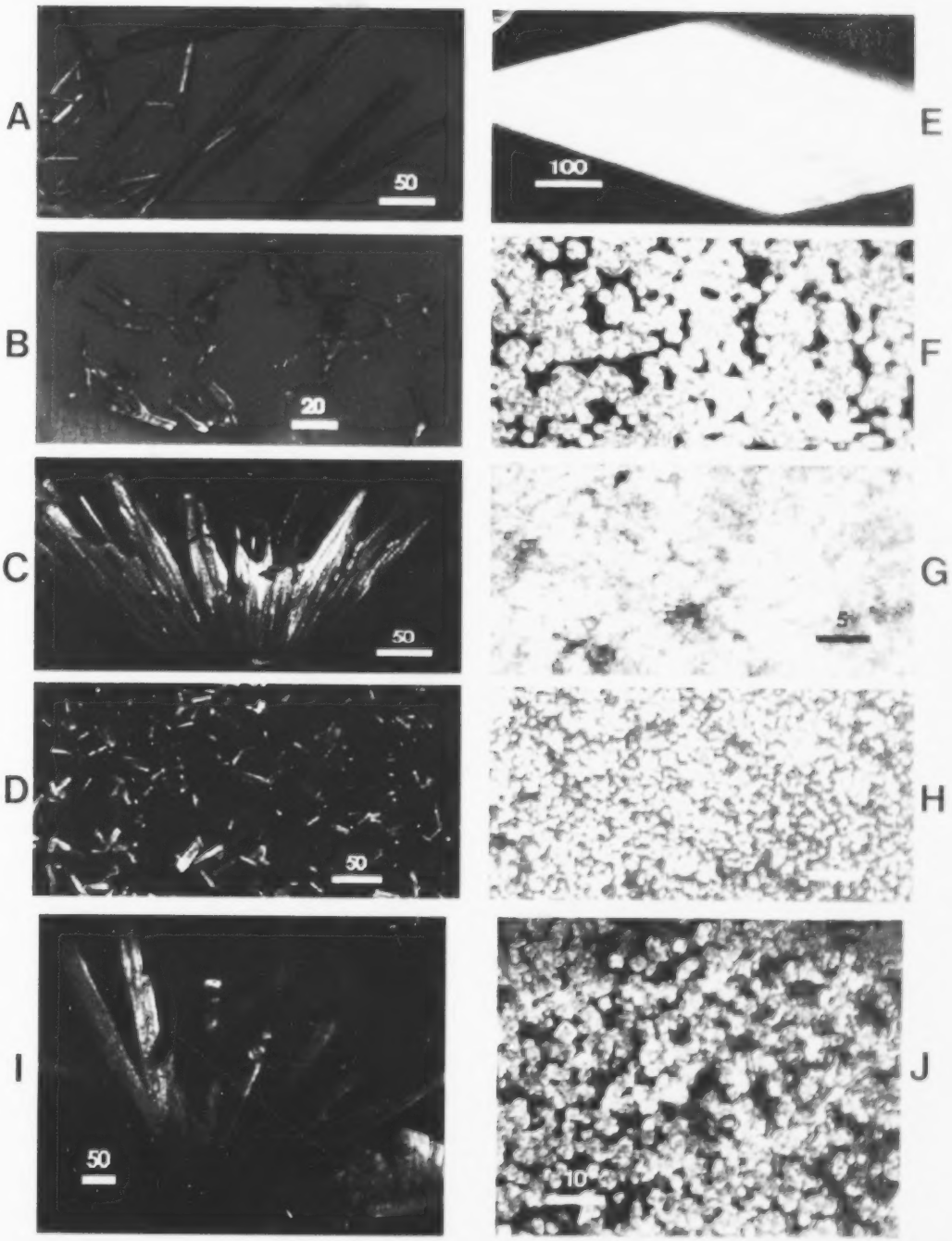
A
50
B
20
C
50
D
50
I
50
E
100
F
G
5
H
J
10

comparison, the images of the same samples prepared on a stainless steel probe are shown in Figures 4.2C and 4.2D.

The images in Figures 4.2A-D clearly show that the analyte is incorporated into the crystals. This is also confirmed by examining individual sections of images that construct the overall images shown in Figures 4.2A-D. In the regions where the analyte is most concentrated the image appears green. In the areas where there is little or no analyte, the red colour of the phase-contrast image dominates and in areas where the analyte is less concentrated the green colour of the analyte overlaps with the red colour of the background and the image appears yellow. A striking feature revealed by these images is that the analyte is not uniformly distributed between the crystals and within the matrix crystals. For the samples prepared with the typical matrix-to-analyte ratio and concentration used in an MALDI experiment (e.g., 100 fmol to 5 pmol for the labelled insulin), regions containing a higher concentration of analyte or analyte domains can be observed in crystals formed on the entire sample probe surface. Careful inspection of the individual crystals on the sample probe surface, as shown in Figure 4.2A-D, does not indicate any correlation between the location of the analyte domains and the physical appearance of the matrix crystals. Some crystals appear to grow to full length, but only part of the crystal contains analyte. In some crystals, the analyte resides inside the crystal, but not on the surfaces. Other crystals can have the opposite distribution. These findings suggest that (a) the analyte and matrix form cocrystals and (b) the cocrystallisation process is not in equilibrium with the dried droplet sample preparation method.

Crystallisation occurs in two phases: nucleation and particle growth. Nucleation takes place as the matrix molecules aggregate or the small particles already present in the matrix solution or on the sample substrate (e.g., the rough edges of the probe surface) act as the nucleation and particle growth sites. The cocrystallisation equilibrium is expected to affect many experimental parameters including the properties of the sample substrate, solvent conditions, and the speed of crystal formation. With the use of the dried-droplet sample preparation method, the nonuniform analyte distribution in matrix crystals was observed for samples prepared on either glass or stainless steel substrate. The variation of the ratio of the

solvent composition does not yield crystals with more uniformly distributed analyte. However, the analyte was much more uniformly distributed in large crystals produced by a controlled, slow-growth process. This is shown in Figure 4.2E for the image of bovine insulin-FITC in large crystals using sinapinic acid as the matrix. In addition, unlike the dried-droplet method, all large crystals grown in this slow process contain the analyte. The same results were obtained using 2,5-dihydroxybenzoic acid as the matrix. Clearly the rate of crystal growth affects analyte incorporation. The slow growth process seems to provide adequate time to establish an equilibrium for the matrix crystals to more uniformly entrain the analyte. Thus, one has to be cautious in extrapolating the findings observed from the crystals grown by the slow crystal growth process to the rapid methods more commonly used for MALDI crystal formation.[1b)]

Some experimental observations are worth noting regarding the possible correlation between the analyte domain and the resultant MALDI analyte signal. In MALDI with samples prepared by the dried-droplet method, it is often necessary to search for a spot that gives an analyte signal. The MALDI instrument used in this experiment is equipped with a CCD camera to aid in the search for the sample spot. Often, when the laser beam is directed to a crystal, only the matrix background signal can be seen and no analyte signal is observed. Note one report shows there is a correlation between the analyte distribution and the MALDI analyte signals.[2] Confocal imaging results seem to provide further evidence of this correlation. Strong and much more reproducible analyte signals can be obtained from the crystals containing the analyte while the regions containing little or no analyte give only matrix peaks.[2] As reported earlier, for large crystals formed by the controlled slow growth process, it is easier to obtain analyte signal.[1b)] Moreover, signal variation from pulse to pulse and from spot to spot is small, compared with the dried-droplet method. This again seems to correlate well with the observation of a more uniform analyte distribution in the large crystals.

While the use of large crystals for MALDI provides better signal reproducibility, this method of sample preparation is impractical for many routine analytical applications due to the time required for preparation and its inefficiency in using the analyte. The inefficiency

is because a large portion of analyte would be entrained into the bulk of the crystal where laser desorption is not accessible.

In contrast to the formation of large crystals by the slow growth process, small crystals or microcrystals can be formed using rapid solvent evaporation. Weinberger and co-workers reported a method using a vacuum to evaporate the matrix/sample solution to form small crystals on an MALDI probe rapidly.[14] Better signal reproducibility is shown. Vorm et al. reported an alternative method of forming microcrystals.[12] In their method, sinapinic acid matrix solutions are prepared in acetone. A drop of matrix solution is applied to the MALDI sample probe. The droplet spreads and dries very quickly, leaving a thin layer of matrix crystals. Analyte samples are then placed on top of the matrix layer and allowed to dry. This method gives improved performance compared with the dried-droplet method for certain applications, such as peptide analysis. Notably, the MALDI analyte signal variations from shot-to-shot are small.

Figure 4.2F shows the analyte image of a sample prepared using the fast solvent evaporation method with the use of sinapinic acid as the matrix on a stainless steel probe. The green colour-contrast reflects the relative intensity of the analyte. The overall crystal shape is imaged and represented in red. The overlap of red and green in different proportions shows the relative ratio between the analyte and matrix (yellow). For example, the analyte content is higher in the green region than the yellow region. Figure 4.2F shows that microcrystals are formed and within the individual microcrystal, the analyte is not uniformly distributed. However, across the entire sample deposition area, the analyte is more uniformly distributed, compared with the dried-droplet method. It appears that the matrix microcrystals prepared by the fast solvent evaporation act as the nucleation sites. The addition of the analyte, in the second step of this method, redissolves a small amount of matrix molecules in the outer layer of the crystals. The dissolved matrix molecules incorporate the analyte during the recrystallisation process. However, the latter is a rapid nonequilibrium cocrystallisation process. This results in the nonuniform analyte distribution in individual crystals. On the macroscopic scale, it is the large number of microcrystals that make the entire sample appear more uniformly distributed in analyte.

These results suggest that densely packed smaller crystals would be statistically in favour of more uniform analyte distribution across the sample area. Since a laser beam of finite dimension is used to desorb the sample, many more crystals would be intercepted by the laser beam from densely packed crystals. Consequently, the averaged number of analyte molecules desorbed would become more even from spot to spot, resulting in better spectral reproducibility. A recent report shows that by varying the solvent conditions used in the fast solvent evaporation method, control of crystal size is achievable, making it a versatile sample preparation method for different applications including direct analysis of serum samples.[15]

Attempts to prepare the matrix crystals using the fast solvent evaporation method on a microscope slide failed. Instead, the sample morphology is similar to that prepared by the dried-droplet method. This result shows that the surface property of the sample substrate must play an important role in forming microcrystals. In contrast to the smooth surface of the glass slide, the "polished" stainless steel probe surface consists of many micro-structures from which the microcrystals are grown. The crystals grown in this manner are less susceptible to being washed away during the on-probe sample cleanup process.

Another very effective method in providing more reproducible MALDI spectral signals is the one reported by Xiang and Beavis.[1e] In this method, the matrix crystals formed on the probe are physically crushed into small crystals or particles. Then a drop of a mixture of matrix and analyte solution is placed on top of the small particle layer. The confocal image of the sample crystals prepared using the crushed-crystal method is shown in Figure 4.2G. This image again shows that the analyte is uniformly distributed on the macroscopic scale. Note that the crystal size is not uniform, but the crystals are densely packed on the sample probe surface. The crystal size is dependent on how hard the larger crystals are crushed. For analytical applications, this method is particularly useful for the detection of proteins while the fast evaporation method often gives no or small signals for these compounds.

This confocal imaging work shows that the salient feature of the fast evaporation method and the crushed-crystal method is the generation of microcrystals that contain the analyte. To produce microcrystals, the presence of nucleation sites on the sample probe may

be very important in both methods. Based on this observation and the notion that densely packed microcrystals statistically favour more uniform analyte distribution, a modified sample preparation method was developed, that is useful for routine analysis of both peptides and proteins. It involves the use of fast solvent evaporation to form small crystals (as in the first step of the fast evaporation method), followed by deposition of a mixture of matrix and analyte solution on top of the crystal layer (as in the sample/matrix deposition step of the crushed-crystal method). The confocal image of the samples prepared with this method, as shown in Figure 4.2H, revealed that the analyte is macroscopically uniformly distributed. On a microscopic level, there are regions where the analyte is more concentrated than in other regions; but, within the confocal microscopic resolution, there are essentially no regions where the matrix is without analyte. The confocal image also shows that the crystals formed are very small (less than 1 μm), uniform and densely packed. Note that the size and density of the crystals can be controlled in the modified method with the use of different solvent composition for matrix solution preparation. Also note, that success with this method is highly dependent upon the quality of the first layer. A highly polished, clean sample probe is necessary to form a uniform submicrocrystalline first layer.

A notable difference in MALDI performance between this uniform submicron-crystal formation method and the fast evaporation method is that this method provides high sensitivity and excellent spot to spot reproducibility for proteins. The enhancement is likely due to the increase of the matrix-to-analyte ratio and improved separation or reduced interaction of analyte molecules as the result of depositing the analyte solution containing matrix molecules on top of the microcrystals, instead of using only the analyte solution. Because of the enhanced sensitivity and the use of submicron crystals, optimizing the mass resolution in MALDI experiments is easier. As an example, Figure 4.3 shows a mass spectrum of trypsinogen obtained with the time-lag focusing linear instrument using a 1-m flight tube. This spectrum shows a mass resolution of 1300 fwhm with a total sample loading of 0.6 pmol of the protein.

Clearly, analyte molecules are not homogeneously distributed within each crystal in all the sample preparation techniques, except the slow crystal growth technique. Within the

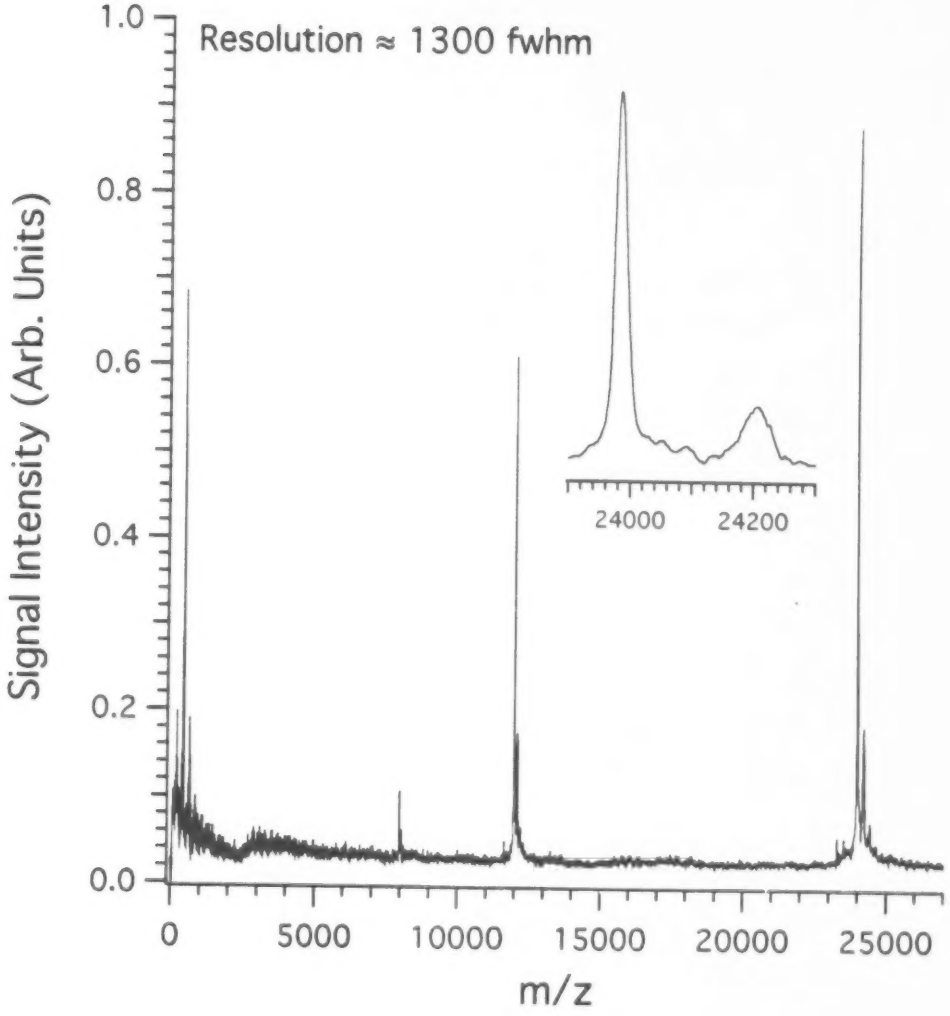

Figure 4.3 MALDI mass spectrum of trypsinogen. The sample was prepared by dissolving sinapinic acid in a solvent mixture of 39% acetone, 60% methanol, 1% of 0.1% trifluoroacetic acid (aq.) (v/v) and depositing 1 μL to the sample probe to form a thin layer of matrix crystals, followed by adding a 0.5 μL of a 1:1 mixture of 1.2 pmol/μL trypsinogen (aq.) and sinapinic acid dissolved in 30% acetonitrile, 20% methanol, 50% water (v/v) to the top of the first matrix layer.

area of the desorption laser beam however, the three microcrystalline techniques provide a more homogeneous sample distribution, statistically favoring improved shot-to-shot spectra reproducibility and sensitivity. Packing more crystals into a smaller area seems to provide improved MALDI performance. While the microcrystalline techniques provide thinner sample preparations than the dried-droplet method, this alone cannot be taken as evidence of superior MALDI performance since the slow-growth method provides good MALDI signals but also the thickest preparations.

Besides the ability to examine the analyte distribution in different sample preparation protocols, the confocal imaging approach can potentially be very useful for quantitative MALDI method development. In quantitative MALDI, an internal standard is often required. An optimal sample preparation method with an appropriate internal standard should provide coherent distribution between the standard and the analyte molecules.[2] To aid in the design of better internal standards and the development of optimal sample preparation methods, two-colour fluorescence imaging may be used to map the individual species distribution in the matrix crystals prepared with a mixture of molecules with different labelling groups. Examples of this double-labelling approach are shown in Figures 4.2I and 4.2J. The confocal microscope was used to examine matrix containing insulin-FITC (8 pmol/μL) and a tetramethylrhodamine-labelled trisaccharide (0.1 pmol/μL). The colour-coded image of the two analytes was obtained by superimposing the image from insulin-FITC (in green) with the image from the tetramethylrhodamine-labelled trisaccharide (in blue). The phase-contrast background image is represented in red. The overall image is a mixture of all three colours in varying intensities. The pink region represents the area where the phase-contrast image and tetramethylrhodamine-labelled trisaccharide image are of about equal intensity, whereas, the white areas represent about equal intensity among all three images. Figure 4.2I shows a double-labelled analyte image of samples prepared using the dried-droplet method with 2,5-dihydroxybenzoic acid as the matrix. This figure clearly shows that the two different analyte molecules are not homogeneously distributed in the matrix. One type of analyte may reside in one region of a crystal and another region of the crystal may contain the other analyte only. This is also true for microcrystals prepared with the fast evaporation method,

as illustrated in Figure 4.2J.

There is an obvious limitation to confocal imaging. The best lateral resolution, provided by the confocal instrument used, was 0.17 μm laterally and 0.54 μm vertically. Jones et al.[4] have shown, using X-ray photoelectron spectroscopy, that for the crushed-crystal method the concentration of protein near the surface of the sinapinic acid crystals is higher than in the bulk of the crystals. While, for large crystals one can distinguish between analyte in the bulk of the crystal and analyte on or near the surface, for the microcrystalline methods, crystal size approaches the resolution limitation of the confocal instrument. Therefore, one cannot distinguish between bulk and surface analyte for the microcrystalline methods with confocal microscopy.

In conclusion, confocal microscopy not only provides information on the morphology of the MALDI crystals, but also gives analyte distribution information for samples containing fluorescently-labelled analyte. This can be useful in the development of sample/matrix preparation methods for improved sensitivity or quantitation or both. Analyte distribution can be quite different among different sample preparation methods. The confocal microscopic approach can also be used to address other important questions. For example, how does an impurity affect the analyte incorporation into the matrix crystals or the analyte distribution within the crystals for a given sample preparation method? What experimental conditions are required to incorporate analyte into matrix crystals in the presence of potential MALDI interferents? In MALDI, to have the analyte located only in the area where laser desorption takes place is preferable. The confocal-microscopy method can be used to guide the development of such a method in that, for example, the analyte is only deposited onto the top layers of the matrix crystals.

4.4 Literature Cited

(1) a) Doktycz, S. J.; Savickas, P. J.; Krueger, D. A. *Rapid Commun. Mass Spectrom.* **1991**, *5*, 145-148. b) Strupat, K.; Karas, M.; Hillenkamp, F. *Int. J. Mass Spectrom. Ion Processes* **1991**, *111*, 89-102. c) Chan, T-W. D.; Colburn, A. W.; Derrick, P. J.; Gardiner, D. J.; Bowden, M. *Org. Mass Spectrom.* **1992**, *27*, 188-194. d) Preston,

L. M.; Murray, K. K.; Russell, D. H. *Biomed. Mass Spectrom.* **1993**, *22*, 544-550. e) Xiang, F.; Beavis, R. C. *Rapid Commun. Mass Spectrom.* **1994**, *8*, 199-204. f) Perera, I. K.; Perkins, J.; Kantartzoglou, S. *Rapid Commun. Mass Spectrom.* **1995**, *9*, 180-187. g) Westman, A.; Huth-Fehre, T.; Demirev, P.; Sundqvist, B. U. R. *J. Mass Spectrom.* **1995**, *30*, 206-211.

(2) Gusev, A. I.; Wilkinson, W. R.; Proctor, A.; Hercules, D. M. *Anal. Chem.* **1995**, *67*, 1034-1041.

(3) Beavis, R. C.; Bridson, J. N. *J. Phys. D: Appl. Phys.* **1993**, *26*, 442-447.

(4) Jones, D. S.; Robinson, K. S.; Thompson, S. P.; Humphrey, P. In *Proceedings of the 43rd ASMS Conference on Mass Spectrometry and Allied Topics*; Atlanta, GA, May 21-26, 1995; p 692.

(5) Li, L.; Golding, R. E.; Whittal, R. M. "Single Cell Analysis by Mass Spectrometry", submitted.

(6) King, R. C.; Owens, K. G. In *Proceedings of the 42nd ASMS Conference on Mass Spectrometry and Allied Topics*; Chicago, IL, May 29-June 3, 1994; p 977.

(7) Brakenhoff, G. J.; Van der Voort, H. T. M.; Oud, J. L. In *Confocal Microscopy*; T. Wilson, Ed.; Academic Press: San Diego, CA, 1990; pp 185-197.

(8) Inoue, S. In *Handbook of Biological Confocal Microscopy*; J. B. Pawley, Ed.; Plenum Press: New York, 1989; pp 1-14.

(9) Whittal, R. M.; Li, L. *Anal. Chem.* **1995**, *67*, 1950-1954.

(10) a) Zhao, J. Y.; Dovichi, N. J.; Hindsgaul, O.; Gosselin, S.; Palcic, M. M. *Glycobiology* **1994**, *4*, 239-242. b) Zhang, Y.; Le, X.; Dovichi, N. J.; Compston, C. A.; Palcic, M. M.; Diedrich, P.; Hindsgaul, O. *Anal. Biochem.* **1995**, *227*, 368-376.

(11) Karas, M.; Hillenkamp, F. *Anal. Chem.* **1988**, *60*, 2299-2301.

(12) Vorm, O.; Roepstorff, P.; Mann, M. *Anal. Chem.* **1994**, *66*, 3281-3287.

(13) Haugland, R. P. *Handbook of Fluorescent Probes and Research Chemicals;* 5th ed.; Molecular Probes Inc.: Eugene, OR, 1992, p 421.

(14) Weinberger, S. R.; Böernsen, K. O.; Finchy, J. W.; Robertson, V.; Musselman, B. D. In *Proceedings of the 41st ASMS Conference on Mass Spectrometry and Allied Topics*; San Francisco, CA, May 31-June 4, 1993; pp 775a-b.

(15) Whittal, R. M.; Palcic, M. M.; Hindsgaul, O.; Li, L. *Anal. Chem.* **1995**, *67*, 3509-3514.

Chapter 5

Direct Analysis of Enzymatic Reactions of Oligosaccharides in Human Serum Using Matrix-Assisted Laser Desorption/Ionisation Mass Spectrometry[a]

5.1 Introduction

Mass spectrometry using fast atom bombardment, electrospray, and matrix-assisted laser desorption/ionisation (MALDI) has recently been developed for the analysis of products of enzymatic reactions in biological fluids. For example, fast atom bombardment mass spectrometry is reported for analysis of endogenous met-enkephalin and β-endorphin from their respective precursors in human cerebrospinal fluid[1] and dynorphin A, dynorphin B and α-neodynorphin from the prodynorphin precursor in human pituitary.[2] More recently, MALDI time-of-flight mass spectrometry is shown as an effective method for mass analysis of the products of in vitro processing involving dynorphin A[3] and cyclosporin A[4] in human blood and neuropeptide Y in human cerebrospinal fluid.[5] Electrospray mass spectrometry is used as an assay for peptidyl-α-hydroxyglycine α-amidating lyase enzyme.[6] Although these techniques require an extensive sample cleanup (except that of Costello et al.[5]) through extraction, filtration, or chromatographic separation, the mass spectrometric approach provides high molecular specificity for the identification of the reaction products.

Reported herein is the development of an MALDI method for the rapid and sensitive

---

[a] A form of this chapter has been published as: R. M. Whittal, M. M. Palcic, O. Hindsgaul, L. Li "*Direct Analysis of Enzymatic Reactions of Human Serum Using Matrix-Assisted Laser Desorption Ionization Mass Spectrometry*" *Anal. Chem.* **1995**, *67*, 3509-3514. The enzyme assays were done by Professor M. M. Palcic and Ms. C. Compston. The synthesis of the tetramethylrhodamine-labelled saccharides was done by Professor O. Hindsgaul's research group.

detection of the product of a glycosyltransferase enzyme reaction. Blood group-B galactosyltransferase enzyme occurs naturally in the serum of blood group B individuals. This enzyme transfers a galactose residue from uridine diphosphogalactose (UDP-Gal) in α-linkage to OH-3 of the galactose residue in oligosaccharide chains ending in the sequence αFuc(1→2)βGal producing the blood group-B antigenic determinant αFuc(1→2)[αGal(1→3)]βGal. This is an ideal model system for the development of sensitive assays for the product(s) of enzymes involved in oligosaccharide biosynthesis and/or degradation since this enzyme is present in very low abundance in an extremely crude sample: human serum. Serum of individuals lacking this enzyme activity, e.g., blood group O or A individuals, is additionally available as a control.

This fast MALDI assay represents one of the so-called mass tracer methods currently being developed. By analogy to well-established radioassay tracer and fluorescent tracer techniques, mass tracer methods are based on mass spectrometry for monitoring chemical, enzymatic, or other changes in biological systems, with no or minimum sample preparation. In the MALDI method, an appropriate functional group is linked to the target molecules and then MALDI is used to follow the transformation of the labelled molecular species. After experimenting with different labelling groups, it was found that tetramethylrhodamine derivatives of oligosaccharides are ~100-fold more sensitive than underivatized oligosaccharides. Moreover, a sample preparation method was developed for mixing samples and matrix for on-probe sample cleanup. With this method, salts, buffers, and other potential interfering contaminants in serum are washed away, and yet the tetramethylrhodamine labelled species are selectively retained on the sample probe.

5.2 Experimental

5.2.1 Preparation of labelled oligosaccharides. Chart 1 lists the structures and their respective abbreviation for the labelled oligosaccharides that pertain to this work. Le^b-OCH_3, Le^b-MCO[7], αFuc(1→2)βGal-MCO (disac-MCO), and αFuc(1→2)[αGal(1→3)]βGal-MCO (B-MCO)[8] were available from earlier work. The conversion of MCO glycosides to their tetramethylrhodamine derivatives was carried out as previously described.[9]

Chart 1

Structure	Abbreviation
αFuc(1→2)βGal —	disac-
αFuc(1→2)[αGal(1→3)]βGal —	B-
αFuc(1→2)βGal(1→3)[αFuc(1→4)]βGlcNAc —	Le^b-
-O-$(CH_2)_8COOCH_3$	-MCO
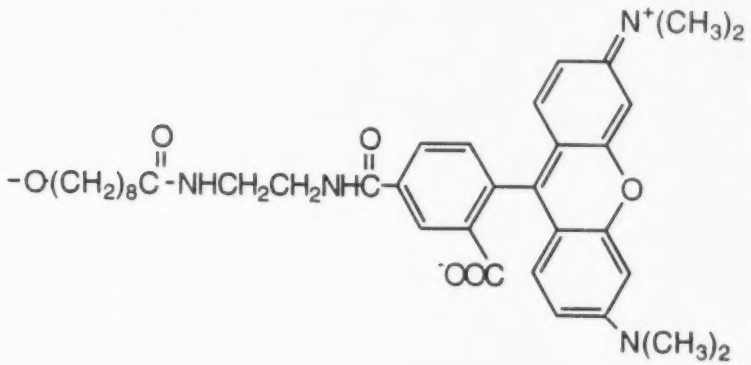	-TMR

5.2.2 Enzyme reactions. 5 nmol of αFuc(1→2)βGal-TMR (acceptor) in aqueous solution at 1 mg mL^{-1} was added to an Eppendorf tube and lyophilised to dryness. After drying, 50 μL of human serum (blood group B), 2 μL of 2.5 mM UDP-Gal (donor), 0.6 μL of 0.5 M $MnCl_2$, and 5 μL of 0.5 M sodium cacodylate buffer (pH 7.1) were added. The mixture was incubated at 37°C for 90 min and an aliquot was used to check for the presence of the product through MALDI analysis. The introduction of the tetramethylrhodamine substituent has a minor affect on the galactosyltransferase reaction, under the conditions employed for the in vitro conversion, the rate of reaction is 90% of the parent αFuc(1→2)βGal-$O(CH_2)_7CH_3$ by standard radiochemical assay methods.[10]

A 15 μL aliquot of the incubated serum was added to a C-18 SepPak, washed with water, eluted with methanol, and lyophilised to dryness in an Eppendorf tube. To this was added 30 μL of 100 mM citrate buffer at pH 5.0. To half of this solution was added 0.15

units of Limpet sulphatase type V for a total volume of 16.5 μL. To the other half was added 0.14 units of Abalone sulphatase type VIII for a total volume of 16 μL. The vials were incubated at 37°C for 120 min. An aliquot was used for MALDI analysis.

5.2.3 MALDI sample preparation. All nonserum samples were prepared for MALDI analysis using the dried-droplet method of sample preparation (see for example Hillenkamp et al.[11]). 2,5-Dihydroxybenzoic acid matrix solution was prepared at a concentration of 10 mg mL^{-1} in 30% acetonitrile/water (v/v). α-Cyano-4-hydroxycinnamic acid matrix solution was prepared as a saturated solution (~7 mg mL^{-1}) in 30% acetonitrile/water (v/v). The matrix solutions were mixed on a vortex mixer for 1 min and then centrifuged to remove undissolved matrix crystals. A 0.5 µL aliquot of matrix solution and 0.5 to 1.0 µL of analyte solution were placed on the sample probe and allowed to dry.

For samples analysed from buffered human serum, α-cyano-4-hydroxycinnamic acid was used as the matrix. The matrix solution was prepared at a concentration of 20 mg mL^{-1} in 70% acetonitrile/water (v/v). A 0.5 µL aliquot of matrix solution was applied to the probe tip and allowed to dry. The high-concentration matrix solution produced a dense layer of matrix on the sample probe of ~2 mm diameter giving a surface density of 17 nmol mm^{-2}. The serum sample was diluted in half with 50% ethanol/water (v/v). On top of the matrix, 0.5 to 1.0 µL of the serum supernatant was applied. Just before the sample dries (~1 min), the probe tip is dipped into pure room-temperature water for 45 s. Excess water was removed by gently touching a wiper to the edge of the sample probe. Washing the probe tip just before the sample dries proved more effective at removing the high concentration of buffers and other species present in serum. The washed probe tip was then inserted into the mass spectrometer.

5.2.4 Time-of-flight mass spectrometry. A linear, time-lag focusing time-of-flight mass spectrometer was used to collect all mass spectra. The MALDI instrument was designed and constructed at the University of Alberta. A detailed description of this system is given in Chapter 2. In brief, it consists of an acceleration region containing a repeller plate and an ion extraction plate to which 12 kV voltages are applied. After the laser desorption/ionisation takes place, a pulse voltage (1 kV) is applied to the repeller for ion

extraction. The time delay between the ionisation and ion extraction events was optimized at 280 ns and used throughout the work presented herein. The total flight tube length is about 1 m. A nitrogen laser (Photochemical Research Associates LN1000) was used to generate the MALDI ions. The mass spectrum was captured using either a LeCroy 9310M or 9350M digital oscilloscope. The major difference is the sampling rate. The 9350M scope provides a sampling rate of up to $1x10^9$ samples/s or a time resolution of 1 ns/point whereas the 9310M scope has a time resolution of 10 ns/point. High-resolution mass spectra were collected on the 9350M oscilloscope. All mass spectra are the result of signal averaging of 100 laser shots. Signal averaging was done on the oscilloscope without selection. The averaged mass spectrum was then downloaded to a computer for processing.

5.3 Results and Discussion

Underivatized oligosaccharides can be ionised by MALDI.[12] However, the limit of detection for underivatized carbohydrates is 100 fmol (for reference standards in clean samples), which is higher than that obtained for peptides of similar mass.[13] For direct analysis of reaction products in serum, the sensitivity of MALDI needs to be improved. Peracetylation of neutral oligosaccharides enhances the sensitivity 10-fold[13] and permethylation enhances the sensitivity of glycolipids 100-fold.[14] After experimenting with different labelling groups, it was found that tetramethylrhodamine derivatives of oligosaccharides are ~100-fold more sensitive than underivatized oligosaccharides.

Figure 5.1 shows the MALDI mass spectrum of a mixture of three derivatives of a model Le^b blood group active tetrasaccharide: 10 pmol of Le^b-OCH_3 (a simple methyl glycoside derivative), 1 pmol of Le^b-MCO (a more lipophilic derivative with an 8-methoxycarbonyloctyl aglycone) and 0.2 pmol of Le^b-TMR (with the tetramethylrhodamine label attached to the MCO group). The spectra shown in Figure 5.1 are obtained using 2,5-dihydroxybenzoic acid as the matrix. 2,5-Dihydroxybenzoic acid is a superior matrix for the analysis of neutral oligosaccharides among several substituted benzoic acids, cinnamic acids and coumarins, including α-cyano-4-hydroxycinnamic acid and 3-amino-4-hydroxybenzoic acid.[13] The neutral oligosaccharides in the spectrum show two peaks due to cationisation with both sodium and potassium. The peak observed for Le^b-TMR arises from protonation

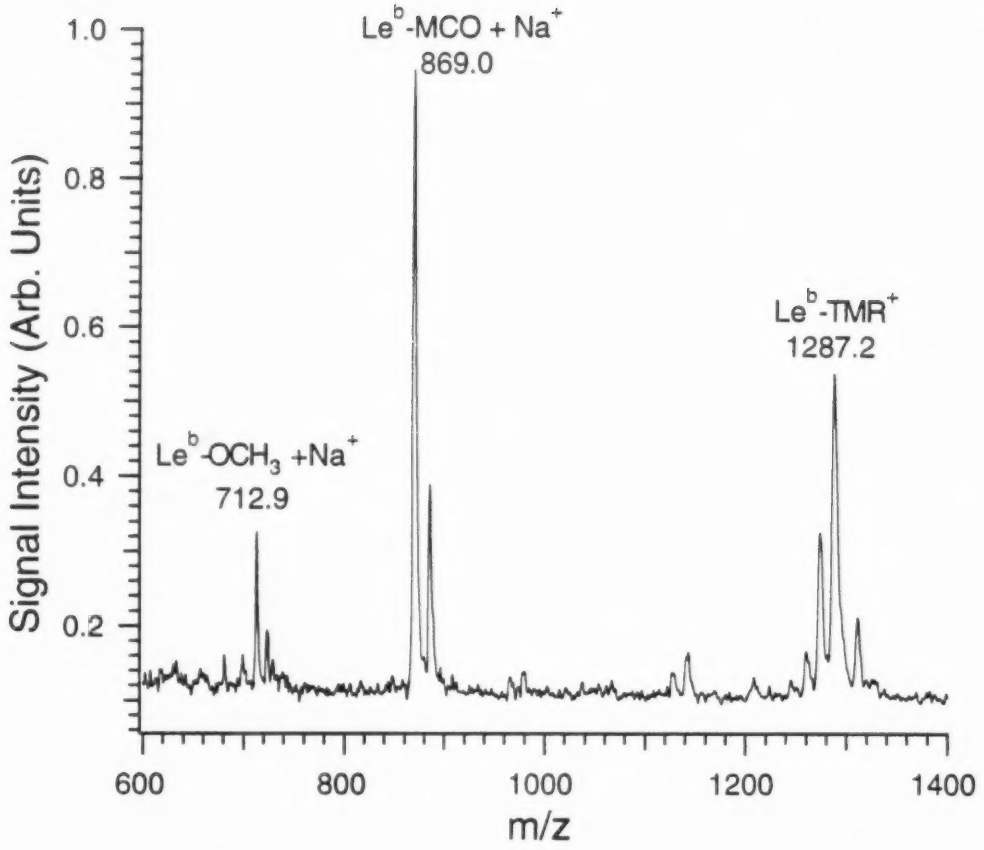

Figure 5.1 MALDI mass spectrum of a mixture of three derivatives of an oligosaccharide using 2,5-dihydroxybenzoic acid as the matrix: 10 pmol Le^b-OCH_3, 1 pmol Le^b-MCO and 0.2 pmol Le^b-TMR.

of the tetramethylrhodamine zwitterion, although at this time it is unknown whether protonation occurs in the gas phase or if the tetramethylrhodamine ion is desorbed preformed (see Chart 1). There is also a predominant peak (at M-14) possibly due to the loss of CH_2 from tetramethylrhodamine. The signal-to-background-noise ratios for Le^b-OCH_3, Le^b-MCO and Le^b-TMR are 21, 82 and 42, respectively. The mass spectra obtained from more concentrated or more dilute solutions of the mixture used in Figure 5.1 display similar relative responses. Le^b-TMR is generally about 2-3-fold more sensitive than Le^b-MCO and 100-fold more sensitive than Le^b-OCH_3 with 2,5-dihydroxybenzoic acid.

The cinnamic acid derivative α-cyano-4-hydroxycinnamic acid can also provide good MALDI spectra for the tetramethylrhodamine-labelled oligosaccharides. Figure 5.2 shows the MALDI spectrum of 0.2 pmol of Le^b-TMR acquired using α-cyano-4-hydroxycinnamic acid as the matrix. The peak at (M-14) intensifies and additional fragment peaks are observed at m/z 1142.5 (loss of fucose) and 981.5 (loss of fucose and galactose). This finding is not surprising considering that others have noted fragmentation increases with α-cyano-4-hydroxycinnamic acid in reflectron time-of-flight systems.[15] Fragmentation can take place during the time-lag period (280 ns). Figure 5.2 also shows that the signal-to-background-noise ratio improves to 60, a 50% improvement over 2,5-dihydroxybenzoic acid. On the other hand, for Le^b-OCH_3 and Le^b-MCO the signal-to-background-noise ratio drops below three if the same quantity of neutral oligosaccharide is loaded as in Figure 5.1. Several other tetramethylrhodamine-labelled oligosaccharides have been examined and similar results are obtained. In general, with a sample loading between 100-200 fmol or a concentration of 100-200 fmol μL^{-1}, a well defined molecular ion signal (analyte signal-to-background-noise ratio >50) can be obtained for tetramethylrhodamine-labelled species using α-cyano-4-hydroxycinnamic acid.

To analyse these labelled species in a buffered serum sample, sample/matrix preparation becomes very important. The MALDI technique is known to tolerate salts and buffers to some extent. This is particularly true for peptide and protein analysis.[11] The dried droplet method of preparing matrix crystals followed by on-probe sample washing is a simple technique, but often not effective in removing a high concentration of contaminants.

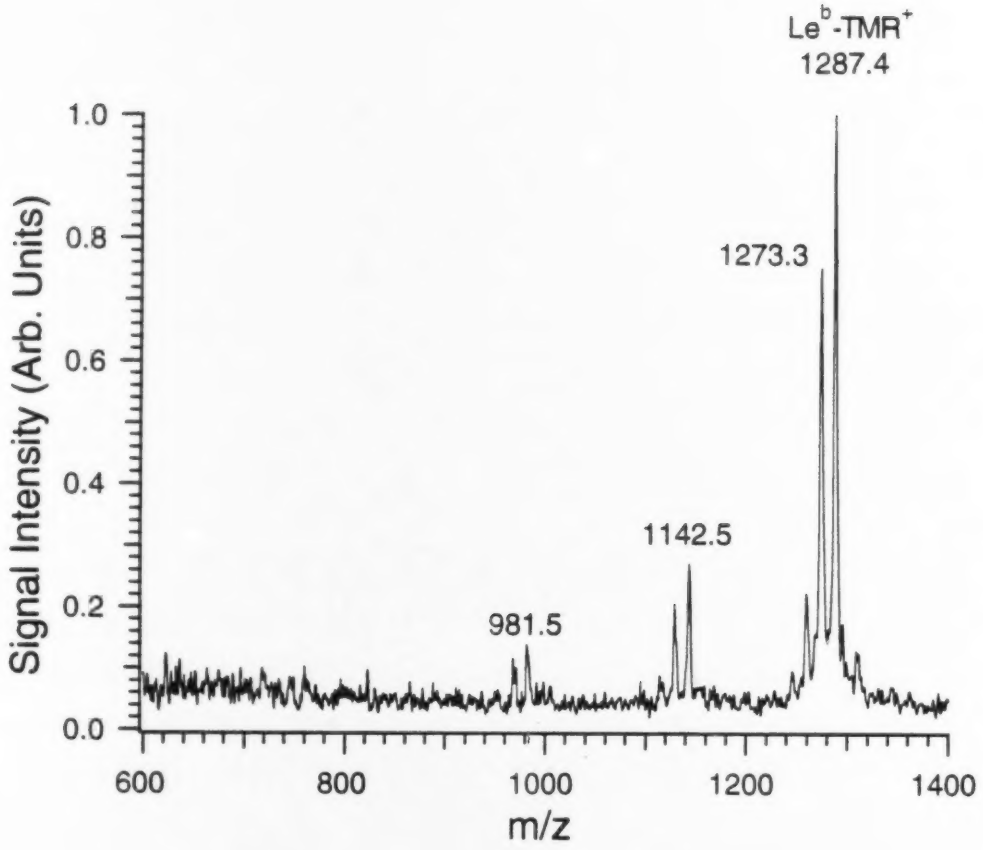

Figure 5.2 MALDI mass spectrum of 0.2 pmol Le^b-TMR obtained using α-cyano-4-hydroxycinnamic acid as the matrix.

For buffered serum, the dried droplet method using either 2,5-dihydroxybenzoic acid or α-cyano-4-hydroxycinnamic acid fails to form crystals and a spectrum of only background noise is obtained (not shown). Several other methods are reported to wash away potential interfering contaminants on the probe. In particular, the fast evaporation method of Vorm et al.[16] and the pressed crystal sample cleanup method developed by Xiang and Beavis[17] are effective for removing salts and glycerol from peptide and protein samples. However, using these methods, positive results are not obtained for analysing oligosaccharides in buffered serum. For all of the matrices tested, the underlying matrix layer completely redissolves upon deposition of sample and does not recrystallise.

A two-step sample preparation method was developed, which is a modification of the method described by Vorm et al.,[16] to analyse labelled oligosaccharides in serum. In preparing the matrix layer on the probe, a high surface density of matrix is necessary to prevent the complete redissolution of the matrix layer when serum is added. Deposition of α-cyano-4-hydroxycinnamic acid from a 20 mg mL^{-1} 70% acetonitrile solution gives small matrix crystals and a high surface density (17 $nmol/mm^2$). To prepare the analyte, an aliquot of serum is diluted with an equal amount of 50% ethanol/water (v/v), which precipitates some serum proteins. This is an effective first step in the sample analysis procedure, since, proteins cannot be readily washed away from the matrix/analyte mixture on the sample probe. The supernatant is then deposited directly on top of the matrix layer. The matrix layer partially redissolves, then recrystallises presumably entrapping the analyte. On-probe sample washing then follows. Note that matrices, such as 2,5-dihydroxybenzoic acid, that have a high solubility in aqueous solution are unsuccessful with this approach.

For the analysis of the labelled oligosaccharides from serum, this method is facile and effective for removing salts and other contaminants in serum. As an example, Figure 5.3 shows the MALDI spectrum of a mixture of 30 pmol of Le^b-OCH_3, 10 pmol of Le^b-MCO, and 0.5 pmol Le^b-TMR spiked into human serum with buffers and other reagents added. Of the three oligosaccharides loaded, only Le^b-TMR (m/z 1287.4) is detected from this buffered serum sample with a signal-to-background-noise ratio of 11. Therefore, the signal-to-background-noise ratio for serum samples decreases by a factor of 14 over the nonserum

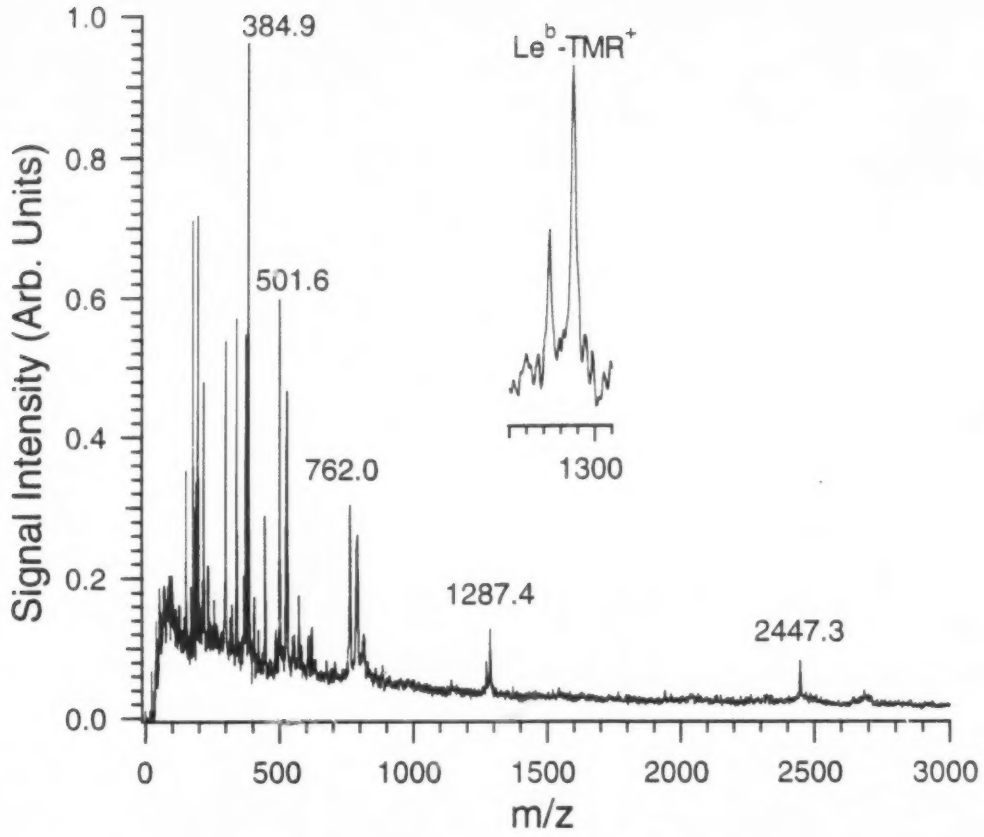

Figure 5.3 MALDI mass spectrum of a mixture of 30 pmol Le^b-OCH_3, 10 pmol Le^b-MCO, and 0.5 pmol Le^b-TMR spiked into human serum with buffers and other reagents added. α-Cyano-4-hydroxycinnamic acid is used as the matrix with the new sample/matrix preparation method. Le^b-TMR is the only oligosaccharide derivative observed. The inset graph is an expansion of the peak at m/z 1287.4.

samples. Peaks are observed at 384.9, 501.6, 762.0 Da and there is also a weaker peak at 2447.3 Da. These peaks are from unidentified serum components. Other tetramethylrhodamine-labelled di-, tri-, and tetrasaccharides have also been studied and similar findings are obtained. Note that the tetramethylrhodamine derivatives are very soluble in water, whereas α-cyano-4-hydroxycinnamic acid is not. The tetramethylrhodamine derivatives may preferentially either form cocrystals with the matrix or adsorb onto the matrix crystals. During the sample washing step, salts, buffers, and other potential contaminants are effectively washed away. In the example of Figure 5.3, Le^b-OCH_3 and Le^b-MCO may also be washed away. This illustrates that by properly designing the label group in conjunction with an optimal sample/matrix preparation protocol, selective analyte retention and ionisation can be achieved.

High mass measurement accuracy is essential for unambiguous identification of chemical species based on molecular weight information. In MALDI, the presence of impurities in a sample can potentially degrade the mass resolution and mass accuracy. Thus, an ideal sample preparation method must remove interfering contaminants that would reduce mass accuracy. The mass measurement accuracy for the detection of oligosaccharides was investigated using the time-lag focusing linear time-of-flight mass spectrometer. Figure 5.4A shows the molecular ion region of the MALDI mass spectrum of the blood group B active tetramethylrhodamine-labelled trisaccharide (B-TMR) obtained with a pure reference sample using the 1 gigasample/s digitizer (LeCroy 9350M oscilloscope). The total sample loaded is 200 fmol or 1.0 μL of a sample solution with a concentration of 2×10^{-7} M. As Figure 5.4A illustrates, the isotope peaks are well resolved. With a signal-to-background-noise ratio of 34 for the major isotope peak, the mass resolution is 2600 fwhm. The theoretical exact mass of B-TMR is 1099.50 Da. The measured mass of the monoisotopic peak utilizing a two point external calibration is 1099.45 Da; thus, the error in mass measurement is 46 ppm. For comparison, the mass spectrum of B-TMR obtained from buffered serum, using the sample preparation method described above, is shown in Figure 5.4B. To maintain a comparable signal to background ratio, B-TMR is spiked into human serum to a concentration of 6×10^{-7} M. One microlitre of the sample is loaded to the probe, followed by washing. The MALDI

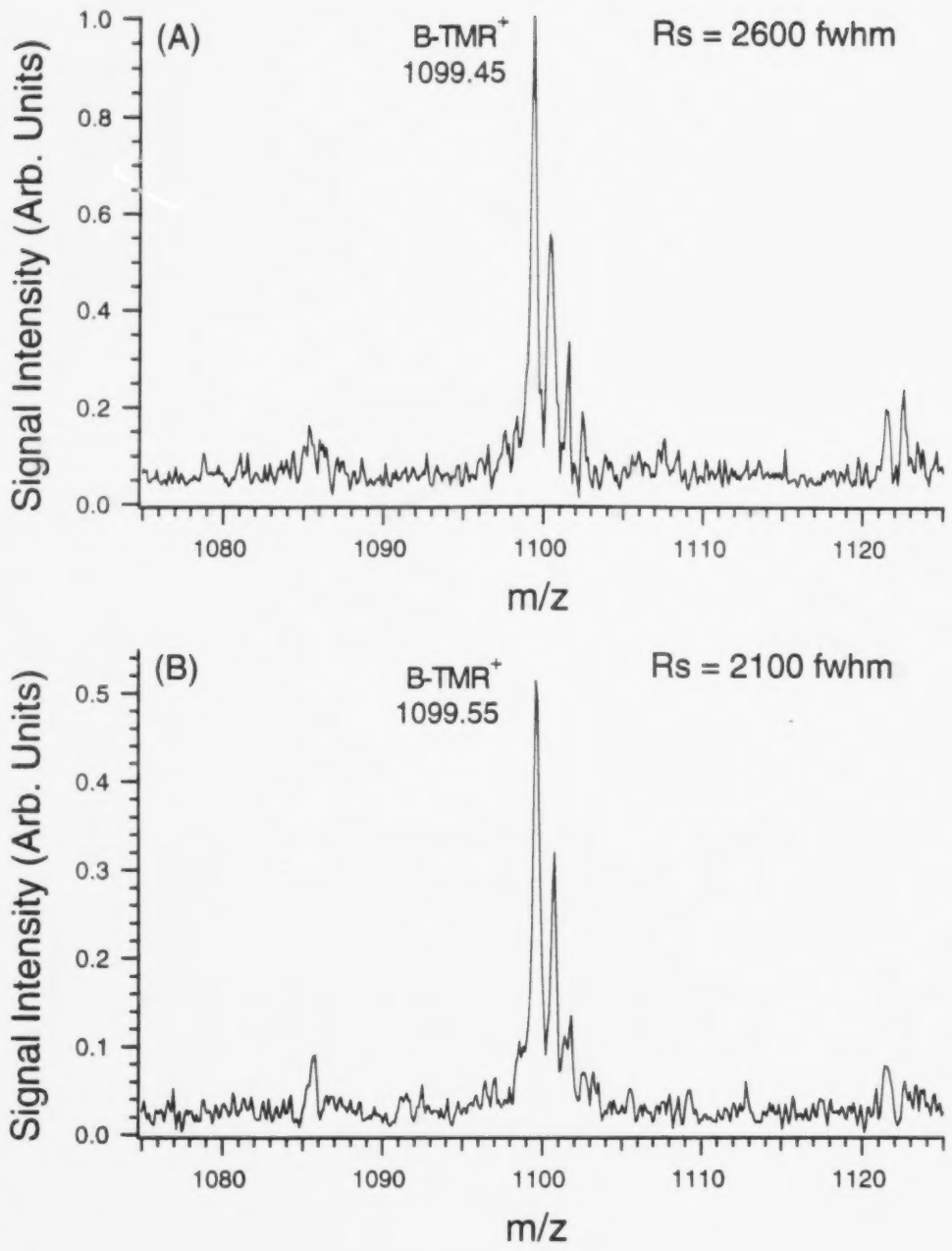

Figure 5.4 MALDI mass spectra of B-TMR obtained with A) a pure sample and B) from buffered serum spiked with B-TMR. α-Cyano-4-hydroxycinnamic acid is used as the matrix with the new sample/matrix preparation method. Spectra collected with a 1ns/point digitizer. The theoretical exact mass of B-TMR is 1099.497 Da.

spectrum shown in Figure 5.4B has a mass resolution of 2100 fwhm. The observed mass of the monoisotopic peak is 1099.55 Da giving an error in mass measurement of 52 ppm using a two point external calibration. More generally, repeat measurements (n = 8) show a mass accuracy of 50±20 ppm. The calibrants used for Figure 5.4 are disac-TMR and Le^b-TMR dissolved in water at a concentration of 1×10^{-6} M. This example shows that there is a degradation in mass resolution between the pure reference sample and the buffered serum sample, but not to the point where mass accuracy suffers.

Direct monitoring of the in vitro αGal(1→3)transferase (blood group B galactosyl transferase) enzyme reaction is accomplished using this MALDI analysis technique. This enzyme uses UDP-Gal as the donor and αFuc(1→2)βGal-TMR (disac-TMR) as the acceptor to produce B-TMR. A known amount of disac-TMR (5 nmol in 57.6 μL of serum solution) along with sodium cacodylate buffer (45 mM, pH 7.1) and manganese chloride (5 mM) are added to the serum. The mixture is incubated for 90 min. Figure 5.5A shows the MALDI spectrum when no UDP-Gal donor is added to the incubation. As expected, a product ion is not present in this spectrum. The peak at m/z 938.1 and 960.0 are the molecular ions of the starting material disac-TMR due to protonation and sodium cationisation, respectively. The peak at m/z 1039.4 is found only in the incubated samples. The origin of this peak is unknown. Figure 5.5B shows the spectrum taken when 5 nmol of UDP-Gal donor is added to the starting mixture and it is incubated for 90 min. A new peak appears at 1100.3 Da. B-TMR is the expected reaction product from the transferase enzyme reaction with a theoretical average mass of 1100.2 Da. For the B-TMR peak the signal-to-background-noise ratio is 3.

This example illustrates that the MALDI technique can be used for monitoring an enzymatic reaction directly from crude serum without the use of traditional time-consuming separation processes. While this enzymatic reaction can be studied by other tracer techniques, the mass spectrometric technique shown here provides chemical identification. In monitoring an enzymatic reaction in a biological sample, there are concerns that the reaction conditions used, or the presence of other unanticipated enzymes, may change the course of the reaction of interest. For example, for the incubation analysed in Figure 5.5, fucosidase catalysed hydrolysis of the starting material may take place to form free fucose

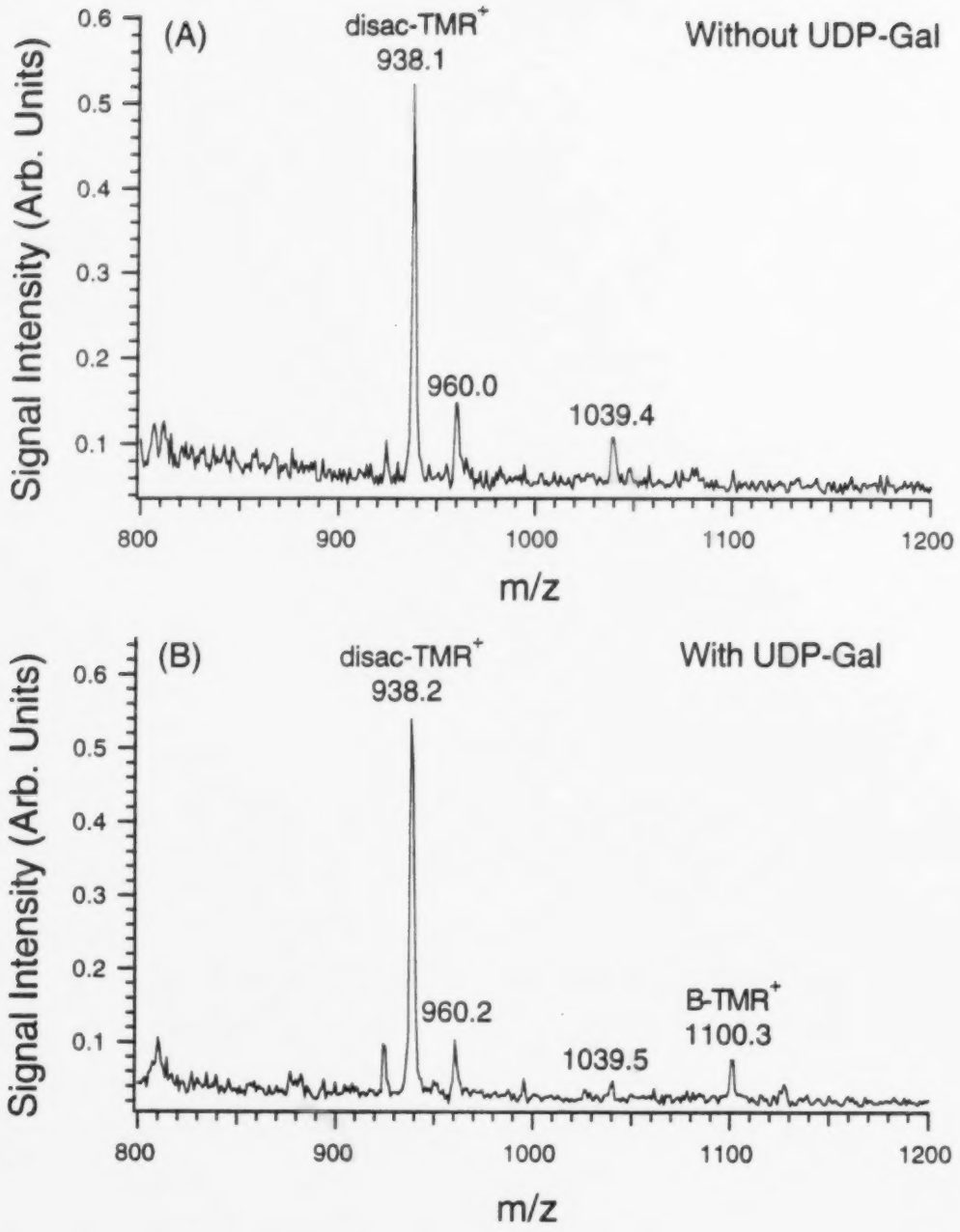

Figure 5.5 MALDI for monitoring the αGal(1→3) transferase enzyme reaction in vitro. MALDI mass spectra of the serum samples after a 90-min incubation with no UDP-Gal donor added (A) and with UDP-Gal donor added (B) α-cyano-4-hydroxycinnamic acid is used as the matrix with the new sample/matrix preparation method.

and the tetramethylrhodamine-labelled monosaccharide βGal-TMR. Radiochemical assay methods would not detect this hydrolysis. High-performance liquid chromatography would also fail to identify the products unless mass spectrometry is used for detection. Further investigation of the unknown peak was undertaken. Figure 5.6A is the MALDI spectrum of the disac-TMR incubated with serum for 90 min at 37°C, collected using the high-resolution oscilloscope (Lecroy 9350M). In addition to the disac-TMR$^+$ peak, there is a peak 102.0 mass units higher. Two possible compounds that could be products with this mass are (disac-TMR + SO_3Na - H) and (disac-TMR + PO_3HNa - H). A sulphate product would give a peak 102.05 mass units higher while a phosphate product would give a peak 101.97 mass units higher. This small mass difference cannot be confidently distinguished as the difference corresponds to 1 ns or one data point on the digitizer. However, if the sample is then incubated with Limpet sulphatase type V, the peak at 102.0 mass units higher than the disac-TMR disappears (Figure 5.6B), suggesting that the unknown peak is a sulphate product. The peak also disappears if the sample is incubated with Abalone sulphatase type VIII. The position to which the sulphate is attached cannot be determined from the spectrum. This points to a limitation of the MALDI technique with the current setup. MALDI combined with MS/MS can provide some structural information. For example, phosphate is easily distinguished from sulphate.[18] Additionally, one can determine to which saccharide the sulphate is attached (the fucose or the galactose for the disac-TMR) but still not be able to determine the position of the sulphate on that saccharide.[19]

An ideal mass tracer method should provide quantitative information rapidly. Quantitative information, about the reaction product(s), can be provided with MALDI if an internal standard is used.[4,13,20] To quantify the yield of B-TMR formed in Figure 5.5 a calibration curve was generated using the relative signal intensity of B-TMR with respect to the signal intensity of Le^b-TMR. The disac-TMR ion intensity was not used since the concentration of disac-TMR changes during incubation. To develop the calibration curve, shown in Figure 5.7, B-TMR and Le^b-TMR are spiked to buffered human serum and analysed. The concentration of B-TMR was varied between 0.22 and 2.1 pmol μL^{-1} while the concentration of Le^b-TMR was fixed at 2.1 pmol μL^{-1}. The relative intensity of the

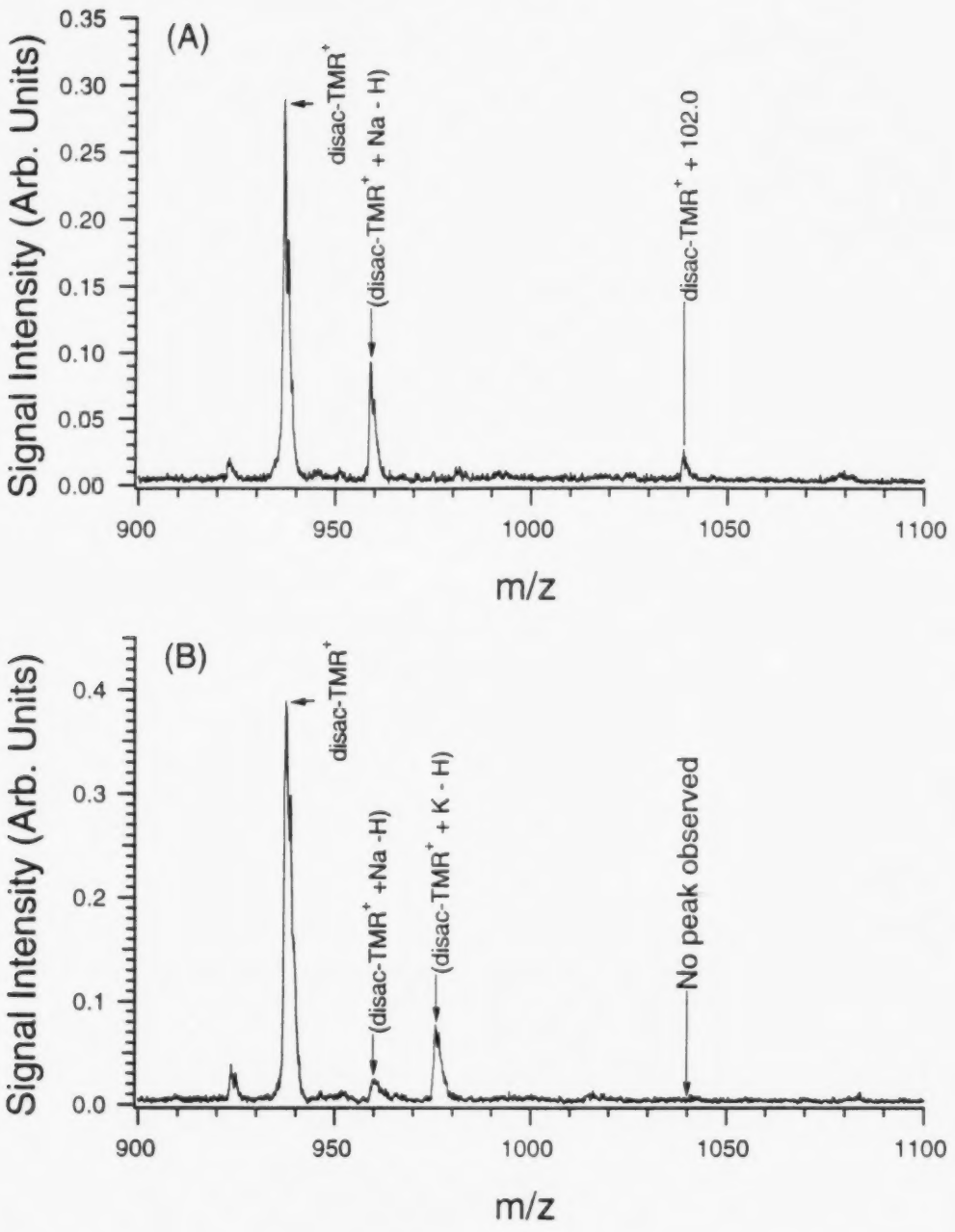

Figure 5.6 MALDI spectra of the acceptor disac-TMR after a 90-min incubation in human serum. (A) An unexplained peak appears at 102.0 mass units above the disac-TMR$^+$ peak. (B) After a 120 min incubation of the sample in (A) with Limpet sulphatase, the unexplained peak disappears.

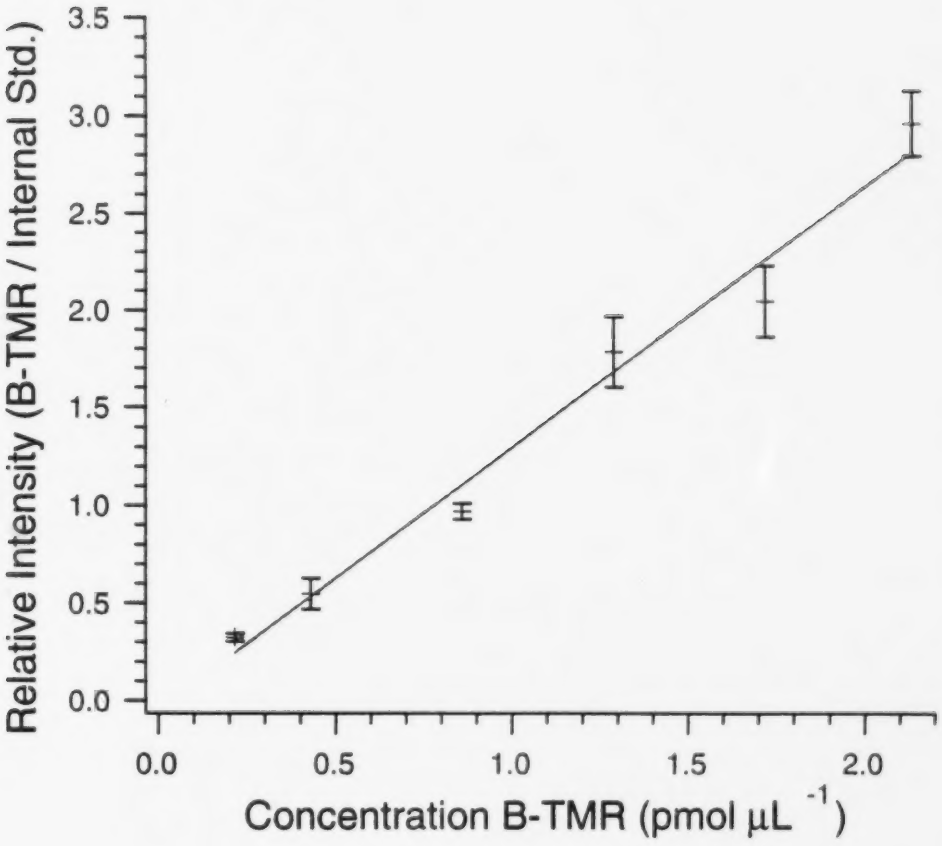

Figure 5.7 Calibration curve for quantitation of B-TMR product. The peak intensity of B-TMR is measured relative to Le^b-TMR. The error bars represent ±2 SD for five samples at each concentration.

molecular ion peak of B-TMR to Le^b-TMR is plotted as a function of B-TMR concentration. A linear response is obtained (r=0.99). The error bars represent ± two SD for five samples at each concentration. For the sample analysis, Leb-TMR is spiked to the sample followed by immediate MALDI analysis. From the calibration curve, the concentration of B-TMR formed after the 90 min incubation of disac-TMR is 0.50±0.09pmol μL^{-1} or a total product yield of 29±5 pmol. Also, from the calibration curve the concentration detection limit of B-TMR in human serum can be estimated as 0.11 pmol μL^{-1} (detection limit defined as 3 SD of the background signal level / sensitivity).

Note that the ability to do analyte quantitation directly from a crude sample as illustrated in this example is very significant. This method averts the problems of possible sample loss or quantitative variations often associated with conventional sample cleanup, extraction, and chromatographic procedures. In addition, the calibration curve can be constructed in a much shorter time. A detailed investigation on the quantitative aspect of this mass tracer method should be completed in the future. In particular, the linear dynamic range and the rational selection of internal standards in the calibration curve method should be studied. The possibility of using standard addition for quantitation should also be investigated. In addition, a correlation study between the MALDI work and other quantitative methods should be carried out to establish the validity of the MALDI quantitation method.

In summary, a tracer method based on the MALDI technique for the assay of glycosyltransferases in human serum was developed. This rapid, sensitive, and molecular specific detection system should be useful for reaction monitoring and enzyme kinetic studies of oligosaccharides from crude samples including crude cell tissue and organ extracts. This work also shows the importance of the molecular structure or other physical and chemical properties of the analyte on sample preparation or crystal formation in MALDI. Further investigation of this phenomenon in the future is anticipated to design better mass tracers and extend this work to other biomolecules.

5.4 Literature Cited

(1) Liu, D.; Wood, G. W.; Desiderio, D. M. *J. Chromatogr.* **1990**, *530*, 235-252.

(2) Silberring, J.; Brostedt, P.; Thornwall, M.; Nyberg, F. *J. Chromatogr.* **1991**, *554*, 83-90.

(3) Chou, J. Z.; Kreek, M. J.; Chait, B. T. *J. Am. Soc. Mass Spectrom.* **1994**, *5*, 10-16.

(4) Muddiman, D. C.; Gusev, A. I.; Proctor, A.; Hercules, D. M.; Venkataramanan, R.; Diven, W. *Anal. Chem.* **1994**, *66*, 2362-2368.

(5) Costello, C. E.; Juhasz, P.; Ekman, R.; Heilig, M.; Ågren, H. In *Proceedings of the 42nd ASMS Conference on Mass Spectrometry and Allied Topics*; Chicago, IL, May 29-June 3, 1994; p 25.

(6) Unsworth, E. J.; Treston, A. M. In *Proceedings of the 42nd ASMS Conference on Mass Spectrometry and Allied Topics*; Chicago, IL, May 29-June 3, 1994; p 154.

(7) Spohr, U.; Morishima, N.; Hindsgaul, O.; Lemieux, R. U. *Can. J. Chem.* **1985**, *63*, 2664-68.

(8) Lemieux, R. U. *Chem. Soc. Rev.* **1978**, *7*, 423-452.

(9) a) Zhao, J. Y.; Dovichi, N. J.; Hindsgaul, O.; Gosselin S.; Palcic, M. M. *Glycobiol.ogy* **1994**, *4*, 239-242. b) Zhang, Y.; Le, X.; Dovichi, N. J.; Compston, C. A.; Palcic, M. M.; Diedrich, P.; Hindsgaul, O. *Anal. Biochem.* **1995**, *227*, 368-376.

(10) Palcic, M. M.; Heerze, L. D.; Pierce, M.; Hindsgaul, O. *Glycoconjugate J.* **1988**, *5*, 49-63.

(11) Hillenkamp, F.; Karas, M.; Beavis, R. C.; Chait, B. T. *Anal. Chem.* **1991**, *63*, 1193A-1203A.

(12) Stahl, B.; Steup, M.; Karas, M.; Hillenkamp, F. *Anal. Chem.* **1991**, *63*, 1463-1466.

(13) Harvey, D. J. *Rapid Commun. Mass Spectrom.* **1993**, *7*, 614-619.

(14) Juhasz, P.; Costello, C. E. *J. Am. Soc. Mass Spectrom.* **1992**, *3*, 785-796.

(15) Karas, M.; Bahr, U.; Ehring, H.; Strupat, K.; Hillenkamp, F. In *Proceedings of the 42nd ASMS Conference on Mass Spectrometry and Allied Topics*; Chicago, IL, May 29-June 3, 1994; p 7.

(16) Vorm, O.; Roepstorff, P.; Matthias, M. *Anal. Chem.* **1994**, *66*, 3281-3287.

(17) Xiang, F.; Beavis, R. C. *Rapid Commun. Mass Spectrom.* **1994**, *8*, 199-204.

(18) Lipniunas, P. H.; Townsend, R. R.; Burlingame, A. L.; Hindsgaul, O. *J. Am. Soc. Mass Spectrom.* **1996**, 7, 182-188.

(19) Ii, T.; Ohashi, Y.; Ogawa, T.; Nagai, Y. *Glycoconjugate J.* **1996**, *13*, 273-283.

(20) Nelson, R. W.; McLean, M. A.; Hutchens, T. W. *Anal. Chem.* **1994**, *66*, 1408-1415.

Chapter 6

Characterization of End-Labelled Polyethylene Glycol by High Resolution Matrix-Assisted Laser Desorption/Ionisation Time-of-Flight Mass Spectrometry[a]

6.1 Introduction

Matrix-assisted laser desorption/ionisation (MALDI) is widely used for biopolymer analysis with many applications.[1] The use of MALDI in industrial polymer analysis is more recent.[2] Products from condensation,[3] pulsed-laser,[4] and group transfer[5] polymerizations have been analysed by MALDI. The ability to find the molecular weight, molecular weight distribution, and end-group mass both quickly and accurately makes MALDI a favourable technique.[6] Analysis of modified end groups requires the mass spectrometric method provide

---

[a] A form of this chapter has been published as i) R. M. Whittal, L. Li, S. Lee, M. A. Winnik "*Characterization of pyrene end-labeled poly(ethylene glycol) by high resolution MALDI time-of-flight mass spectrometry*", *Macromol. Rapid Commun.* **1996**, *17*, 59-64.

ii) S. Lee, M. A. Winnik, R. M. Whittal, L. Li "*Synthesis of Symmetric Fluorescently Labeled Poly(ethylene glycols) Using Phosphoramidites of Pyrenebutanol and Their Characterization by MALDI Mass Spectrometry*", *Macromolecules* **1996**, *29*, 3060-3072. The pyrene labelled poly(ethylene glycol) polymers were synthesized by Dr. S. Lee in Dr. M. A. Winnik's research group at the University of Toronto. Dr. Lee collected the gel permeation chromatogram of the product. Also, Dr. Lee collected the ^{1}H NMR data presented as a comparison.

iii) R. M. Whittal, D. C. Schriemer, L. Li "*Matrix-Assisted Laser Desorption/ Ionization of Polymers Using Time-Lag Focusing Time-of-Flight Mass Spectrometry*", in preparation.

high mass measurement accuracy to confirm the structure(s) of the modified end group(s) and to decide whether one or both ends of the polymer are modified.

The analysis of end-group modified poly(ethylene glycol) using time-lag focusing MALDI is described herein. The modifications include poly(ethylene glycol) end-labelled with pyrenebutyric acid, acetaminophen, ephedrine, and bis(phosphates) of pyrenebutanol. Time-lag focusing MALDI provides high resolution (~1000 fwhm) and good mass measurement accuracy (better than 70 ppm) for polymers. This allows identification of the doubly-labelled product and can confirm the presence of singly-labelled impurity.

Chemically modified polymers have been used for a variety of diverse applications. Poly(ethylene glycol) labelled with common pharmaceuticals are used as oral delivery agents of slow-release drugs.[7] Winnik et al.[8,9] uses fluorescence techniques to study the morphology and dynamics of polymer systems. Polymers that contain covalently attached chromophores are used for these studies. Typically, the molecular weights of the labelled chains must be determined accurately to interpret the fluorescence measurements. For example, polymers end-labelled with pyrene, such as **1**, are used for cyclization studies. In the past, these polymers were characterized by gel permeation chromatography, NMR, UV-VIS spectroscopy, and fluorescence decay measurements. MALDI can provide some important information, which cannot be determined using any of the previous methods alone.

Time-lag focusing is a mass dependent energy compensation technique. Thus, considering if time-lag focusing is an appropriate method for polymer analysis is fair. Polymers have molecular weight distributions with peaks over a wide mass range. The best energy compensation is accomplished over a narrower range than the width of the polymer distribution. However, as shown here, the observed resolution is higher across most of the distribution using time-lag focusing than using continuous extraction. More important, time-lag focusing optimized for different regions of the mass spectrum does not generate an error in the value of the number average molecular weight, M_n, or the weight average molecular weight, M_w, since the relative peak area is unchanged. M_n and M_w are determined using equations (1) and (2).[10] The area under the oligomer peak is given by N_i and the observed oligomer molecular weight is given by M_i, i.e.,

$$M_n = \frac{\sum N_i M_i}{\sum N_i}, \tag{1}$$

$$M_w = \frac{\sum N_i M_i^2}{\sum N_i M_i}. \tag{2}$$

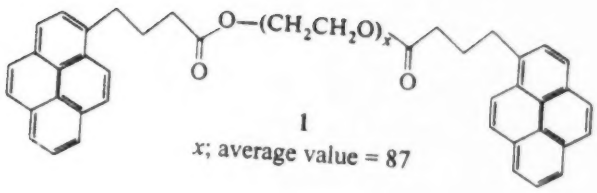

1

x; average value = 87

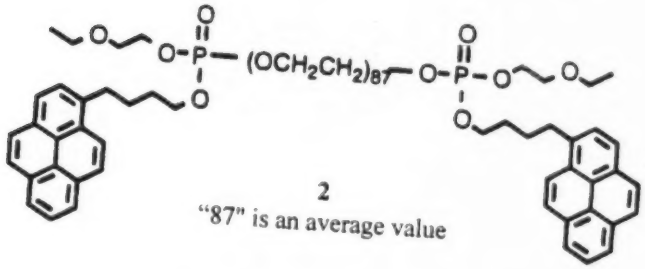

2

"87" is an average value

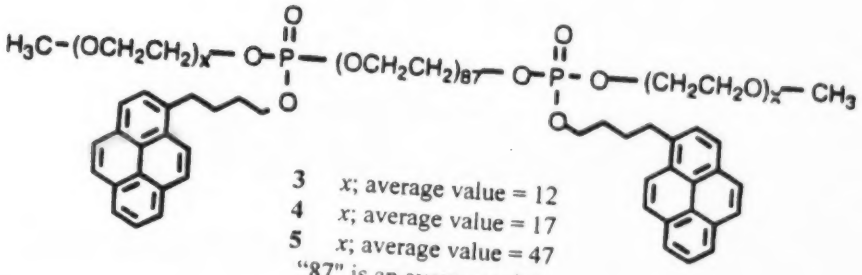

3 *x*; average value = 12

4 *x*; average value = 17

5 *x*; average value = 47

"87" is an average value

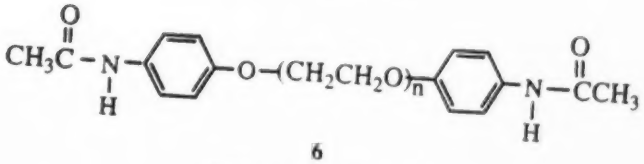

6

n; average value = 74

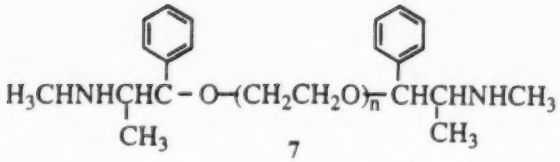

7

n; average value = 74

6.2 Experimental

6.2.1 Synthesis of α,ω-poly(ethylene glycol)-di-4-(1-pyrenyl)butyrate (1) The starting material for **1** was poly(ethylene glycol) 4100, a molecular weight standard, purchased from Polymer Laboratories (Amherst, MA). The product, **1**, was obtained by direct acid-catalysed esterification of the hydroxyl ends of the polymer with 4-(1-pyrenyl)butyric acid.[11]

6.2.2 Synthesis of α,ω-poly(ethylene glycol 4100) bis[methoxy poly(ethylene glycol X) 4-(1-pyrenyl)butyl phosphate] The same starting material was used in the synthesis of **2** to **5**. The synthesis of these compounds is described in detail elsewhere.[12] In brief, 4-(1-pyrenyl)butanol was added to phosphorus trichloride to yield the phosphorodichlorodite. Addition of diisopropylamine gives the phosphoroamidochlorodite. This product was reacted with poly(ethylene glycol), which has been terminated on one end with a methyl group, of the appropriate molecular weight to yield the corresponding phosphoramidites. The phosphoramidites were reacted with the poly(ethylene glycol) starting material in the presence of tetrazole to yield the bis(phosphate) final products.

6.2.3 Materials The poly(ethylene glycol) 2000, 3350, 10000 and poly(ethylene glycol) end-labelled with acetaminophen **6** and ephedrine **7** were purchased from Sigma. The matrix, 2-(4-hydroxyphenylazo)benzoic acid, was purchased from Aldrich and used without further purification.[13]

6.2.4 MALDI Mass Spectrometry Poly(ethylene glycol) polymers and modified polymers were dissolved in methanol at a concentration of 1-2 mg mL^{-1}. 2-(4-Hydroxyphenylazo)

benzoic acid was dissolved in 1, 4-dioxane at a concentration of 0.05 M. The polymer solutions were then mixed with 2-(4-hydroxyphenylazo)benzoic acid solution to a final concentration of 10^{-4} M. One microlitre of 0.02 M NaCl or KCl was typically added to 100 μL of the above solution. One microlitre of the mixture was placed on the stainless steel sample probe and allowed to dry. The MALDI experiment was carried out in a time-lag focusing linear time-of-flight mass spectrometer. The details of the instrument have been described.[14]

6.2.5 Gel Permeation Chromatography and ^{1}H NMR Samples were run on a Varian Associates 5000 liquid chromatography pump connected to a Waters R401 differential refractive index detector and a Kratos 970 fluorescence detector. The excitation source was set at 345 nm, and a 370 nm cutoff filter was placed in front of the photodetector. The mobile phase was tetrahydrofuran at a flow rate of 0.8 mL min^{-1}. For molecular weight analysis, the polymers were analysed using three Waters μ-Styragel columns (500, 10^3, and 10^4 Å). Poly(ethylene glycol) standards from Polymer Laboratories were used for calibration.

^{1}H NMR spectra were recorded on a Varian Associates VXR-400 spectrometer at 399.952 MHZ. The M_n values were obtained by comparing the intensity of the peak at ~3.39-3.55 ppm, due to the bold faced protons $MeOCH_2C\mathbf{H}_2(OC\mathbf{H}_2C\mathbf{H}_2)_{x-2}OC\mathbf{H}_2CH_2OP$ and $POCH_2C\mathbf{H}_2(OC\mathbf{H}_2C\mathbf{H}_2)_{y-2}OC\mathbf{H}_2CH_2OP$ with that of the multiplet between 7.69 and 8.20 ppm, representing the 18 pyrenyl protons, for each polymer.

6.3 Results and Discussion

6.3.1 Time-Lag Focusing MALDI and Polymer Analysis

Figure 6.1 shows the MALDI spectra for a mixture of poly(ethylene glycol) 2000 and 4100 collected under (A) continuous extraction and time-lag focusing with (B) a 1.40 kV pulse and (C) a 2.00 kV pulse. The observed peaks represent the sodium cationised oligomers. The peaks are equally spaced at 44 mass units apart, representing the individual oligomers that differ by the molecular weight of the repeating oxyethylene unit. The resolution, listed in the figure, and sensitivity are improved using time-lag focusing. The resolution for the poly(ethylene glycol) 4100 does not appear to change at the two pulse

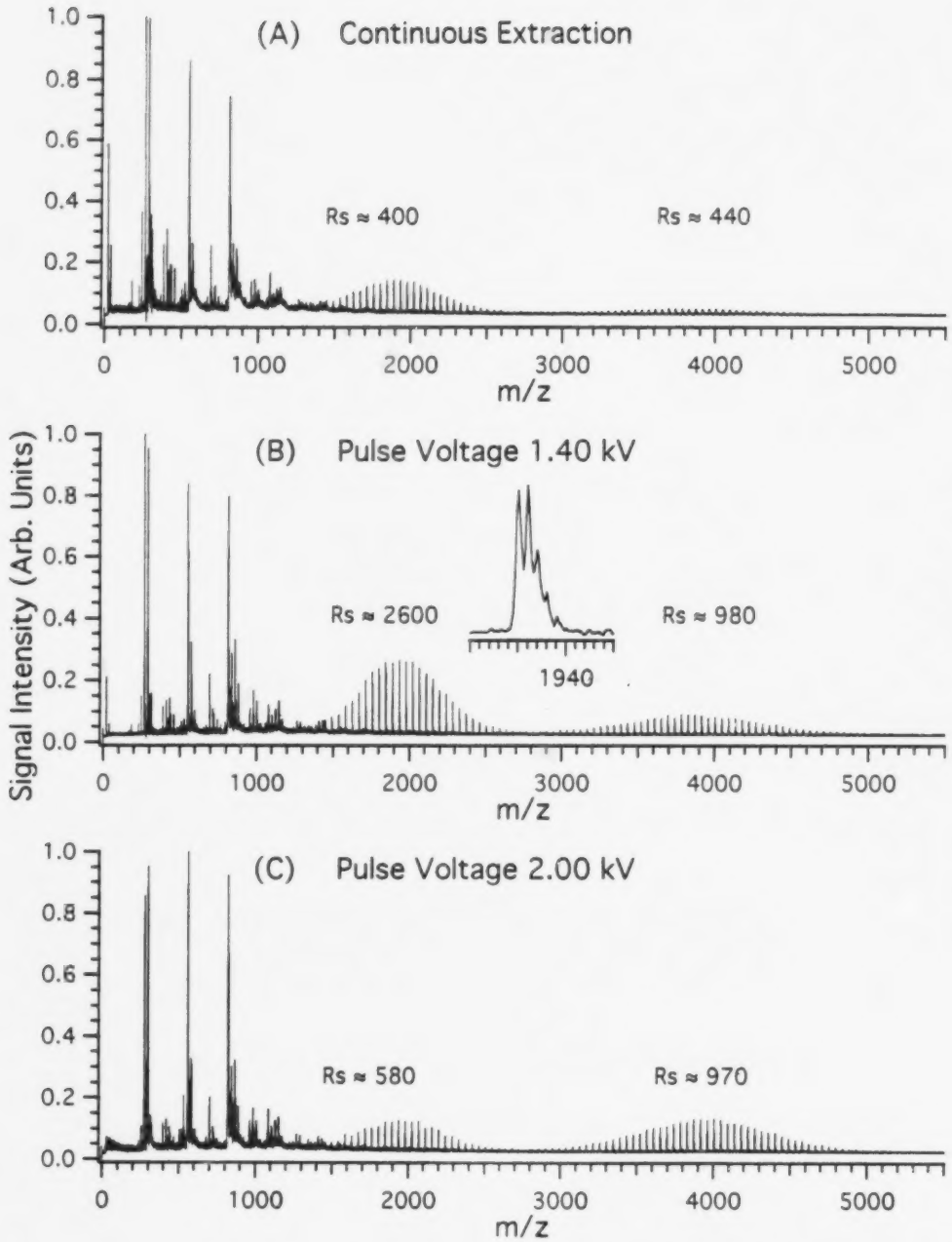

Figure 6.1 MALDI spectra of a mixture of poly(ethylene glycol) 2000 and 4100 in (A) continuous extraction and time-lag focusing with (B) a 1.40 kV pulse and (C) a 2.00 kV pulse.

potential settings. In fact, the resolution is limited by the isotope (mainly carbon 13) distribution for poly(ethylene glycol) at this mass. Therefore, the instrumental resolution is higher than the apparent resolution when the pulse potential is optimized for the 4 kDa mass range. The improved resolving power of the time-lag instrument is clearly shown in Figure 6.2 using poly(ethylene glycol) 10000. Each oligomer of this compound is resolved in time-lag focusing but only a single broad peak is observed under continuous extraction. The time lag was set to optimize focusing at 13 kDa where the resolution is ~1100 fwhm. The resolution is ~700 fwhm at 9 kDa and ~350 fwhm at 4 kDa. In figure 6.2A, the maximum resolution in continuous extraction is ~280 fwhm at 4 kDa. Therefore, resolution is higher across most of the distribution in time-lag focusing than in continuous extraction. From continuous extraction, M_n and M_w may be determined but with time-lag focusing the repeat unit (44 Da) and the end groups may additionally be determined.

It is known that time-lag focusing is a mass dependent energy compensation method. Thus, one should consider the appropriateness of this method with polymers that have a distribution over wide mass ranges. Figure 6.3 shows the MALDI spectrum of poly(ethylene glycol) 3350 collected at two different pulse voltages. A pulse voltage of 1.80 kV is optimum for masses at ~3 kDa and gives values for M_n and M_w of 3262.1 and 3321.0, respectively. A pulse voltage of 2.19 kV is optimum for masses at ~5 kDa and gives values for M_n and M_w of 3261.3 and 3322.4, respectively. Within experimental error, these values may be considered the same. This result is not surprising; although the resolution changes at different pulse potentials, the relative peak area does not change. An extension of this type of analysis has been carried out with polystyrenes over the mass range from 3 kDa to 14 kDa.[15] It is found that the values of M_n and M_w do not change within the experimental standard deviation of 1.6%.

6.3.2 Applications of Time-Lag Focusing MALDI to Polymer Analysis:

Figure 6.4 shows the MALDI mass spectrum of the starting material for **1**. The main peaks are from the sodium cationised oligomers. A series of smaller peaks is also observed at 16 mass units higher than each of the main peaks. This is due to the corresponding potassium cationised chains. The calculated molecular weights from the MALDI results are

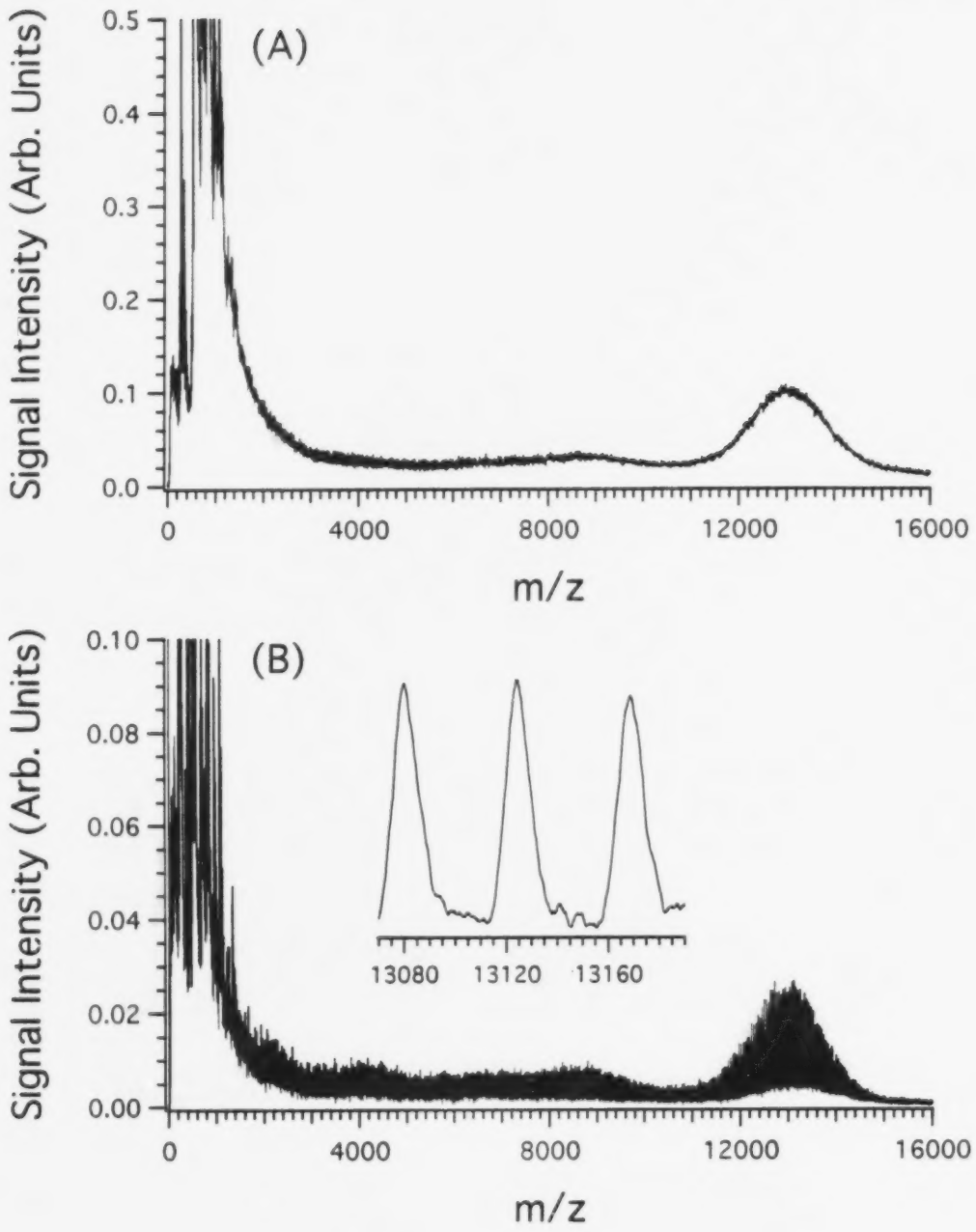

Figure 6.2 MALDI spectra of poly(ethylene glycol) 10000 in (A) continuous extraction and (B) time-lag focusing extraction. The resolution in (B) is ~1100 fwhm at 13 kDa.

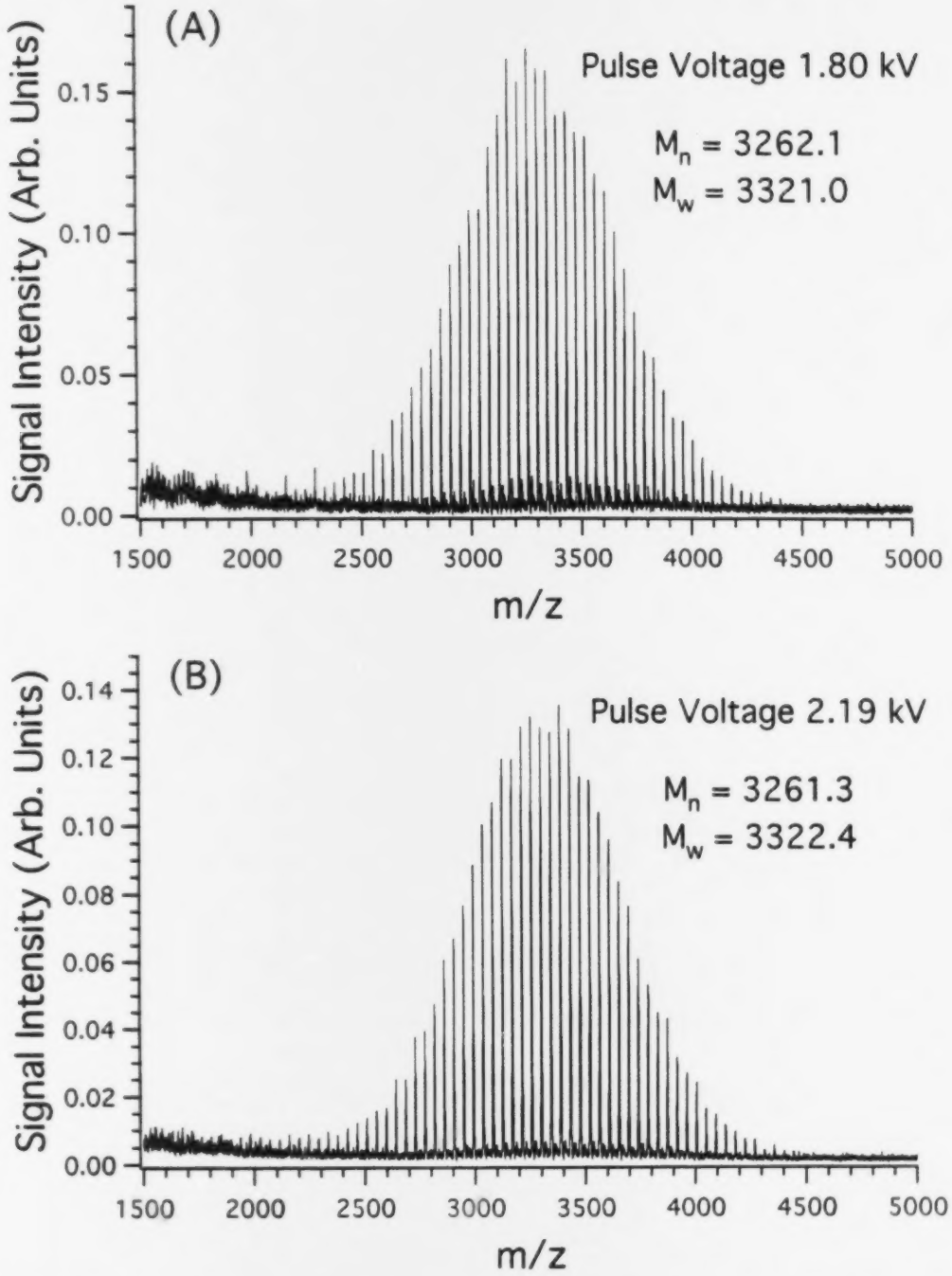

Figure 6.3 Spectra of poly(ethylene glycol) 3350 collected at two different pulse potentials. (A) the pulse potential is optimized for ~3 kDa and (B) the pulse potential is optimized for ~5 kDa.

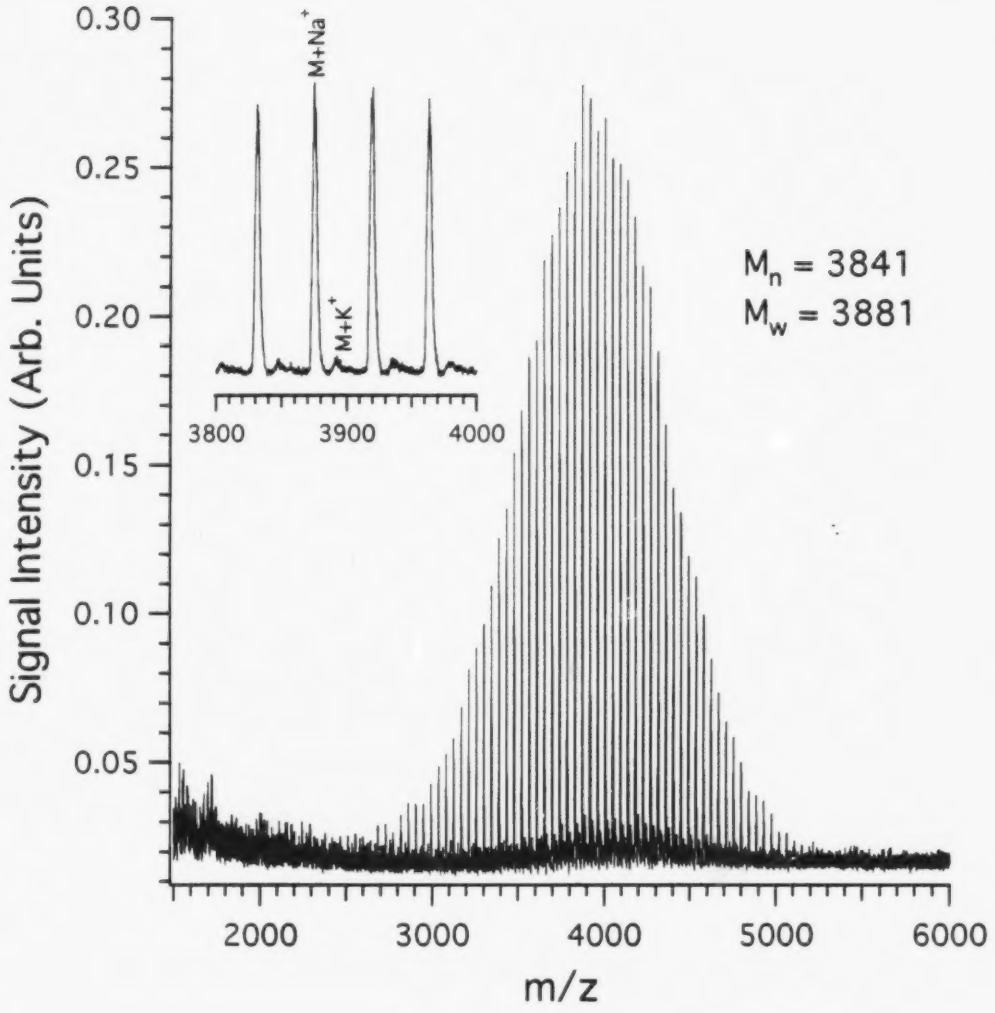

Figure 6.4 MALDI mass spectrum of the poly(ethylene glycol) 4100 molecular weight standard used as the starting material in the esterification reaction with pyrenebutyric acid, i.e., to make **1**.

shown in Table 6.1 and are consistent with those obtained by other methods. The dispersity, M_w/M_n, obtained by MALDI is narrower than that of the two gel permeation chromatography results. This is most likely the result of broadening of the solute bands in the gel permeation chromatography columns for this low molecular weight polymer.

Table 6.1 Molecular Weight Data for the Poly(ethylene glycol) Used as the Starting Material for **1**, **2**, **3**, **4**, and **5**

Method	Molecular Weight	M_w/M_n
Vapour Pressure Osmometry [a]	M_n = 3927	-
Viscometry [a]	M_v = 4083	-
Gel Permeation Chromatography [a]	M_n = 3791 M_w = 3907 M_p = 4084	1.03
Gel Permeation Chromatography [b]	M_n = 3721 M_w = 3908 M_p = 4290	1.05
MALDI Mass Spectrometry [b]	M_n = 3841 M_w = 3881	1.01

[a] Data provided by the supplier.
[b] Results obtained from this work.

The product, α,ω-poly(ethylene glycol)-di-4-(1-pyrenyl)butyrate (**1**), was obtained by direct acid-catalysed esterification of the hydroxyl ends of this poly(ethylene glycol) with 4-(1-pyrenyl)butyric acid. Expecting that **1** will be contaminated with some corresponding chains esterified with pyrenebutyric acid at one end is reasonable. Removing such an impurity from the product is very difficult. Samples of **1**, free of low molecular weight fluorescent impurities, were obtained by repeated precipitation followed by fractionation using gel permeation chromatography.

This method of purification did not provide enough material to assess the extent of functionalisation by UV-VIS spectroscopy. Instead, the value was estimated using fluorescence decay. This approach is described in detail elsewhere.[16] Analysis showed 80 ± 2% of the chains were doubly labelled. However, fluorescence decay measurements do not

provide information about the identity of the singly-labelled species. Supporting evidence from gel permeation chromatography analysis is needed to show that this species is the singly-labelled poly(ethylene glycol) and not, for example, free pyrene.

The gel permeation chromatography trace of **1** shows only one peak, which is expanded in Figure 6.5. Analysis of this peak gave M_p = 5660, M_w = 5196, M_n = 4131, and M_w/M_n = 1.03. The absence of other peaks in the trace suggests that the singly-labelled poly(ethylene glycol) oligomers have a similar length to the doubly-labelled **1**.

Figure 6.6 shows the MALDI mass spectrum of **1**. The distribution of chains in the sample is clearly resolved. Two major series (D and S1 in the insert) and one minor series (S2) of peaks were observed. One advantage of using the time-lag focusing MALDI instrument is the improved mass resolution and mass measurement accuracy. The mass resolution for each individual peak across the entire mass region shown in Figure 6.6 is between 900 and 1150 fwhm. Using the starting material as an external mass calibrant, the average error for mass measurement for individual oligomers shown in Figure 6.6 is better than 70 ppm. In Figure 6.6, the major series of peaks, or D series, is the sodium cationised **1**. The masses of the S1 series correspond to the sodium cationised sodium salt of singly-labelled poly(ethylene glycol) chains ($MNa + Na^+$, where M is singly-labelled poly(ethylene glycol)). The S2 series is most likely sodium cationised singly-labelled poly(ethylene glycol) ($M + Na^+$). Note that, under the MALDI conditions used to obtain Figure 6.6, molecular ion fragmentation is minimized. This was confirmed using *trans*-3-indoleacrylic acid and 2,5-dihydroxybenzoic acid as matrices, potassium and lithium as cationising agents and varying the laser power. The relative intensity of these three series of peaks was independent of the matrices, cationising agent, and laser power used. Figure 6.6 illustrates that the sample contains impurities that are likely from the polymer chains containing the 4-(1-pyrenyl)butyrate group at one end only, whose molecular weight is lower than that of **1** by 270. Previously, the best evidence for the presence of these chains was provided by fluorescence decay measurements. These chains are now seen clearly in the MALDI mass spectrum.

The molecular weight distribution of the doubly-labelled poly(ethylene glycol) was

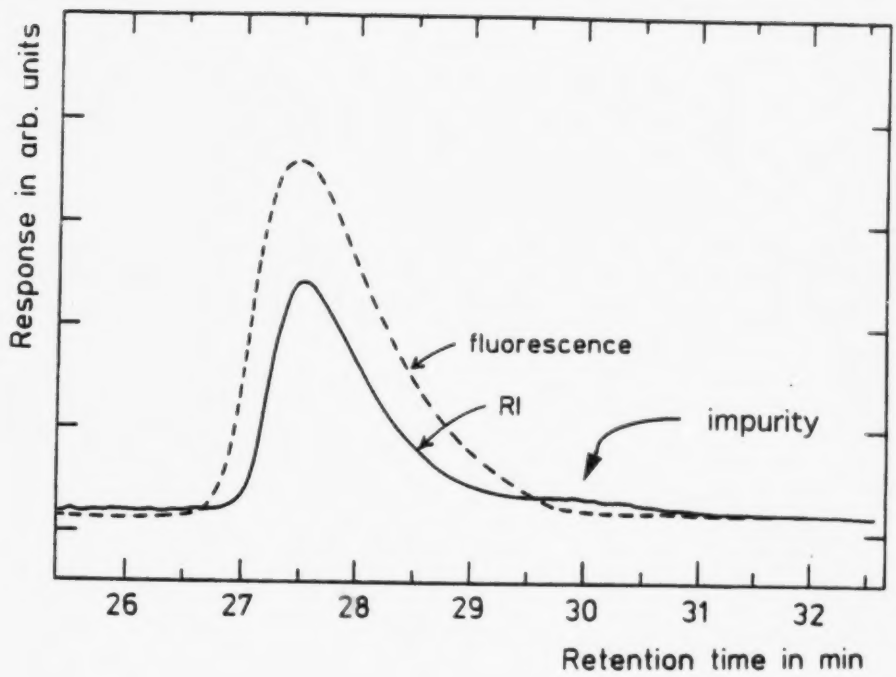

Figure 6.5 Gel permeation chromatography trace of **1**. Solid line: refractive index detector. Dashed line: fluorescence detector measuring the excitation signal at 345 nm. The minor, nonabsorbing impurity at low molecular weight is unidentified.

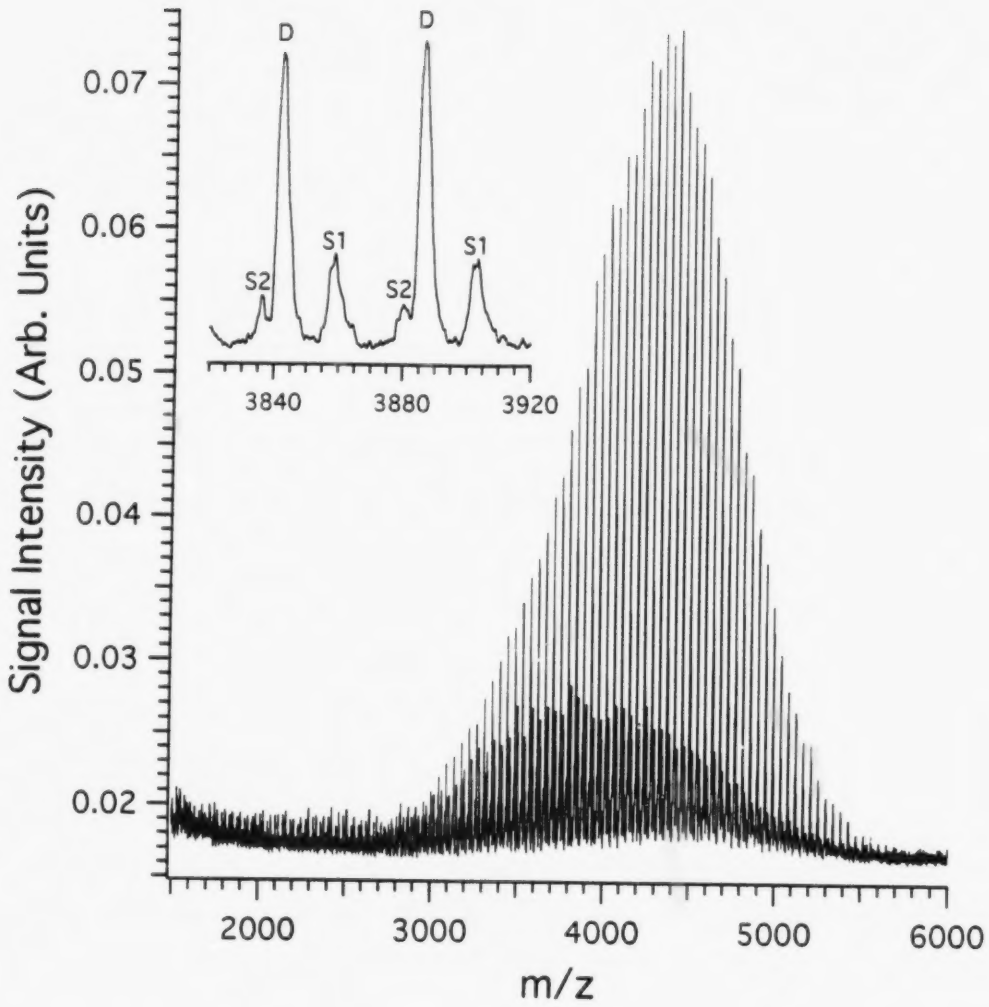

Figure 6.6 MALDI mass spectrum of **1**. D represents the doubly-labelled **1**. S2 is singly-labelled **1**. S1 is most likely the sodium salt of S2. All peaks are sodium cationised. See text for details.

calculated, from three trials, to be: M_w = 4269 ± 9 and M_n = 4232 ± 11. This gives a dispersity of M_w/M_n = 1.01. The molecular weight distribution from the singly-labelled poly(ethylene glycol) S1 series is M_w = 3708 ± 18 and M_n = 3619 ± 21. For the S2 series, M_w and M_n are calculated to be 2985 ± 170 and 2884 ± 181, respectively. The values of M_n and M_w for the S2 series do not likely reflect the true value of M_n and M_w for the singly-labelled poly(ethylene glycol); since, the intensity of the S2 series is low and at masses above 4650 Da the S2 peak can no longer be separated from the base of the D peak although the singly-labelled distribution continues. The relative peak areas in the mass spectra from three trials are 66% for series D, 26% for series S1, and 8% for series S2. Note that, since different polymers have different response factors for the MALDI experiment, the MALDI result shown in Figure 6.6 does not provide quantitative information.

1 was also examined by ^{1}H NMR. After correction for the fraction of singly-labelled chains in the sample (20%, determined by fluorescence decay measurements) M_n was found by end-group analysis to be 4136 ± 110. This value agrees well with the MALDI result. Thus, the higher molecular weight distribution from gel permeation chromatography can be attributed to the effect of the end groups on the hydrodynamic volume of **1**.

The bis(phosphate) end-labelled poly(ethylene glycols), **2** to **5**, are shown in Figures 6.7-6.10. Three series of peaks are resolved. The peaks in each expanded spectra represented by D are from the ions with masses corresponding to the bis(phosphate). Again, no fragmentation of the molecular ion was observed. In all samples, the molecular weight of each peak corresponds to the sodium cationised oligomer having the expected bis(phosphate) structure (within the experimental error of less than 70 ppm).

The peak labelled X1 is 14 mass units higher than D (i.e., M + 14) and the peak labelled X2 is 28 mass units higher than "D" (i.e., M + 28). A close examination of these series of peaks reveals that the X1 peaks are from the partial overlap of two different species. For most of the peaks in the series X1, the major component of this peak is M + 14 and the minor component is M + 16. Sometimes, the intensity of the M + 14 peak may be smaller than the M +16 peak. The M + 16 peak is likely the potassium cationised D. The M +14 and M + 28 peaks are most likely products with structures that are similar to that formed from

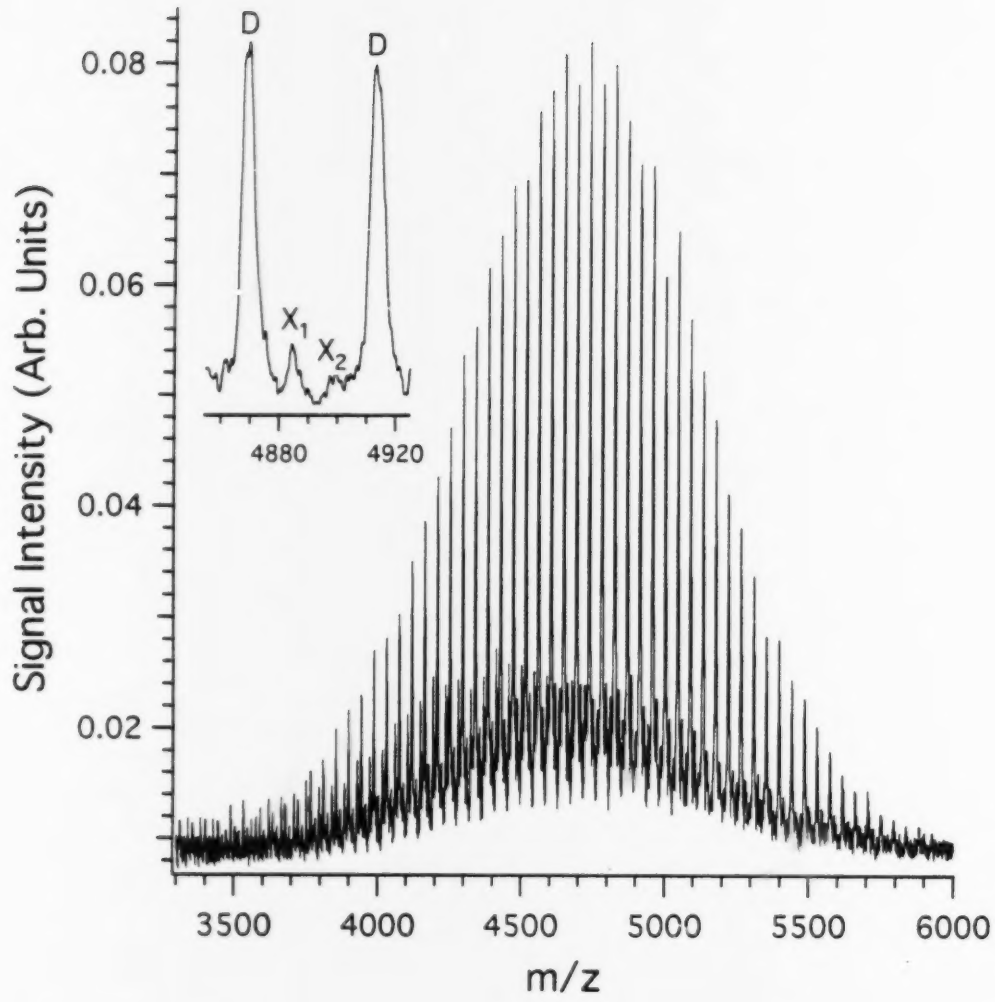

Figure 6.7 MALDI spectrum of **2**. M_n = 4692, M_w = 4714. See text for details.

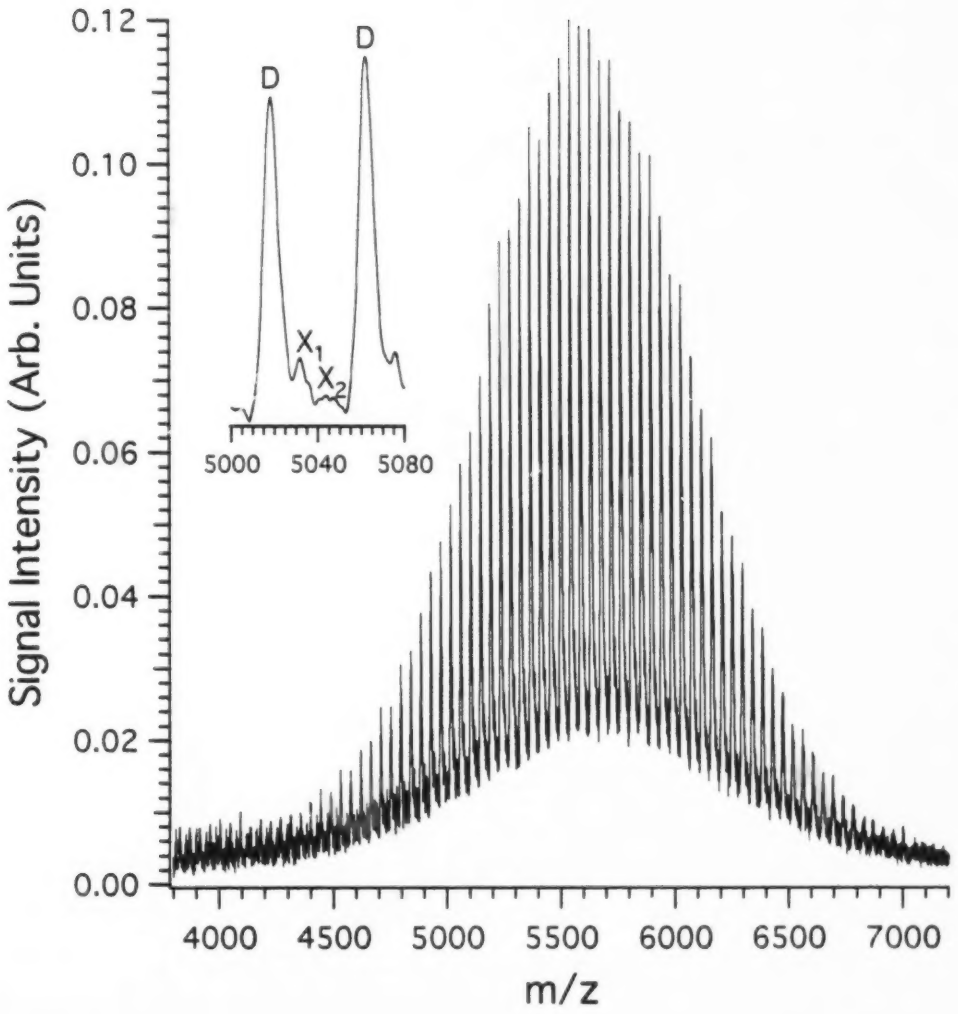

Figure 6.8 MALDI spectrum of **3**. M_n = 5607, M_w = 5628. See text for details.

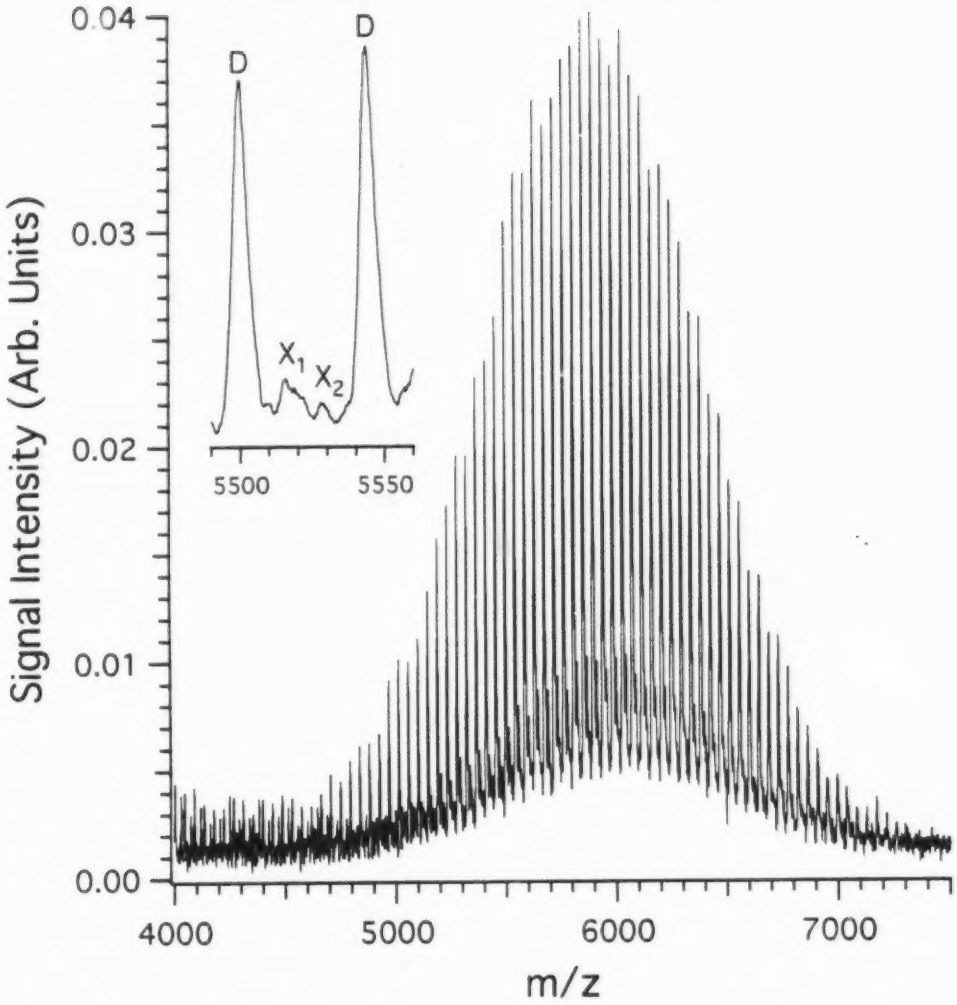

Figure 6.9 MALDI spectrum of **4**. M_n = 5897, M_w = 5920. See text for details.

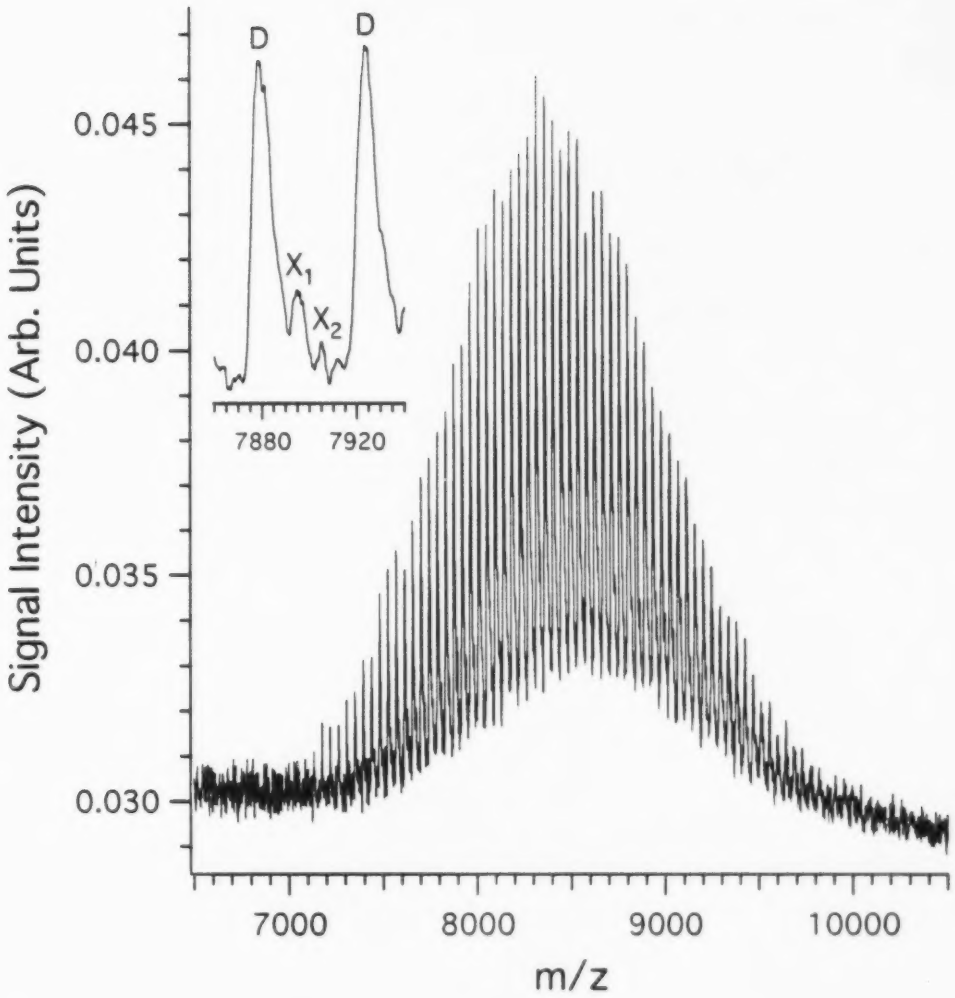

Figure 6.10 MALDI spectrum of **5**. M_n = 8409. M_w = 8427. See text for details.

the oxidation of the alkyl pyrene moiety during workup, with the likely structures of **8** and **9**. The oxidised compounds cannot be separated from their corresponding unoxidised forms using any known methods. Thus, the ability to detect these two species by MALDI is significant, since it provides information about the purity of the products and the possible structure of the impurities.

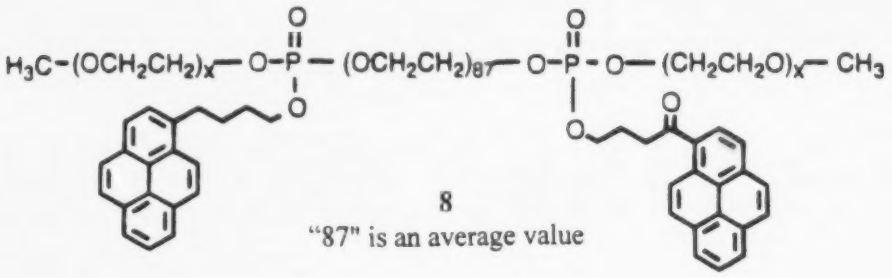

8

"87" is an average value

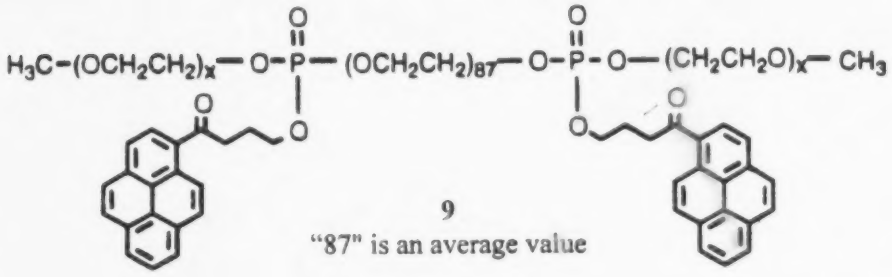

9

"87" is an average value

Table 6.2 summarizes the results obtained for the values of M_n and M_w for the products **2** to **5**. The results compare well with each other (except the gel permeation chromatography results for **4** and **5**) and with the expected values calculated from the molecular weights of the monomethoxy poly(ethylene glycol) end chains and the central chain. Since the gel permeation chromatography results were obtained using poly(ethylene glycol) molecular weight standards, the molecular weights of the poly(ethylene glycol) derivatives interpolated from the calibration curve might differ from their true M_w and M_n values. Therefore, the most useful molecular weight data is provided by the MALDI technique. Note that in this technique, the calculated molecular weight of each peak corresponds to that of the oligo(ethylene glycol) chain containing the expected 4-(1-pyrenyl)

butyl and methoxy groups, within experimental error (less than 70 ppm). This provides the most convincing evidence for the structures **2** to **5**.

Table 6.2 Summary of the Molecular Weight Data for the Bis(phosphates), Obtained by MALDI, Gel Permeation Chromatography (GPC), and ^{1}H NMR Spectroscopy, and Their Comparison with the Calculated M_n Values

polymer	M_w	M_n	M_w/M_n	technique
2	4714±11	4692±12	1.01	MALDI
	5017	4821	1.04	GPC
		4899±452		^{1}H NMR
		4657±12		calc. value[a]
3	5628±8	5607±8	1.00	MALDI
	5818	5465	1.07	GPC
		5818±176		^{1}H NMR
		5621±62		calc. value
4	5920±6	5897±7	1.00	MALDI
	5156	4983	1.04	GPC
		5939±474		^{1}H NMR
		6061±156		calc. value
5	8427±13	8409±11	1.00	MALDI
	6677	6484	1.03	GPC
		8714±705		^{1}H NMR
		8683±264		calc. value

[a] M_n (bis(phosphate)) = $2M_n$(end chain) + M_n(central chain) + 640, where M_n(end chain) was determined by ^{1}H NMR and MALDI; M_n(central chain) = 3839. The residual mass of 640 corresponds to the two $P(O)O(CH_2)_4C_{16}H_9$ units. The uncertainty in the calculated M_n of the bis(phosphates) represents only those which arise from the end chains.

It was surprising to find the average molecular weight of **1** to be lower than expected. M_w and M_n of **1** should be 540 mass units higher than that of its poly(ethylene glycol) precursor. The actual differences are 388 for M_w and 391 for M_n. This result is interpreted to mean that the polymer chain of the functionalised poly(ethylene glycol) is shorter than its original length by an average of three or four monomer units. During the labelling process, the poly(ethylene glycol) chains may be shortened by hydrolysis or fractionated during

polymer isolation.

The chain-shortening phenomenon was also found for other end-group modified poly(ethylene glycol)s, such as slow-releasing drugs, where one or two of the end groups are functional drug compounds. Figure 6.11 and 6.12 are the MALDI mass spectra of **6** and **7**, respectively. A comparison of Figure 6.3 with Figure 6.11 shows that some product peaks of **6** are of lower mass than the starting material. The masses of these peaks correspond to a doubly-labelled product that shifts the mass of a starting material oligomer up by 266.30 Da. Thus, it appears likely that the poly(ethylene glycol) partially hydrolysed during the addition of the end groups. However, the values of M_n and M_w for poly(ethylene glycol)bis(acetaminophen) (**6**) are higher than expected. As previously mentioned, M_n and M_w for the starting material are 3262.1 and 3321.0, respectively. M_n and M_w for **6** are 3559.7 and 3664.0, respectively. The shift in M_n and M_w due to the end groups is ~300 Da but a shift of 266.3 is expected. M_n and M_w for **7** are 3714.7 and 3766.8, respectively. The shift in M_n and M_w due to the end groups is ~450 Da but a shift of 294 is expected. Obtaining the poly(ethylene glycol) 3350 and end-labelled poly(ethylene glycol) 3350 from the same batch from Sigma was not possible. It was assumed that the starting material for the labelled products had a higher average molecular weight than the poly(ethylene glycol) 3350 supplied. Nonetheless, the previous suggestion that fractionation of the high mass oligomers led to the lower than expected mass shifts for **1** can be dismissed; hydrolysis appears the more likely reason. This work suggests that relying on the mass shift of M_w and M_n to infer whether one or two end groups are modified is not reliable. Accurate mass measurement of individual oligomer is required.

Further examination of Figure 6.11 shows that two, not one, acetaminophen groups are attached to the poly(ethylene glycol). For the peak with an observed mass of 3831.44 Da, if this peak represents an oligomer with only one modified end group then the mass would be 3830.57 Da. However, if this peak represents an oligomer with two modified end groups then the expected mass is 3831.56 Da. The mass error, if there are two end groups, is 31 ppm; whereas, the error, if there is one acetaminophen, is 227 ppm. Since the error in analysis is typically less than 70 ppm, two acetaminophen groups must be attached. This

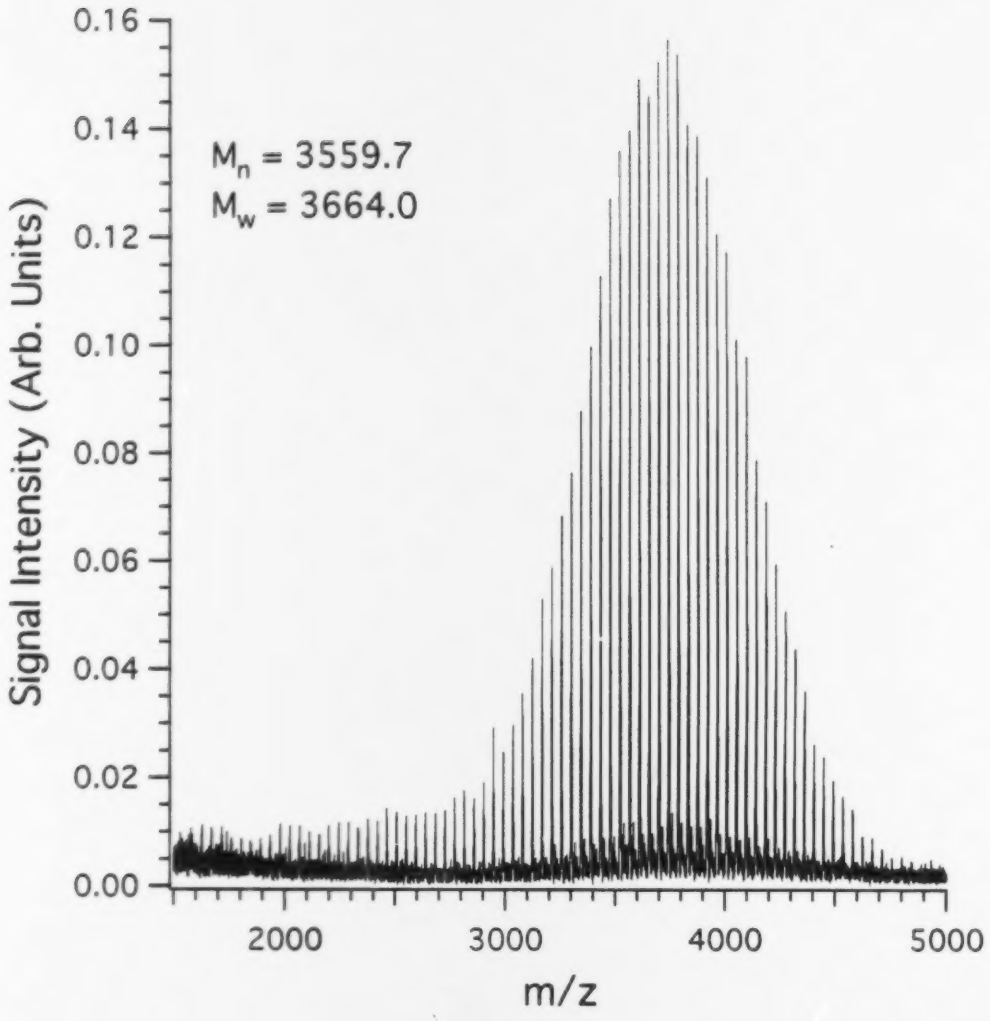

Figure 6.11 MALDI spectrum of **6**. The mass accuracy is 56 ± 38 ppm external for poly(ethylene glycol) bis(acetaminophen). See text for details.

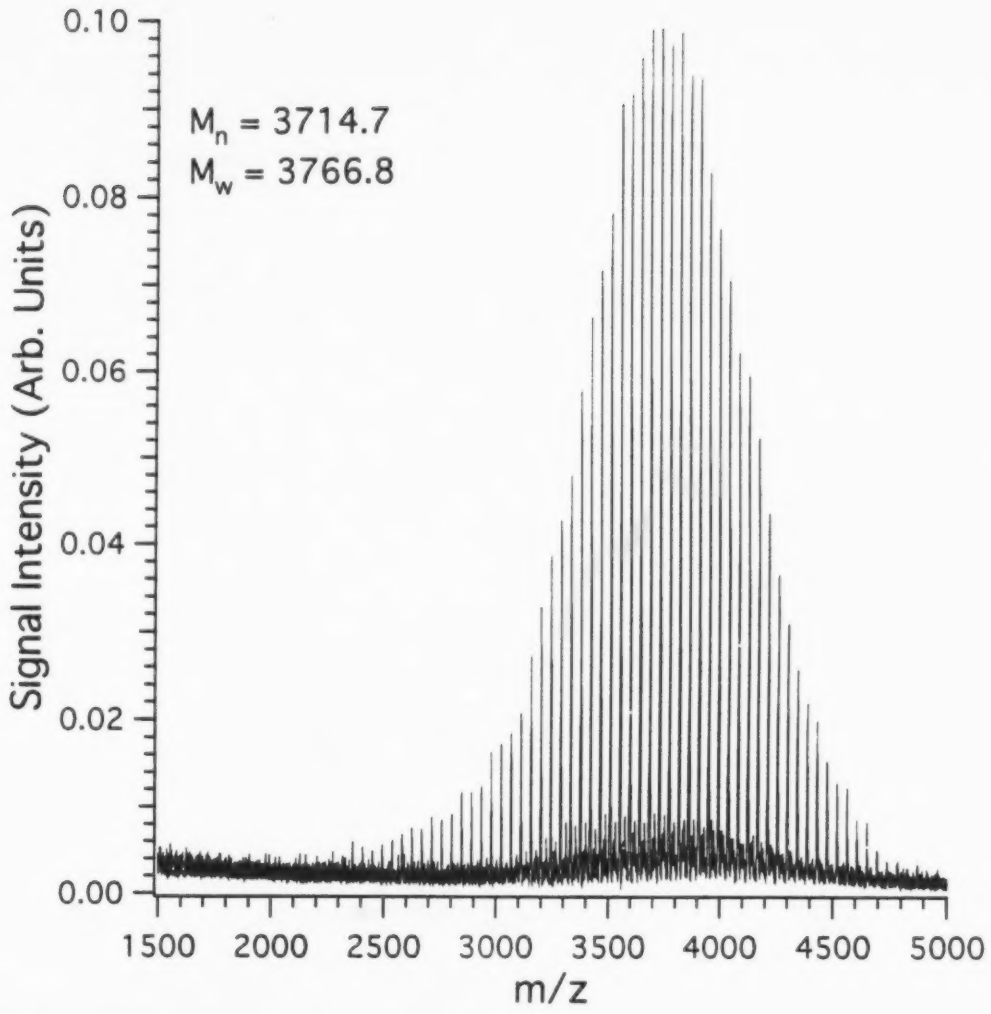

Figure 6.12 MALDI spectrum of **7**. The mass accuracy is 40 ± 35 ppm external for poly(ethylene glycol) bis(ephedrine). See text for details.

type of analysis is not possible in a conventional continuous extraction instrument where external mass accuracy in this mass range is usually 500 to 1000 ppm. Analysis of end-group modified polymers requires high resolution and mass accuracy, which is readily provided with time-lag focusing MALDI analysis.

6.4 Literature Cited

(1) Hillenkamp, F.; Karas, M.; Beavis, R. C.; Chait, B. T. *Anal. Chem.* **1991**, *63*, 1193A-1203A.

(2) a) Creel, H. S. *Trends Polym. Sci.* **1993**, *1*, 336. b) Bahr, U.; Deppe, A.; Karas, M.; Hillenkamp, F. *Anal. Chem.***1992**, *64*, 2866-2869. c) Danis, P. O.; Karr, D. E.; Mayer, F.; Holle, A.; Watson, C. H. *Org. Mass Spectrom.* **1992**, *27*, 843-846.

(3) Bürger, H. M.; Müller, H.-M.; Seebach, D.; Börnsen, K. O.; Schär, M.; Widmer, H. M. *Macromolecules* **1993**, *26*, 4783-4790.

(4) Danis, P. O.; Karr, D. E.; Westmoreland, D. G.; Piton, M. C.; Christie, D. I.; Clay, P. A.; Kable, S. H.; Gilbert, R. G. *Macromolecules* **1993**, *26*, 6684-6685.

(5) Danis, P. O.; Karr, D. E.; Simonsick, W. J.; Wu, D. T. *Macromolecules* **1995**, *28*, 1229-1232.

(6) Montaudo, G.; Montaudo, M. S.; Puglisi, C.; Samperi, F. *Macromolecules* **1995**, *28*, 4562-4569.

(7) Zalipsky, S.; Gilon, C.; Zilkha, A. *Eur. Polym. J.* **1983**, *19*, 1177-1183.

(8) Cheung, S.-T.; Winnik, M. A.; Redpath, A. E. C. *Makromol. Chem.* **1982**, *183*, 1815.

(9) Winnik, M. A. *Acc. Chem. Res.* **1985**, *18*, 73-79.

(10) Mattern, D. E.; Hercules, D. M. *Anal. Chem.* **1985**, *57*, 2041-2046.

(11) Cuniberti, C.; Perico, A. *Eur. Polym. J.* **1977**, *13*, 369-374.

(12) Lee, S.; Winnik, M. A.; Whittal, R. M.; Li, L. *Macromolecules* **1996**, *29*, 3060-3072.

(13) Juhasz, P.; Costello, C. E. Biemann, K. *J. Am. Soc. Mass Spectrom.* **1993**, *4*, 399-409.

(14) Whittal, R.M; Li, L. *Anal. Chem.* **1995**, *67*, 1950-1954.

(15) a) Whittal, R. M.; Schriemer, D. C.; Li, L. "*Matrix-Assisted Laser Desorption/ Ionisation Using Time-Lag Focusing Time-of-Flight Mass Spectrometry*" manuscript in preparation. b) Schriemer, D. C.; Whittal, R. M.; Li, L. In *Proceedings of the 44th ASMS Conference on Mass Spectrometry and Allied Topics*; Portland, OR, May 12 - 16, 1996.

(16) Boileau, S. B.; Méchin, F.; Martinho, J. M. G.; Winnik, M. A. *Macromolecules* **1989**, *22*, 215-220.

Chapter 7

Microspot Matrix-Assisted Laser Desorption/Ionisation and Its Application to Single Cell Analysis[a]

7.1 Introduction

In a typical matrix assisted-laser desorption/ionisation (MALDI) experiment, 0.5–1.0 μL of a 1-μM solution of analyte is loaded along with the matrix to a 3–10 mm^2 sample probe for mass analysis. However, most of the sample is not used as the desorption laser beam intercepting the sample is usually only 50–300 μm in diameter. Improving the sensitivity of MALDI can be accomplished partially by more efficient use of the analyte and through the development of better sample or matrix preparation procedures. Previous reports using chemical etching or laser drilling of a picolitre-volume hole directly on the sample probe show improved sensitivity compared with the conventional sample loading method.[1,2] The detection limit is tens of attomoles for the examples shown. The method described herein uses fused silica capillaries to deliver picolitre to low nanolitre quantities of sample solution unto a specific location on the sample probe. Laser desorption is aimed at this location only, such that the analyte is used efficiently.

This microspot MALDI method can find application in preserving precious low-volume samples. Multiple analysis, including both capillary electrophoresis and MALDI mass spectrometry could be completed from less than 1μL of sample. Additionally, microspot MALDI can be applied to the study of single cells.

Single cell analysis can provide an insight to the detailed chemistry of a cell on individual bases, which allows exploration of the heterogeneity of the cells and the

---

[a] A form of this chapter was submitted for publication as: L. Li, R. E. Golding, R. M. Whittal "The Analysis of Single Cells by Mass Spectrometry" submitted. Mr. R. E. Golding constructed the sample loading device and loaded the samples. Ms. Y. Dai collected the image of the sample.

relationship to their overall biological functionality.[3,4] However, because of the small sample volume, trace quantity of analytes, and complex cellular matrix, the chemical analysis of single cells remains formidable. Recent advances in microcolumn-separation methods, such as capillary electrophoresis and open-tubular liquid chromatography, with the arrival of miniaturized and highly sensitive detection schemes have led the way to detecting cellular components in single cells.[5] Among them, electrochemical and fluorescence detection systems provide the most sensitive approaches, although information on chemical identity deduced from these techniques is often limited.

On the other hand, mass spectrometry can potentially provide chemical analysis at the cellular level with the benefit of unsurpassed chemical specificity. A few reports on the analysis of cellular components in single large biological cells exist.[6] The analysis of cellular proteins from small populations (i.e., 5–20 cells) of human erythrocytes using electrospray ionisation mass spectrometry combined with capillary electrophoresis is also reported.[7] However, the analysis of single small-volume cells has not been as successful. The major obstacles to analysing these small cells lie in the limited sensitivity that a mass spectrometric method can provide and the need for special sample handling techniques for cell presentation to the mass spectrometer. Application of microspot MALDI can provide the sensitivity and sample handling capability required to detect small-volume samples. The analysis of cellular proteins from a single erythrocyte with a total cellular volume of 87 fL is shown. The success in analysing such a tiny cell suggests this method be applicable to the analysis of other important mammalian cells as well.

7.2 Experimental

7.2.1 Sample Preparation. All samples were prepared for analysis on a polished stainless-steel MALDI Probe. The 4-mm-diameter probe was polished with 600 mesh sandpaper to give an even surface. The probe was then successively polished with 4000, 8000, and 12000 mesh Micromesh sheets (ISOMass Scientific). Finally, the surface was polished with a suspension of 0.3-μm aluminum oxide powder. The surface was cleaned by ultrasonication for ~5 min in 1:1 methanol/water, acidified with formic acid (~5%). After ultrasonication the probe was rinsed with water followed by methanol.

The matrices, sinapinic acid and α-cyano-4-hydroxycinnamic acid were purchased from Aldrich. The sinapinic acid was used as received but the α-cyano-4-hydroxycinnamic acid was recrystallised before use. The bradykinin, substance P, human insulin, and equine myoglobin were purchased from Sigma and used as received. Water used throughout the experiment was from a Milli-Q Plus Ultrapure water system (18.2 MΩ•cm).

7.2.1.1 Preparing the Capillaries. The samples for analysis were loaded from deactivated fused-silica capillaries. The capillaries were deactivated with GlassClad 18 (silylation fluid) (United Chemical Technologies; Bristol, PA). GlassClad 18 was prepared as a 0.2% solution in water. The solution was drawn into the capillary and immediately ejected three times using a syringe attached to one end of the capillary. The capillary was then rinsed five to six times with water. Curing of the capillary was done by heating the capillary to 110°C for ½ hr, with a constant flow of nitrogen through the tube.

7.2.1.2 Peptide Analysis. All peptides were analysed using α-cyano-4-hydroxycinnamic acid as the matrix. The matrix was applied to the MALDI probe in two layers. The first layer was a 0.9-μL aliquot of a 5-mg mL^{-1} solution of the matrix in 60% methanol/acetone (v/v). The matrix spreads across the probe surface and dries very quickly, leaving a thin layer of very small crystals. The second layer was a 0.35-μL aliquot of the matrix prepared as a saturated solution in 25% methanol/water (v/v). The second matrix layer was allowed to dry and then checked under microscopic examination to ensure a good quality layer. The aqueous solution of peptide was loaded on top of the second matrix layer.

7.2.1.3 Protein Analysis. All proteins were prepared using sinapinic acid as the matrix, using a two-layer preparation method. The first layer was a 0.9-μL aliquot of a 6-mg mL^{-1} solution of the matrix in 60% methanol/acetone (v/v). The second layer was a 0.35-μL aliquot of a 2.5-mg mL^{-1} solution of the matrix in 20% acetonitrile/water (v/v). The second matrix layer was allowed to dry and checked ensure a good quality layer. For human insulin analysis, the aqueous protein solution was loaded on top of the second matrix layer using the capillary delivery system. To analyse myoglobin, the protein was premixed with the second layer matrix solution and loaded using the microcapillary system.

7.2.1.4 Loading the Analyte. For peptide and protein analysis a 10-μm capillary was

used to load samples. The capillary was filled by drawing solution into the capillary using a syringe attached to the opposite end (see Figure 7.1). A small amount of air was drawn into the capillary to prevent evaporation of the sample solution. The exact volume of solution was measured under the microscope using a calibrated scale in the ocular lens. The MALDI probe was then placed on the microscope stage in a holder that allows exact placement of the sample to the centre of the probe. The sample was deposited on top of the preloaded matrix. The MALDI probe was inserted into the time-lag focusing MALDI instrument for analysis.

7.2.1.5 Analysis of Cells. Whole human blood was obtained from a male subject. The whole blood (~4 mL) was placed in a tube containing 2 mL of a pH 5.5 118 mM citrate, 16 mM phosphate, and 160 mM dextrose solution (an anticoagulant and preservative solution). The tube was cooled to 4°C for ~1 hr. The tube was spun in a centrifuge at 4°C at x1000g for 5 min. The supernatant was removed and discarded. A 2-ml aliquot of the citrate-phosphate-dextrose solution was added, the tube was gently mixed, and then spun again for 5 min. The cycle was repeated three times. The packed button of cells was resuspended in 2 mL of the citrate-phosphate-dextrose solution. The mixture was transferred as 200-μL aliquots to microcentrifuge tubes, which were stored at 4°C until needed. The preservative solution provided a cell lifetime of 28 days without lysis.

The 20-μm-ID capillary used for manipulating a suspension of cells was first etched at one end. The polyimide coating was removed from one end by quickly passing it through a flame and then removing the charred coating with methanol. A syringe was attached to the opposite end of the capillary and the end to be etched was placed in a 40% hydrofluoric acid solution for ~40 min while maintaining a positive pressure on the syringe. The capillary was rinsed several times with a 2% solution of sodium bicarbonate, followed by water, and finally methanol. Part of the etched end ~1 mm was removed from the capillary to ensure a constant internal diameter. The etched capillary had an external diameter of 48 μm. Following etching the capillary was deactivated using the silylation fluid as previously described.

Before analysis the supernatant was removed from the microcentrifuge tube. The packed button of cells was resuspended as a 0.13% solution (v/v) in isotonic saline (0.85% (w/w) NaCl) giving a concentration of ~10–14 cells nL^{-1}. Part of the suspension was placed

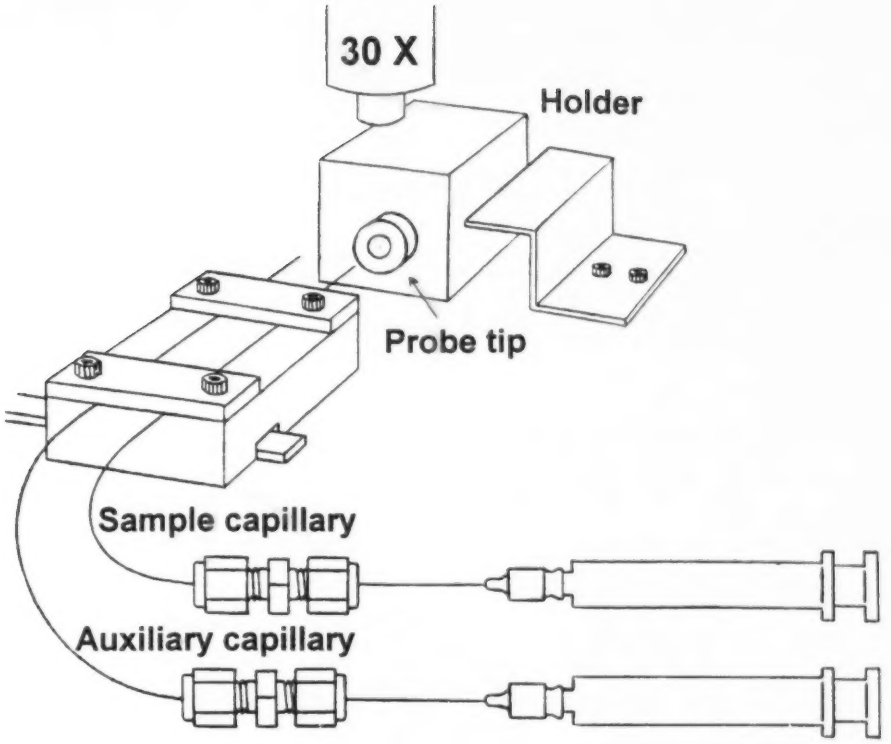

Figure 7.1 Microspot MALDI delivery system. It consists of a sample and probe tip holder and a movable x-y stage. Two fused silica capillaries are attached to the x-y stage and connected to disposable syringes. During sample loading, the sample vial is placed on the sample holder and the x-y stage is moved to allow the capillary to contact the sample solution. A measured volume of a sample is then withdrawn using the syringe under microscopic observation. Some air is then drawn into the capillary. The sample vial is replaced with the MALDI probe that is precoated with a thin layer of a matrix. The capillary loaded with the sample is then moved to the probe surface and the sample is deposited onto the matrix layer. For protein analysis, a second layer of matrix is loaded on top of the sample.

in a 1.3 mm deactivated-glass tube (see Figure 7.2A). The tube was placed in a holder on the microscope stage. The capillary was preloaded with ~0.5–1 nL of water, followed by a small amount of air. Some cell suspension was drawn into the capillary under microscopic examination (30x magnification), with the volume dependent upon the number of cells desired (~100 pL for one cell). Cell counting was then completed using a higher (100x) microscope magnification (see Figure 7.2B). Returning to 30x magnification, the cell suspension tube was replaced with a prepared MALDI probe and the capillary contents were transferred to the probe (see Figure 7.2C). It was assumed that cell lysis occurred as the cell suspension and water mixed upon transfer to the MALDI probe.

The MALDI probe was prepared similarly to the analysis of proteins. To a clean probe was loaded 0.9 μL of 6-mg mL^{-1} sinapinic acid in 60% methanol/acetone (v/v). Loading of the cell suspension followed. An auxiliary capillary (50-μm ID) was used to load 20 nL of 2.5-mg mL^{-1} sinapinic acid in 20% acetonitrile/water (v/v) on top of the sample spot.

7.2.2 MALDI Analysis. The samples were analysed on a time-lag focusing MALDI time-of-flight, as previously described (see Chapters 2 and 3).[8] The laser optics was aligned such that desorption takes place in the centre of the MALDI probe. The laser spot is ~50×100 μm oval from a focused nitrogen laser (Laser Science Inc. VSL 337ND) beam at 67.5° to the probe normal. A CCD camera is used to monitor the desorption location on the probe. The instrument was operated at 20-kV DC with the pulse voltage and delay set appropriately for the compound of interest.

7.2.3 Sample Imaging. A Molecular Dynamics' Multiprobe 2001 Confocal Laser Scanning Microscope was used to image the MALDI samples shown. An Argon/Krypton laser operating at 568 nm line was used for the excitation of the tetramethylrhodamine-labelled trisaccharide.

The measurement of sample spot size was done by using a fluorescence microscope equipped with a mercury lamp for excitation. Two layers of α-cyano-4-hydroxycinnamic acid were loaded on the probe, as described above, and an aliquot of the tetramethyl-rhodamine-labelled trisaccharide was loaded on top. The sample volume was varied and the

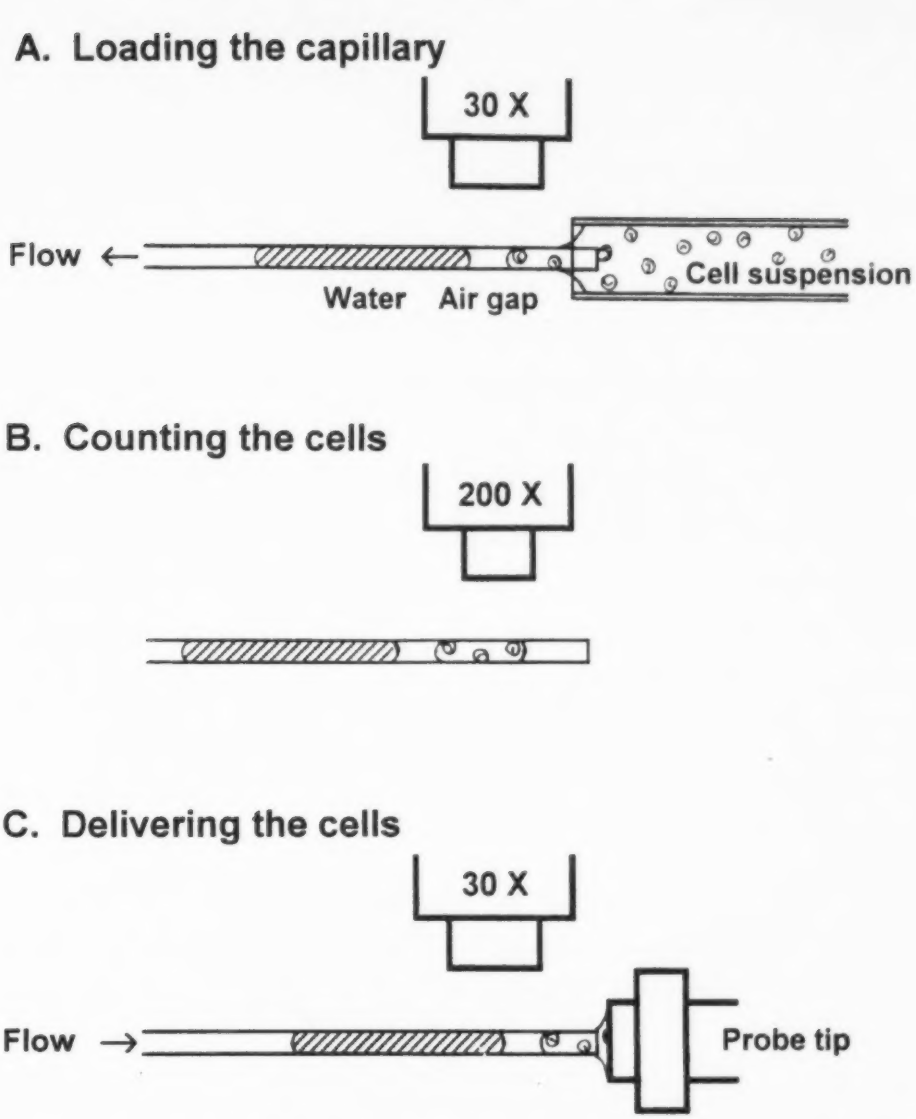

Figure 7.2 Schematic of the cell loading process for human erythrocytes. (A) Before loading the cell suspension the capillary was filled with ~0.5-1 nL of water. The cell suspension was first loaded to a deactivated-glass tube with a diameter of 1.3 mm. The 20-µm-ID sample capillary, whose external diameter was reduced to 48 µm, was inserted in the tube containing the cell suspension. For single cell loading, the volume withdrawn from the cell suspension was ~100 pL. (B) The exact number of cells was verified using a larger microscope magnification. (C) The cell suspension was then delivered to the probe tip that was previously covered with a thin layer of matrix. A second layer of matrix (20 nL) was added on top of the sample using the auxiliary capillary.

sample diameter measured using the fluorescence microscope.

7.3 Results and Discussion

The idea of microspot MALDI is to reduce the sample presentation surface with respect to the laser desorption site and ion acceptance volume in the mass spectrometer to improve the sampling efficiency. In this approach the sample solution is first drawn into a small-diameter capillary with the volume determined by the length of the sample plug (see Figure 7.1). A small air amount of air is drawn into the capillary to reduce solvent evaporation. The evaporation rate was found to be 1.6 pL min^{-1} for a 10-μm-ID capillary filled with an aqueous solution; the rate increases with the capillary diameter. Figure 7.3A is a confocal microscopy image of 0.35 μL of sample loaded using the conventional sample preparation technique (see Chapter 4).[9] The diameter of the spot is ~1.5 mm. Whereas, the sample spot observed for microspot loading of 230 pL of sample is ~150 μm. The size of the sample spot is dependent upon how much solution is delivered and the diameter of the capillary used, as shown in Figure 7.4.[10] There is a rapid decrease in the analyte spot area as the volume is reduced. Thus, the concentration of analyte per unit area is higher at low volumes (especially below 400 pL), which should result in a more intense MALDI signal. As little as 20 pL of sample solution can be accurately delivered onto the matrix layer producing an ~100-µm-diameter spot on the probe surface. The laser desorption spot is an ~50×100-µm oval. By rotating the sample probe, MALDI mass spectra are recorded from different areas in the sample spot until most or the entire sample is used.

The quality of the matrix layer plays an important role in the sensitivity of microspot MALDI. A two-layer deposition approach gave the best results (see Chapter 4 for more discussion on this subject). The two-layer matrix deposition method relies on the first matrix layer crystals to act as nucleation sites for the second matrix layer. Highest sensitivity is achieved if the second matrix layer is a densely packed but thin layer of small crystals. Achieving this goal requires careful preparation of the matrix and the MALDI probe itself. To have small well-packed crystals in the second layer, the first-layer crystals must be small.

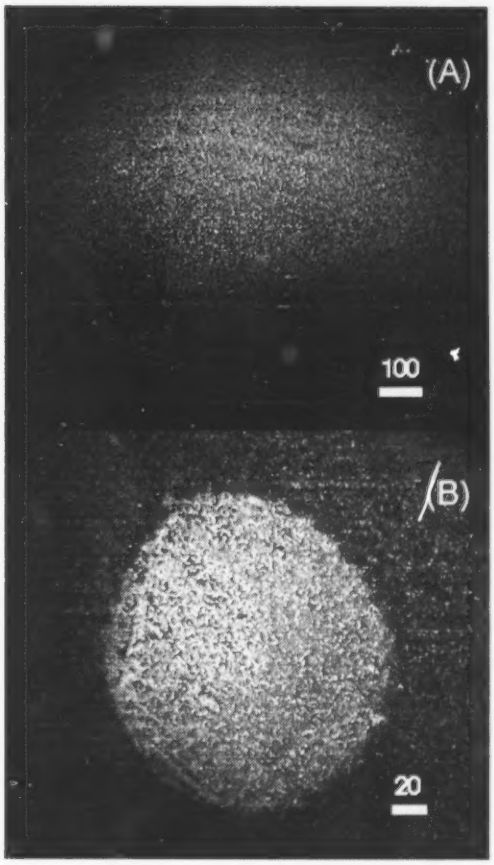

Figure 7.3 (A) Confocal fluorescence microscopic image of a conventional sample preparation and (B) a microspot MALDI sample preparation of a tetramethylrhodamine labelled trisaccharide loaded on the second layer of α-cyano-4-hydroxycinnamic acid.

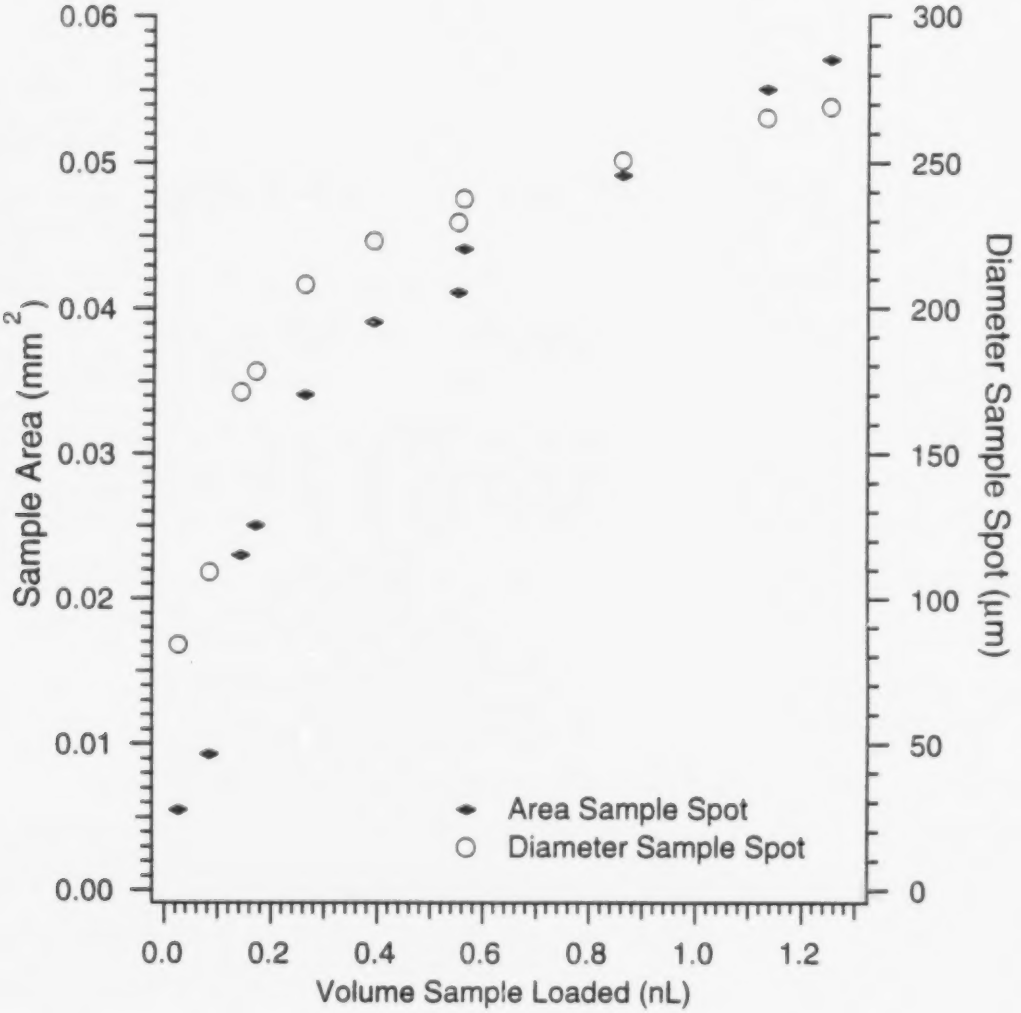

Figure 7.4 The sample spot area and diameter which is observed by fluorescence microscopy for a tetramethylrhodamine-labelled trisaccharide on α-cyano-4-hydroxycinnamic acid for a 10-μm-ID and 144-μm-OD capillary.

The size of the crystals in the first layer depends upon the rate of their formation and the number of nucleation sites. Changing the type and amount of solvent allowed control over the solvent evaporation rate and thus crystal formation rate and size. A 60% methanol/acetone (v/v) mixture gave good control over the rate at which solvent dried and crystals formed from 0.9μL of solution. The concentration of the matrix was also important. The concentration must be high enough to cover the 4-mm MALDI probe sufficiently but if the concentration is too high then agglomerates of matrix form or the crystals become too large or both. A highly-polished MALDI probe reduces the number of nucleation sites on its surface. Final polishing with 0.3-μm aluminum-oxide powder gave a smooth mirror-like finish on the probe. Thorough cleaning of the probe allowed the matrix solution to spread and dry evenly on the surface. The matrix concentration and the type and amount of solvent used for the second layer affected the size and density of the crystals formed. The best second layer was achieved using the conditions given above.

The MALDI spectra in Figures 7.5 and 7.6 show the sensitivity attainable with microspot MALDI. Figure 7.5 is the MALDI mass spectra of substance P (oxidized form) with a total sample loading of 0.97 amol (195 pL of a 5.0-nM solution) and bradykinin with a loading of 4.6 amol (230 pL of a 20-nM solution). For Figure 7.5A, the signal-to-background-noise ratio is 16 and the mass resolution is sufficient to observe the isotope peaks. For bradykinin (Figure 7.5B), the signal-to-background-noise ratio is 22. Figure 7.6A is a spectrum of 13 amol (260 pL of a 50-nm solution) of human insulin, a protein with a molecular weight of 5807.7. Figure 7.6B is a spectrum of 54 amol of myoglobin (300 pL of 180-nM solution) without its heme prosthetic group. The hemeless myoglobin or apomyoglobin is a 16951.5 Da protein. The peak at ~8.5 kDa is the doubly-charged apomyoglobin molecular ion. A mass filter was used to suppress the ions below 1.5 kDa while collecting the myoglobin spectrum; the rise in the baseline at 1.5 kDa is where the mass filter shuts off. The sensitivity is reduced for proteins but this is true for conventional sample loading also. Further improvement of the sensitivity should be possible by further optimizing the sample and matrix preparation process and the use of a more sensitive

detector.[b]

To illustrate the application of this method to cell analysis, red blood cells were chosen as a model system because they are readily available and small (8-μm diameter and 2-μm thick).[3] In addition, the major cellular protein content (~450 amol) is well within the limit of the microspot MALDI method. The total cell volume is ~87 fL, which is perhaps the smallest biological sample analysed by mass spectrometry.

Figure 7.2 shows the cell intake and loading procedures. First, ~0.5–1 nL of water was drawn into the capillary, followed by the suspension of blood cells (in isotonic saline solution) with a small air gap between the two solutions. Enough water was drawn into the capillary to dilute the saline solution to <0.3% (the concentration that ensures lysis of all cells) when the water and suspension are delivered to the MALDI probe. Although only 3:1 water-to-saline is needed, a 5:1 ratio provided better MALDI sensitivity. The amount of cell suspension loaded was dependent upon the number of cells wanted for analysis. There is one cell in ~100 pL of the suspension. After the suspension was loaded, a small amount of air was drawn into the capillary, cell counting was completed, and the suspension and water were transferred to the MALDI probe preloaded with the first matrix layer. A 20-nL aliquot of the second matrix layer was added on top of the analyte using a 50-μm-ID auxiliary capillary.

Figures 7.7A and 7.7B show the mass spectra from loading three cells and one cell, respectively. The spectra display two intense peaks from the major components in the cell, i.e., the subunits of hemoglobin without the heme prosthetic group. Apohemoglobins A and B have masses of 15126.4 Da and 15867.3 Da, respectively. The peaks observed below 1 kDa are from the matrix; whereas, the peaks at ~7-8 kDa and 5-6 kDa are the doubly-charged and triply-charged molecular ions, respectively. Considering 450 amol of hemoglobin are present in one cell, it is not surprising to observe a strong signal. However, what is

---

[b] Currently, a dual-microchannel-plate detector from the R. M. Jordan Co is used, but a triple-plate design and the newly developed high-dynamic-range microchannel plate from Galileo will provide about a 10-fold enhancement in sensitivity. B. Laprade, W. Fuchs, B. Lincoln In *Proceedings of the 44th ASMS Conference on Mass Spectrometry and Allied Topics*, Portland, OR, 1996. MPB 25.

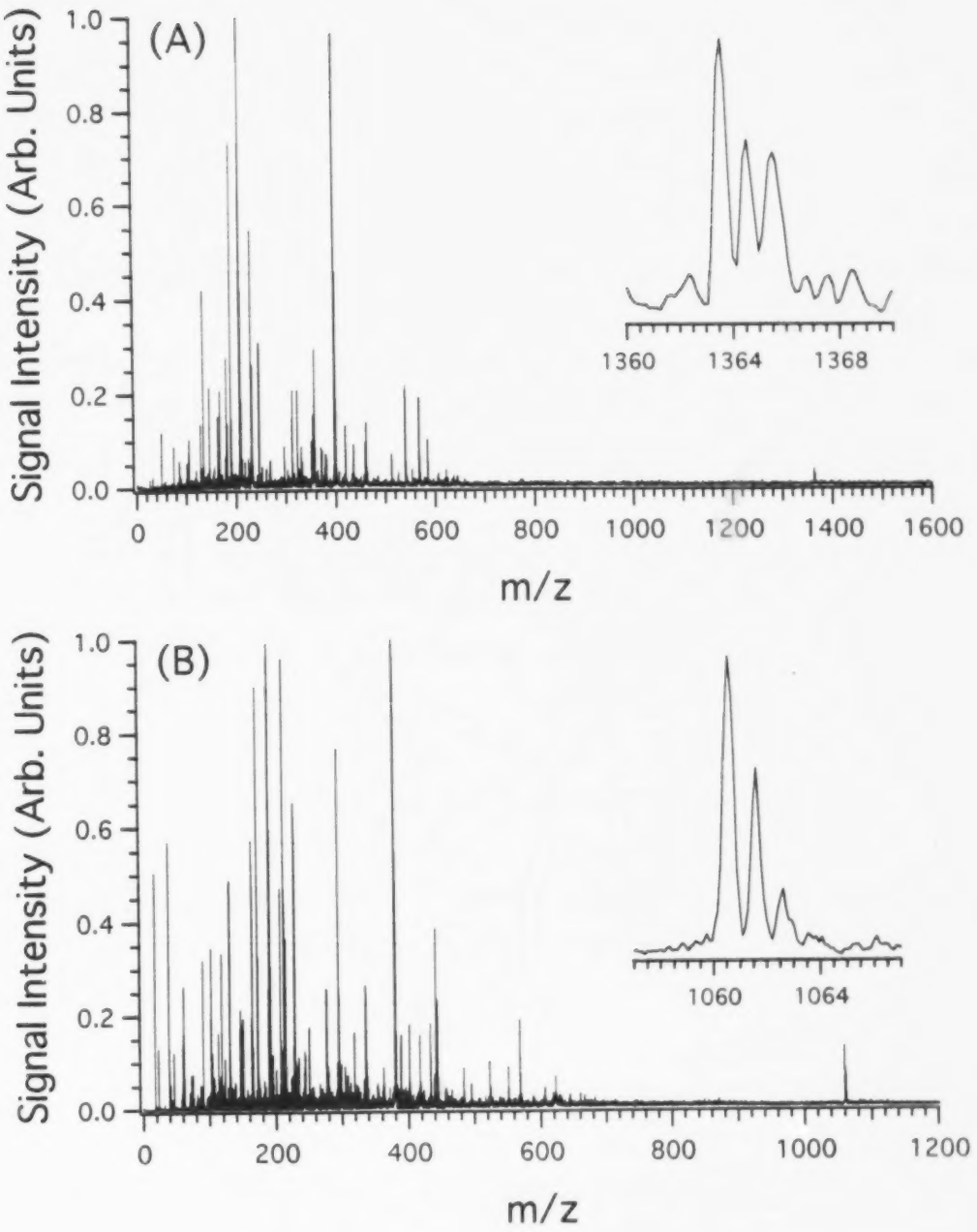

Figure 7.5 Microspot MALDI spectra of (A) 195 pL of a 5.0 nM solution or 0.97 amol of substance P (oxidized form) and (B) 230 pL of a 20 nM solution or 4.6 amol bradykinin. The samples were loaded on top of the second layer of matrix. See the text for details.

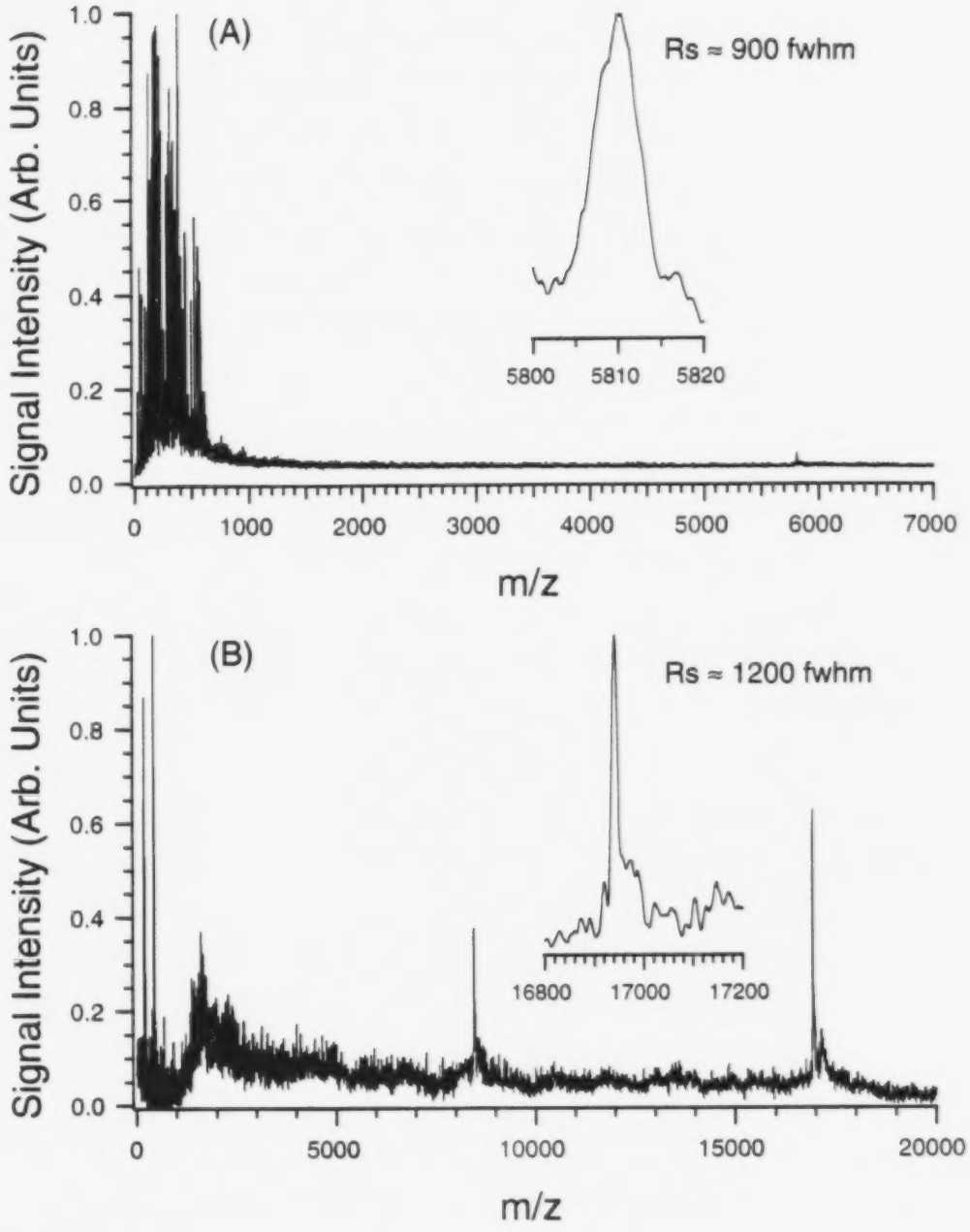

Figure 7.6 Microspot MALDI spectra of (A) 13 amol of human insulin and (B) 54 amol of equine myoglobin using sinapinic acid as the matrix. See the text for details.

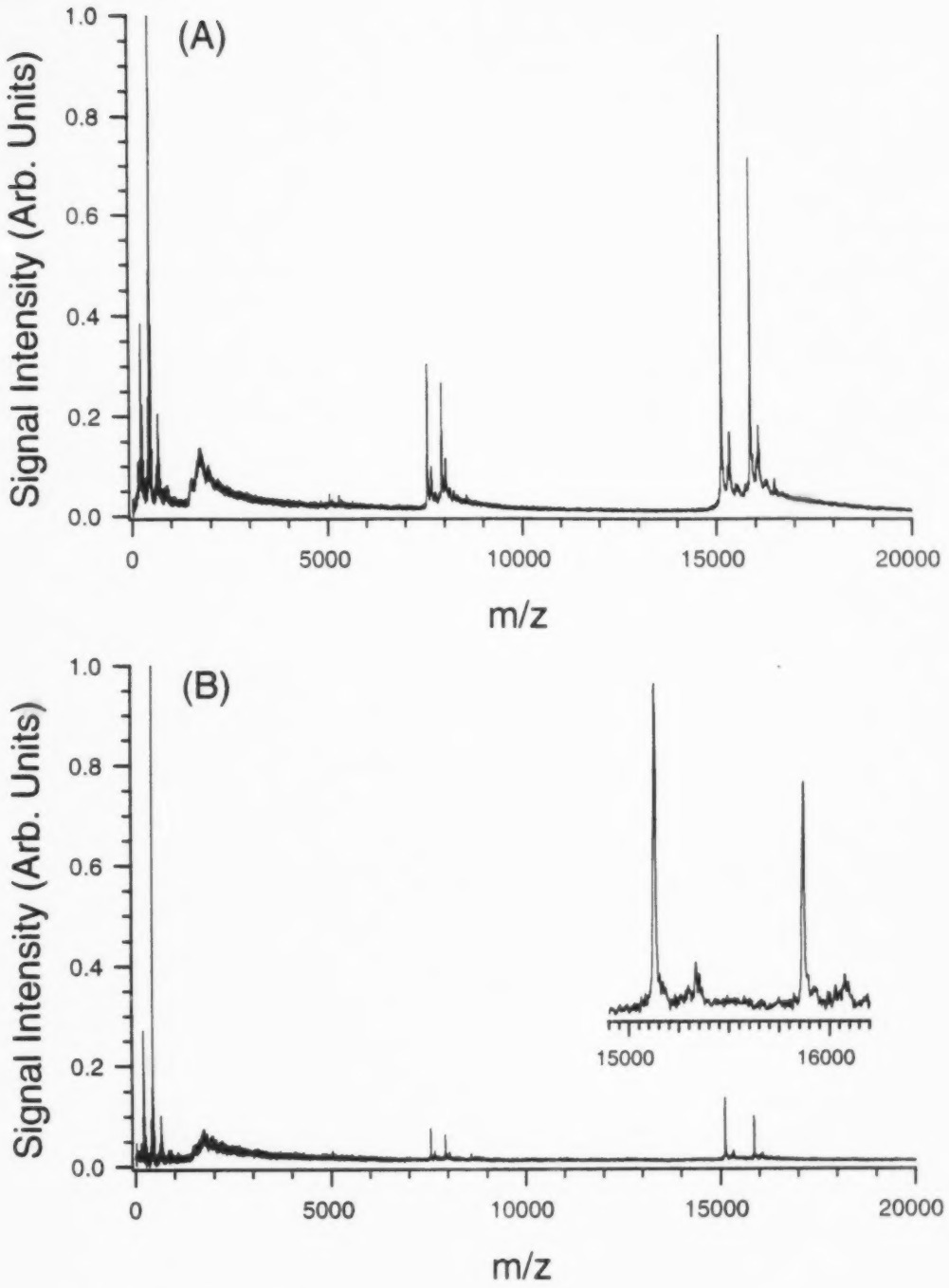

Figure 7.7 Application of microspot MALDI to the analysis of human erythrocytes. (A) three cells loaded and (B) one cell loaded. See text for details.

remarkable is that, despite the high salt content, the mass spectrum shown in Figure 7.7B for the single cell analysis displays a mass resolution of 1500 fwhm. No sample cleaning was employed. The tolerance of MALDI to salts and buffers is clearly an advantage.[11]

The addition of several other features to this technique should further expand the usefulness of this mass spectrometric approach. Some form of chemical separation before mass spectrometric detection should be possible and benefit the analysis of trace components in the presence of a large quantity of other components. The use of affinity separation methods to isolate the compound of interest in a single cell or a subcellular component of a large cell could be explored. Here, the affinity capture sites can be inside the sample delivery capillary. Cell lysis can be accomplished using techniques similar to those used for capillary electrophoresis.[5,12] After isolation, the analyte can be deposited onto the probe. Alternatively, chemical and enzymatic reactions can be done to gain structural information from the mass analysis of the degraded products. For proteins, protein identification can be simplified by mass analysis with peptide and protein library searching. In essence, many strategies and methods currently used for handling larger volumes of a sample can potentially be miniaturized to meet the requirement of handling single cells. Note that many elegant methods are reported for handling single cell and small-volume solutions including enzymatic reactions at picolitre sample volumes.[12] Although these methods are focused on the use of other detection devices, adaptation to mass spectrometric applications should be possible with some modifications. Also note that, besides single cell analysis, the micro-spot MALDI technique should find general use in handling a small amount of material for biological applications, including the analysis of proteins isolated by polyacrylamide gel electrophoresis.

7.4 Literature Cited

(1) Jespersen, S.; Niessen, W. M. A.; Tjaden, U. R.; van der Greef, J.; Litborn, E.; Lindberg, U.; Roeraade, J. *Rapid Commun. Mass Spectrom.* **1994**, *8*, 581-584.

(2) Solouki, T.; Marto, J. A.; White, F. M.; Guan, S.; Marshall, A. G. *Anal. Chem.* **1995**, *67*, 4139-4144.

(3) Yeung, E. S. *Acc. Chem. Res.* **1994**, *27*, 409-414.

(4) a) Wightman, R. M.; Jankowski, J. A.; Kennedy, R. T.; Kawagoe, K. T.; Schroeder, T. J.; Leszczysyn, D. J.; Near, J. A.; Diliberto, E. J.; Viveros, O. H. *Proc. Natl. Acad. Sci. U.S.A.* **1991**, *88*, 10754-10758. b) Chow, R. H.; von Rüden, L.; Neher, E. *Nature* **1992**, *356*, 60-63. c) Alvarez de Toledo, G.; Fernández-Chacón, R.; Fernández, J. M. *Nature* **1993**, *363*, 554-558. d) Shear, J. B.; Fishman, H. A.; Allbritton, N. L.; Garigan, D.; Zare, R. N.; Scheller, R. H. *Science* **1995**, *267*, 74-77. e) Kennedy, R. T.; Huang, L.; Aspinwall, C. A. *J. Am. Chem. Soc.* **1996**, *118*, 1795-1796.

(5) a) Kennedy, R. T.; Oates, M. D.; Cooper, B. R.; Nickerson, B.; Jorgenson, J. W. *Science* **1989**, *246*, 57-63. b) Wallingford, R. A.; Ewing, A. G. *Anal. Chem.* **1988**, *60*, 1972-1975. c) Ewing, A. G.; Mesaros, J. M.; Gavin, P. F. *Anal. Chem.* **1994**, *66*, 527A-537A. d) Chang, H. T.; Yeung, E. S. *Anal. Chem.* **1995**, *67*, 1079-1083.

(6) a) McAdoo, D. J. In *Biochemistry of Characterized Neurons*; Osborne, N. N., Ed.; Pergamon Press: New York, 1978; pp. 19-45. b) Li, K. W.; Hoek, R. M.; Smith, F.; Jiménez, C. R.; van der Schors, R. C.; van Veelen, P. A.; Chen, S.; van der Greef, J.; Parish, D. C.; Benjamin, P. R.; Geraerts, W. P. M. *J. Biol. Chem.* **1994**, *269*, 30288-30292.

(7) Hofstadler, S. A.; Swanek, F. D.; Gale, D. C.; Ewing, A. G.; Smith, R. D. *Anal. Chem.* **1995**, *67*, 1477-1480.

(8) Whittal, R. M.; Li, L. *Anal. Chem.* **1995**, *67*, 1950-1954.

(9) Dai, Y.; Whittal, R. M.; Li, L. *Anal. Chem.* **1996**, *68*, 2494-2500 and the references therein.

(10) Golding, R. E.; Whittal, R. M.; Li, L. *"Nanoscale Sample Manipulation and Preparation Method for MALDI MS"* In *Proceedings of the 43rd ASMS Conference on Mass Spectrometry and Allied Topics*; Atlanta, GA, May 21-26, 1995; p 1223.

(11) Hillenkamp, F.; Karas, M.; Beavis, R. C.; Chait, B. T. *Anal. Chem.* **1991**, *63*, 1193A-1203A.

(12) a) Chang, H. T.; Yeung, E. S. *Anal. Chem.* **1993**, *65*, 2947-2951. b) Lillard, S. J.; Yeung, E. S.; Lautamo, R. M. A.; Mao, D. T. *J. Chromatogr. A* **1995**, *718*, 397-404.

Chapter 8

Conclusions and Future work

Time-lag focusing combined with MALDI provides several benefits over the traditional continuous extraction instrument. Probably, the most important benefit is the improved resolution. Desorption from thin sample layers on a sample probe placed in parallel to the direction of ion flight minimizes spatial aberrations. Consequently, an ion's position and velocity (energy) are directly related before the extraction pulse is applied. Energy compensation can be done in the source to focus ions of the same mass at the detector plane, significantly improving resolution. In Chapter 2 it was shown that a time-of-flight instrument equipped with time-lag focusing can provide mass resolution that is equivalent to ion mirror instruments for peptides. In addition, Chapters 2 and 3 show the resolution achievable by time-lag focusing exceeds that observed with ion mirrors for proteins and for more fragile biopolymers such as DNA. The spectrum of a mixed-base DNA 35-mer has a resolution of ~1200 fwhm.

Decoupling ion desorption from ion extraction reduces the number of collisions that occur in the source. The large kinetic energy deficit observed in continuous extraction instruments, which increases with mass, is not observed with time-lag focusing. As discussed in Chapter 3, the opposite effect is observed, i.e., a kinetic energy excess that increases with mass. This introduces a calibration problem in time-lag focusing MALDI. A method to overcome the problem was introduced, along with its limitations. A small energy deficit was observed with increasing laser power. The deficit appears to decrease slightly with mass, consistent with the proposed reason for the deficit, i.e., discharge of the repeller caused by the impact of anions and electrons. Increasing the capacitance of the ion source decreases this effect. Future work on the design of the instrument should consider the effect of source capacitance. Also, the ability to change the MALDI pulse shape would allow one to construct a pulse that increases in amplitude with time to provide the energy compensation necessary to optimally focus all ions, despite mass, with each pulse, i.e., mass independent time-lag focusing.

Chapter 4 focused on the importance of sample preparation. A time-of-flight instrument capable of high resolution and mass accuracy can still give significant mass errors if samples are prepared carelessly. As discussed previously, minimum spatial distributions are found for samples prepared as thin layers. Any axial spatial aberrations will reduce resolution and mass accuracy. The starting position for the ions moves forward as the sample thickness increases. The ions receive less kinetic energy than anticipated and flight times increase. If the sample is moved forward by 50 μm, then a mass error of +725 ppm would result for an insulin ion under time-lag focusing in a 1-m instrument. In addition, preparing small densely-packed crystals reduces the inhomogeneity of MALDI samples. The macroscopically poor analyte distribution in large crystals can be essentially eliminated using small crystals. The laser samples several crystals with each laser pulse. Shot-to-shot reproducibility is improved.

The MALDI instrument can be applied to the analysis of several different biopolymers and synthetic industrial polymers. In Chapter 5, MALDI was applied as a method to identify the products of an enzymatic reaction in vitro. The anticipated product and an unanticipated reaction product were found. The acceptor in the reaction was tetramethylrhodamine-labelled αFuc(1→2)βGal-$(CH_2)_8COOCH_3$. The unanticipated product was proposed to be a sulphated form of the acceptor, although the position of the sulphate is unknown. MALDI alone cannot determine the position of the sulphate group.

Chapter 6 was devoted to the analysis of end-labelled polyethylene glycol polymers. High mass accuracy and resolution are necessary to confirm the success of synthetic modification. The shift in the value of the number average or weight average molecular weight from the unmodified polymer is not a reliable means of determining the degree of functionalisation; exact mass assignment is necessary. High resolution analysis can separate impurities (singly-labelled product) of similar mass. Future work on the general applicability of MALDI to polymer analysis is required. All spectra shown in Chapter 6 were for polymers of narrow polydispersity. Polymers of wide polydispersity, i.e., $M_w/M_n > 1.5$, need to be analysed. MALDI analysis of these polymers does not yet give accurate values for the weight average and number average molecular weights.

Chapter 7 addressed the problem of sensitivity in MALDI analysis by reducing the sample deposition area such that the sample is used more efficiently. Again, the importance of sample preparation was emphasized. Small matrix crystals improve the sensitivity of analysis. The method was applied to the analysis of hemoglobin (~450 amol) from a single human red blood cell. This work could be extended to other cells, especially the analysis of peptides (perhaps protein digests). Peptides are very sensitive in MALDI. The limit of detection is < 1 amol.

MALDI is less than a decade old. The applications and limitations of the technique are still being explored. Most work reported was done on low resolution continuous extraction time-of-flight instruments. Decoupling ion formation from ion extraction and applying time-lag focusing assists in opening new avenues of research involving MALDI and in better understanding the fundamentals of the technique.